DEVELOPMENT AND MOTION CONTROL ANALYSIS OF AN AUTONOMOUS UNDERWATER VEHICLE

Thesis submitted by

PRITAM GHOSH

Doctor of Philosophy
(Engineering)

DEPARTMENT OF MECHANICAL ENGINEERING

FACULTY COUNCIL OF ENGINEERING &TECHNOLOGY

JADAVPUR UNIVERSITY

KOLKATA, INDIA

2024

JADAVPUR UNIVERSITY

KOLKATA-700032, INDIA

1. Title of the Thesis:

DEVELOPMENT AND MOTION CONTROL ANALYSIS OF AN AUTONOMOUS UNDERWATER VEHICLE.

2. Name, Designation & Institution of the Supervisor(s):

Dr. Pranibesh Mandal

Assistant Professor, Department of Mechanical Engineering,

Jadavpur University, Kolkata-700032

3. List of Publications:

i.   Ghosh, P., and Mandal, P. (2024). "AUV Way-Point Tracking at Constant Velocity: Cross-Track Error (CTE) and Line-of-Sight (LOS) Guidance", Engineering Research Express. DOI: 10.1088/2631-8695/ad36b0. **[Scopus, ESCI]**

ii.   Ghosh, P., and Mandal, P. (2019). "Numerical Study of Depth Control of an Innovative Underwater Vehicle Having Four Ballast Tanks", International Journal of Emerging Technologies and Innovative Research, 6(5), 123-126. DOI: 10.1729/Journal.21175. **[UGC care list]**

iii.   Ghosh, P., and Mandal, P. (2018). "Pressure and Shear Stress Distribution over External Hull of an Autonomous Underwater Vehicle", Journal of Basic and Applied Engineering Research, 2018, 5(5), 452-456. **[UGC care list]**

iv.   Ghosh, P., Das, A., and Mandal, P. (2023). "Analysis of Available Yawing Moment of an Autonomous Underwater Vehicle Model in Simulation Frame", Journal of Graphic Era University, 11(02), 191–206, DOI: 10.13052/jgeu0975-1416.1125.
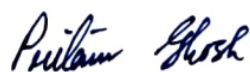
4. List of Patents: Nil

5. List of Presentations in National/International Conferences:

i.   Ghosh, P., and Mandal, P. (2024). "Yaw Motion Control Strategy for Autonomous Underwater Vehicles", 2nd International Conference on Mechanical Engineering (INCOM 2024) on January 5-6, 2024, at Jadavpur University, Kolkata, WB, India.

ii.   Ghosh, P., and Mandal, P. (2021). "Numerical Analysis of Open-Water Propeller Performance and Submarine Hull Drag", 48th National Conference on Fluid Mechanics and Fluid Power (FMFP) on December 27-29, 2021, at BITS Pilani, Pilani Campus, RJ, India.

6. List of Book Chapters:

i.   Ghosh, P., and Mandal, P. (2023). "Numerical Analysis of Open-Water Propeller Performance and Submarine Hull Drag", In: Bhattacharyya, S., Benim, A.C. (eds) Fluid Mechanics and Fluid Power (Vol. 2). FMFP 2021. Lecture Notes in Mechanical Engineering. Springer, Singapore. DOI: 10.1007/978-981-19-6970-6_30. **[Scopus]**

Candidate: Supervisor:

_____   _____ 25.04.2024

    (Pritam Ghosh)   (Dr. Pranibesh Mandal)

Assistant Professor
Dept. of Mechanical Engineering
Jadavpur University, Kolkata-32

JADAVPUR UNIVERSITY
FACULTY OF ENGINEERING AND TECHNOLOGY

STATEMENT OF ORIGINALITY

I, PRITAM GHOSH, registered on 27th April 2018, do hereby declare that this thesis entitled **"DEVELOPMENT AND MOTION CONTROL ANALYSIS OF AN AUTONOMOUS UNDERWATER VEHICLE"** *contains literature survey and original research work done by the undersigned candidate as part of the Doctoral studies.*

All information in this thesis has been obtained and presented in accordance with existing academic rules and ethical conduct. I declare that, as required by these rules and conduct, I have fully cited and referred all materials and results that are not original to this work.

I also declare that I have checked this thesis as per the "Policy of Anti-Plagiarism, Jadavpur University, 2019", and the level of similarity as checked by iThenticate software is **4%.**

Signature of the candidate: _Pritam Ghosh_

(Pritam Ghosh)

Date: 25.04.2024

Certified by Supervisor(s):
(Signature with Date, Seal)

1. _Pranibesh Mandal_ ,25.04.2024

(Dr. Pranibesh Mandal)

Assistant Professor
Dept. of Mechanical Engineering
Jadavpur University, Kolkata-32

This page is left blank intentionally

JADAVPUR UNIVERSITY
FACULTY OF ENGINEERING AND TECHNOLOGY

CERTIFICATE FROM THE SUPERVISOR

*This is to certify that the thesis entitled **"DEVELOPMENT AND MOTION CONTROL ANALYSIS OF AN AUTONOMOUS UNDERWATER VEHICLE"** submitted by Sri PRITAM GHOSH, who got his name registered on 27.04.2018 for the award of Ph.D. (Engineering) degree of Jadavpur University, is absolutely based upon his own work under the supervision of Dr. PRANIBESH MANDAL and that neither his thesis nor any part of the thesis has been submitted for any degree/diploma or any other academic award anywhere before.*

_____ ,25.04.2024

(Dr. Pranibesh Mandal)

Signature of the Supervisor and

date with Official Seal

Assistant Professor
Dept. of Mechanical Engineering
Jadavpur University, Kolkata-32

v

This page is left blank intentionally

Abstract

The complexity of designing a controller for an Autonomous Underwater Vehicle (AUV) has been examined in detail in this dissertation, with particular attention paid to heave motion, yaw motion, propeller performance, and trajectory tracking. By reducing reliance on conventional control surfaces, a novel four-ballast tank mechanism has been devised, revolutionizing AUV manoeuvrability. The study begins with a thorough investigation of the heave motion dynamics. The problem of the hull drag coefficient has been addressed utilizing a dual-methodology approach that combines rigorous CFD analysis with MATLAB-Simulink equations and Ansys-Fluent. The use of PID and PI controllers for depth control, in particular, emphasizes how much better PID is at managing higher-order dynamics.

In this study, a four-bladed B-series propeller has been used for the forward movement of the AUV. The open-water behavior of a B-series four-bladed propeller and submarine hull drag has been studied numerically using the SST k-ω turbulence model in the ANSYS-Fluent software platform. For validation purposes, the results of propeller coefficients obtained from numerical simulation have been compared with the experimental data of Bernitsas et al. (1981). For the comparison it has been estimated that the maximum difference between the thrust coefficients is 6.52% and torque coefficients is 7.5 % which means the numerical results have good accuracy. From the submarine hull analysis, it has been found that as the submarine speed increases drag on the hull also increases, and around the advance ratio (J) of 0.9 the submarine hull drag exceeds the thrust generated by the propeller when the propeller is rotating at its maximum speed. This means the maximum limiting speed of the submarine lies when

J is around 0.9 which meets the demand for this submarine model. Hence it can be concluded that this propeller is suitable for the submarine used in the present study.

Additional research into the physics of yaw motion reveals the complex link between forward velocity, yawing moments, and rudder tilt angle. The Ansys-Fluent software platform has been used to find the relation. It has been found that the yawing moment increases initially with the tilt angle of the rudder, reaching a peak before declining due to stalling effects. Furthermore, the yawing moment has been observed to rise with increasing forward velocity. The identification of critical angles for rudder stalling offers valuable information regarding the ideal operational range. A yaw motion dynamics governing equation is formulated based on the numerical analysis and implemented in MATLAB Simulink. A comprehensive comparison between two control systems: the Proportional-Integral (PI) and the combined Proportional-Integral-Derivative (PID) methods has been conducted for solving the yaw motion dynamics governing equation. The PID-Controller has exhibited superior performance characteristics, with notable reductions in oscillations and errors when compared with the PI-Controller. Furthermore, when the system has been subjected to a trapezoidal input demand, the PID controller has emerged as the optimal choice, outperforming its counterpart consistently. This finding underscores the potential advantages of incorporating an integral component into the control strategy for such applications.

The dissertation further establishes the intricate challenges associated with trajectory tracking for an AUV operating in a 2-D plane. The dynamics and kinematic framework of the AUV have been formulated and line-of-sight guidance has been proposed. For enhanced path-following tracking precision, sliding mode controllers on the 2-D plane are devised by employing both the cross-track error and the line-of-sight approach. This ensures both robustness and precise control, especially when confronted

with large errors. The controller's effectiveness has been evaluated by using four distinct trajectories: linear, linear with sharp turns, curved, and circular. Additionally, stability analysis has been performed to assess the resilience of the controllers against sudden underwater disturbances. Further, perturbation has been introduced in the simulations to simulate real-world conditions more accurately. The results of the simulations confirm the controllers' capability to accurately track various paths from a given starting point.

This page is left blank intentionally

Acknowledgement

I would like to express my deepest gratitude and appreciation to all those who have supported and contributed to the completion of my PhD thesis. Their guidance, encouragement, and assistance have been invaluable throughout this journey.

First and foremost, I am indebted to my supervisor, Dr. Pranibesh Mandal, for his exceptional mentorship and unwavering support. His expertise, insightful feedback, and dedication to my academic development have been instrumental in shaping this research. I am truly grateful for his patience, guidance, and the countless hours invested in supervising and refining this thesis.

I am deeply thankful to my lab mates and fellow researchers who have provided valuable discussions, technical support, and camaraderie. Their intellectual contributions and friendship have made this academic journey more enjoyable and meaningful.

My deepest appreciation goes to my family for their unconditional love, encouragement, and understanding throughout this challenging process. Their unwavering support, patience, and belief in my abilities have been the cornerstone of my success. I am truly grateful for their sacrifices and constant motivation.

Finally, I would like to express my heartfelt gratitude to all the participants who volunteered their time and expertise for this study. Without their willingness to contribute to my research, this work would not have been possible.

In conclusion, I extend my sincere appreciation to all those mentioned above, as well as anyone else who has been involved in my academic journey, directly or indirectly. Your support and contributions have played a pivotal role in completing this thesis, and I am forever grateful.

Thank you all.

PRITAM GHOSH

This page is left blank intentionally

Dedicated to My Parents

Guide

And My Beloved Wife

This page is left blank intentionally

Table of Contents

Abbreviations

AUV   Autonomous Underwater Vehicle

CFD   Computational Fluid Dynamics

CTE   Cross Track Error

DNS   Direct Numerical Simulation

LES   Large Eddy Simulation

LOS   Line of Sight

MPC   Model Predictive Control

PI   Proportional Integral

PID   Proportional Integral Derivative

RANS   Reynolds Average Navier Stokes

RMSE   Root Mean Square Error

SSK   Submersible Ship Killer

SST   Shear Stress Transport

UUV   Unmanned Underwater Vehicle

TKE   Turbulent Kinetic Energy

This page is left blank intentionally

Nomenclature

J	Advance ratio
p	Angular velocity along x-direction
q	Angular velocity along y-direction
r	Angular velocity along z-direction
V_a	AUV forward speed
F_w	AUV gravity force
t	Blade thickness
F_i	Body forces
F_b	Buoyancy force
G	Centre of gravity of rudder
c	Chord of propeller blade
$Y_{\dot{v}}$	Coefficient of added mass due to sway
$Y_{\dot{r}}$	Coefficient of added mass due to yaw
$N_{\dot{v}}$	Coefficient of added mass moment of inertia due to sway
$N_{\dot{r}}$	Coefficient of added mass moment of inertia due to yaw
C_d	Co-efficient of drag
Y_v	Coefficient of sway force due to side slip
Y_v	Coefficient of sway force due to side slip
Y_r	Coefficient of sway force due to yaw
Y_r	Coefficient of sway force due to yaw
N_v	Coefficient of sway moment due to side slip
N_r	Coefficient of sway moment due to yaw
c_i	Control voltage
e	Controller error
D_ω	Cross diffusion term
U_{cx}	Current velocity in x-direction
U_{cy}	Current velocity in y-direction
Z_d	Demand depth
z	Depth
K_d	Differential gain
a	Distance between centre of gravity of AUV and front tip of rudder

Γ_k	Effective diffusivity of k
Γ_ω	Effective diffusivity of ω
Q	Flow rate
X	Force along x-direction
Y	Force along y-direction
Z	Force along z-direction
G_ω	Generation of dissipation
$\widetilde{G_k}$	Generation of TKE
g	Gravitational acceleration
F_{hd}	Hydrodynamics resistance
K_i	Integral gain
L	Length of AUV
u	Linear velocity along x-direction
v	Linear velocity along y-direction
w	Linear velocity along z-direction
K	Moment about x-axis
M	Moment about y-axis
N	Moment about z-axis
I_z	Moment of inertia of the AUV about the yaw axis
P	Pitch of propeller
p_r	Pressure
A_s	Projected surface area
D	Propeller diameter
R	Propeller radius
A_o	Propeller swept area
T	Propeller thrust
k_L	Proportional coefficient of motor-pump
K_p	Proportional gain
F_{br}	Residual buoyancy
M_d	Resisting moment
n	Rotational speed (rps)
F_r	Side force generated by rudder

S_k	Source term of turbulent kinetic energy
S_ω	Source term of turbulent dissipation rate
K_t	Thrust coefficient of propeller
K_q	Torque coefficient of propeller
m	Total Mass
A_E	Total propeller blade area outside of the hub
S_T	Total trajectory path length
M_{yaw}	Yawing moment

Greek Symbols

δ_p	Angle between LOS and existing track
ψ_d	Demand yaw angle
ρ	Density
μ	Dynamic viscosity
g	Gravitational acceleration
η	Propeller efficiency
ε_{cr}	Root Mean Square Error Coefficient
θ_r	Roll angle
φ	Roll angle
θ	Rudder tilt angle
δs	Segmental trajectory length
μ_t	Turbulent eddy viscosity
ψ	Yaw angle

This page is left blank intentionally

List of Figures

List of Tables

This page is intentionally left blank

CHAPTER 1

Introduction

Chapter 1 provides the context for the thesis, briefly discussing the field of underwater vehicles. This chapter also presents the construction of the underwater vehicle, the literature review, the scope of the research, and the thesis outline.

1.1 BACKGROUND TO SUBMARINE ACQUISITION

The acquisition of submarines has always been blended with intricate international politics, economic considerations, and technological advancements. The history of submarines dates back to the late 19th and early 20th centuries, but their strategic importance surged during World War I and II. These wars showcased the submarine's potential to alter naval warfare paradigms, emphasizing stealth, surprise, and the ability to disrupt enemy supply lines. Post the World Wars, the Cold War era marked a significant increase in submarine development and acquisition. Recognizing the strategic advantage of an underwater presence the U.S. and Soviet Union embarked on ambitious programs to develop nuclear-powered submarines. Due to their extended underwater endurance and ability to carry ballistic missiles, these vessels became central pieces in the global strategic deterrence game. Advancements like the Polaris and Trident missile systems were seen in the 1960s and 1970s, enhancing the reach and potency of submarine-launched weapons. However, it was not only superpowers that saw the usefulness of submarine fleets. Regional nations wanted submarine capabilities in response to local conflicts and a desire for deterrence. Countries such as India, China, France, and the United Kingdom have constructed or bought sophisticated submarines to boost their naval capabilities.

Beyond military considerations, economic factors also play a crucial role in submarine acquisition. Submarines are expensive assets, requiring significant investments not just in their development or purchase but also in the infrastructure needed to support and maintain them. The decision to acquire submarines often necessitates careful balancing of defense imperatives against budgetary constraints.

Furthermore, technological access has often been a limiting factor for many nations. Advanced technologies, particularly those related to nuclear propulsion or stealth, are

closely guarded, leading nations to either develop indigenous capabilities or enter strategic alliances to gain access.

In recent times, there has been growing concern surrounding the underwater environment, with particular attention focused on the Arctic region. This area is seen as having the potential to become a new battleground for naval operations due to factors such as melting ice and increased accessibility. As a result, submarine strategies have been undergoing significant adjustments and adaptations to address these emerging challenges and opportunities. As countries strive to protect their interests in these disputed waters, submarines are considered invaluable assets because of their capability to operate stealthily beneath the ice caps.

Unmanned vehicles, commonly referred to as Unmanned eXpeditery Vehicles (UXVs), are gaining traction as tools to enhance naval vessel capabilities (Binns, et al., 2011). Among them, the Unmanned Underwater Vehicle (UUV) stands out, especially in the realm of submarine operations. This is because they can perform many tasks typically assigned to submarines. The global rise in the use of Submersible Ship Killer (SSKs) prompts new challenges for nations operating submarines (Development, Concepts and Doctrine Centre, 2010). Deploying UUVs as part of the naval fleet can decrease risks to manned submarines. They enhance capabilities in Intelligence, Surveillance, Reconnaissance, and Capital Asset Protection, as noted by Purton et al. (2013b).

1.2 LITERATURE REVIEW

Unmanned systems have witnessed remarkable advancements over the past few decades. Initially introduced for underwater operations, the versatility of these systems has been demonstrated not only beneath the water but also in aerial and terrestrial

environments. One of the standout innovations resulting from this progress is the Autonomous Underwater Vehicle (AUV). Since its prototype was first developed in the 1980s, AUVs have expanded their scope of applications. They have found widespread applications, ranging from military operations, as highlighted by Hagen et al. (2003), to more specific applications such as predicting underwater visibility conditions (Kenny et al., 2003; Yu et al., 2002), mapping the seabed (Kenny et al., 2003), and tracing chemical pathways (Farrel et al., 2005). AUVs stand out particularly for their capacity to operate in the challenging terrains of the ocean's deepest parts. Unlike remotely operated vehicles that necessitate constant human intervention, AUVs are designed to function independently in potentially hazardous underwater environments. (Sahoo et al., 2019; Wynn et al., 2014). These vehicles are inherently autonomous, powered by their own propulsion mechanisms, as outlined by Allotta et al. (2015) and equipped with onboard computers that facilitate decision-making. The onboard sensors of AUVs are their data collection tools, recording various marine parameters like temperature, depth, and chemical constituents. The utility of AUVs extends beyond data collection. Their competence in seafloor mapping, as observed by Shome et al. (2012), is vital for projects such as tidal energy plants and constructing marine infrastructures. Equipped with high-definition cameras, they can provide detailed images of the ocean bed. Furthermore, in the gas and oil sectors, AUVs play an indispensable role in evaluating geohazards and inspecting underwater structures for possible damages.

It is essential to provide the necessary power for these advanced machines. Most AUVs rely on lithium-ion batteries due to their superior energy density, providing extended operational durations (Bradly et al., 2001; Raman et al., 2002). Given that AUVs are expected to operate autonomously for prolonged periods across diverse marine terrains, it is important to optimize their energy consumption. A significant

factor influencing their energy use is the resistance they encounter from water during navigation. Comprehensive understanding and optimization of hydrodynamic properties, such as drag, lift, skin friction, and pressure coefficients, are therefore essential in enhancing the efficiency, control, and navigation capabilities of AUVs.

The hydrodynamic characteristics of AUVs are very important in determining their operational performance, stability, and efficiency under the sea. Fossen's (1994) research provides a solid foundation on this subject, detailing essential hydrodynamic principles such as drag, lift, and buoyancy as they relate to AUVs. The geometry of an AUV, particularly its shape and size, greatly influences these properties. Research by Hai et al. (2003) emphasizes the advantages of streamlined designs for reducing resistance and maximizing efficiency. Furthermore, the control mechanisms of AUVs have evolved to rely on sophisticated hydrodynamic models, as elucidated by Whitcomb (2000). Delving into the specifics, various hydrodynamic coefficients important to AUV stability have been discussed by Kim et al. (2002), while Bandyopadhyay (2005) explores the hydrodynamic implications of innovative propulsion systems, especially those inspired by marine creatures. Variables like buoyancy systems, as described by Blidberg (2001) are essential for balancing an AUV's weight, ensuring efficient movement. The AUV's structure itself, especially its hull design, plays a significant role in its hydrodynamics. A study by Alam et al. (2015) explored optimal design considerations. Additions like tails and fins can greatly impact an AUV's maneuverability and stability, as noted by Chen et al. (2013). Modern design and evaluation methods now prominently feature Computational Fluid Dynamics (CFD) tools, exemplified by Turnock et al.'s (2010) research. The natural aquatic environment, with factors like water currents and clarity, can introduce additional hydrodynamic challenges for AUVs, a topic addressed by Ridao et al. in 2010.

5

AUVs rely heavily on precise motion control to operate effectively in intricate underwater environments. At the core of this control, there are the fundamental motions: heave (vertical movement), roll (tilting side-to-side), pitch (tilting forward and backward), and yaw (turning left or right). Heave control ensures depth accuracy, vital for tasks such as seafloor mapping. Roll and pitch control maintain the AUV's stability, preventing undesired tilts which can affect onboard sensors and instruments. Yaw control governs the AUV's heading, ensuring it follows the desired path.

Depth control in AUVs is a vital area of research, emphasizing safety, efficiency, and navigation accuracy in submerged environments. Numerous advancements over the past decade have accentuated the importance and potential of sophisticated depth regulation systems. Supriyanka et al. (2011) were pioneers in exploring adaptive buoyancy systems that can adjust to varying underwater conditions. By 2012, Nor et al. has introduced neural network-based algorithms for more intuitive depth control. Kormushev and Caldwell (2013) has taken a significant lead by combining Proportional-Integral-Derivative (PID) controllers with machine learning techniques, boosting depth regulation efficiency. Studies by Watson and Green (2014) highlighted the integration of swarm intelligence for depth control in multiple AUVs. Through comprehensive underwater simulations, Zheng and Wu (2015) have identified potential challenges in deep-sea depth regulation. Focusing on energy efficiency, Tanakitkorn et al. (2017) have elucidated the design, simulation, and experimental testing of a PID-based diving control system using a Lyapunov-based approach for over-actuated AUVs. The system enables smooth transitions between hover-style and flight-style control, accommodating a broad spectrum of operating speeds. Wei et al. (2018) have investigated the vertical motion control of AUVs using Kalman Filtering. They have incorporated the Kalman filter into the depth data feedback loop to enhance the

accuracy of the feedback data, demonstrating the viability of this approach. All these contributions have highlighted the rapid progression and diverse approaches toward ensuring optimal depth control in AUVs.

The performance of AUV's propellers plays an important role in determining the efficiency, maneuverability, and noise emissions of these vehicles during their underwater missions. Additionally, the interaction between the submarine's hull and propeller is crucial for power calculation. Over the years, there has been significant research focusing on optimizing propeller design and understanding its impact on AUV operations. Due to the robust wake flows behind the hull, particularly at high Reynolds numbers, the performance of the propeller is significantly influenced by the upward flow conditions (Carlton 2011). Additionally, the presence of the propeller behind the hull can impact the flow condition around the submarine due to the relatively low flow velocity. Analyzing the flow field around underwater vehicles can be achieved through both experimental and numerical methods. Although experimental methods have limitations in terms of cost and time, numerical methods have gained popularity over the last few decades. Compared with experimental methods, numerical methods are considerably less expensive and more efficient if employed accurately. Computational fluid dynamics capabilities have advanced with the development of numerical methods, and one regularly used method is the potential flow method (Gao and Davies 2002; Kinnas and Hsin 1992; Ohkusu 1996; Ghassemi 2003). The finite volume method stands as another extensively developed CFD technique. While this method is more time-consuming compared to the potential flow method, it has demonstrated the capability to yield more reliable results, as evidenced by Turnock & Wright (2000). Other notable computational methods include Direct Numerical Simulation (DNS), Large Eddy Simulation (LES), and Reynolds Average Navier Stokes (RANS).

However, due to their computational expense, marine problems are typically addressed using more cost-effective methods such as RANS models.

The Shear Stress Transport (SST) k-ω 2-equation model stands out as one of the most suitable turbulence models for simulating the flow field around submarines and propellers, as utilized in the present study. Extensive investigations into the performance of the SST model have been conducted in numerous cases, offering advantages encompassing both free flow (k-ε) and near-wall (k-ω) models (Gohil et al. 2016). In examining marine propellers, the simplest case is the open water condition. However, when the propeller is positioned behind a floating hull, the flow around the hull creates nonuniform propeller inflow. Assuming a uniform flow condition around a propeller in such scenarios can lead to unrealistic results. To address this, studies have been conducted to predict propeller performance in nonuniform flow conditions. Some of these studies neglect the effect of hull/propeller interaction on performance due to challenges in mesh generation complexity and the substantial computational time involved (Watanabe et al. 2003; Ji et al. 2010; Zhang 2010).

Hayati et al. (2013) explored the performance of a standard propeller positioned behind an autonomous underwater vehicle within a fully turbulent flow regime. This investigation encompassed various angles of attack, employing the computational fluid dynamics method. In a study by Nan et al. (2005), the flow fields around a submarine near the free surface have been computationally analyzed. The results, including resistances and wave patterns, underwent a thorough examination. Gross et al. (2011) have simulated the flow on a SUBOFF bare hull model using an in-house developed Navier-Stoke code. Additionally, RANS calculations have been conducted as a reference using ANSYS CFX, with a focus on investigating the impact of different hull attack angles on friction and pressure coefficients. Chase and Carrica (2013) have

conducted computations on the self-propulsion of the DARPA-SUBOFF generic submarine, utilizing the E1619 propeller in model scale, and subsequently analyzed its propulsion performance. Their study revealed the significant impact of grid refinement on wake calculations. Zhang and Zhang (2014) have delved into the hull/propeller interaction of a submarine model equipped with a high-skew five-blade propeller in submergence and near-surface conditions. They assessed the wave pattern at various depths of submergence and calculated the thrust, torque, and self-propulsion factor of the submarine model. Notably, this study did not explore the effects of sea waves on the propulsion system's performance and hull resistance. Taskar et al. (2016) investigated the influence of waves on the propulsion system, including the propeller and engine, as well as the propeller and hull efficiency of a ship. They presented an effective method for modeling wake in waves, emphasizing the importance of a coupled engine-propeller system for accurate ship performance estimation.

The evolution of yaw motion control in AUVs has been a subject of extensive research over the years, given its fundamental role in maintaining the desired underwater orientation. Key research, such as Fossen's 1994 foundational text on ocean vehicle dynamics, has introduced the community to rudimentary control methods like PID controllers. As AUVs encountered various underwater uncertainties, the demand for adaptive controllers increased, a trend captured in the 2019 study by Yu et al. (2019). Neural networks' potential in predicting yaw motion and enhancing feedback control have been recognized early in 1993 by Healey and Lienard. Alongside, there have been significant strides in sliding mode control, emphasizing disturbance robustness, as illustrated by Swaroop et al. (2000) and Valeriano et al. (2016). Model Predictive Control (MPC) has appeared as a novel approach with research by Lapierre and Soetanto (2007) demonstrating its effectiveness. The 1990s also saw the integration of

fuzzy logic into yaw control strategies, offering enhanced performance under specific conditions, as evidenced by Li et al. (2021) work. Bai et al. (2022) have developed a self-adjusting and adaptive control method for the yaw dynamics of an autonomous underwater vehicle. Here, fuzzy logic has been combined with a classical gain compensator, which, when calibrated, offers consistent control across different conditions. This hybrid controller outperforms standalone fuzzy logic and classical state feedback controllers. Lefeber et al. (2003) have pursued and exemplified a holistic approach integrating yaw control with other motion dimensions, while Roy et al. (2023) showcased blending methodologies like neural networks and sliding mode control. The challenge of disturbances, particularly from underwater currents, was addressed through sliding mode techniques, as presented by Rodriguez et al. in 2019. The turn of the recent decade has ushered in a fresh perspective on deep reinforcement learning, with researchers like Carlucho et al. (2018) emphasizing its significance in AUV control.

AUV trajectory tracking, which involves ensuring that an AUV follows a predefined path, has been the subject of intensive research over the past decades and has given its significance in ensuring efficient and safe AUV missions. According to Nagai et al. (2008), accurate tracking requires a fine balance between onboard sensors and control algorithms. Rezazadegan et al. (2015) have emphasized the importance of adaptive control schemes in addressing uncertainties in AUV dynamics and external disturbances. Building on this, Kim Juhwan, and Son-Cheol Yu (2016) have introduced a neural network-based approach for real-time trajectory corrections. Elmokadem et al. (2016) have highlighted the challenges posed by underwater current disturbances, prompting Gan et al. (2016) to develop a predictive control framework to anticipate and counteract such external forces. As technology progressed, researchers like Thomas and

Jones (2012) began harnessing the power of machine learning for adaptive trajectory tracking. Multi-AUV missions, with their need for synchronized tracking, have been examined in depth by Huang et al. (2016). Yang (2017) took a step further by introducing deep learning techniques for trajectory predictions. Meanwhile, Holovatenko & Pysarenko (2015) have looked into the optimization of energy consumption during trajectory tracking. Zeng et al. (2015) and Zhang et al. (2022) both have emphasized the importance of robust algorithms that can handle unexpected obstacles and re-plan trajectories in real time. More recently, Mourtzis et al. (2023) have discussed the integration of Augmented Reality (AR) to enhance the visualization and tracking process, while studies by Monbroussou & Kukla (2021) and Das et al. (2023) have explored the incorporation of Quantum Computing and Internet of Things (IoT), respectively, in refining trajectory tracking methodologies.

In light of the extensive literature survey on AUVs, several important observations emerge. AUVs have firmly established their significance in vast areas of applications, ranging from scientific research to military operations. Their diverse application areas underscore their versatility and adaptability in addressing varied marine challenges. Central to the AUV's effectiveness is its motion control, where heave, roll, pitch, and yaw emerge as critical dimensions ensuring its precision and stability in the aquatic environment. The design and performance testing of the propeller is important, acting as the heart of the AUV's propulsion, influencing its speed, efficiency, and energy consumption. Lastly, trajectory control stands out as a testament to the sophisticated technology behind these vehicles, ensuring they navigate their underwater journeys with accuracy and adaptability. In sum, the AUV is a harmonious amalgamation of intricate design, advanced control mechanisms, and cutting-edge technology, poised to revolutionize underwater exploration and operations.

1.3 SCOPE OF THE RESEARCH

The major goals of the present investigations are enumerated as follows:

- Innovative implementation of a four-ballast tank mechanism to control the AUV maneuverability, minimizing the dependence on traditional control surfaces.
- Formulation of the governing equation to control the heave and yaw motions of the AUV.
- Numerical simulations to predict the AUV hull drag coefficients during heave and forward motion.
- Conduct a detailed study of open-water tests to analyze the propeller performance and find out AUV's speed limit.
- Investigation of the relationship between yaw motion, rudder tilt angle, and forward velocity of AUV.
- Implementation of suitable controllers for controlling the heave and yaw motions of AUV.
- Establishing the kinematic and dynamic model of the AUV for trajectory tracking control in the 2D plane.

1.4 OUTLINE OF THESIS

The thesis comprises a total of four chapters including this Chapter 1. The background of submarine acquisition, literature survey, and scope of work have been discussed in this chapter.

In Chapter 2, the details of system description and modeling of heave motion, yaw motion, propeller performance, and trajectory tracking of AUV have been discussed. Firstly, In Section 2.2 the model of heave motion dynamics has been formulated and a block diagram has been formed in Matlab-Simulink. In section 2.3, the model of the propeller has been drawn using CAD software and CFD based performance test setup

of the propeller has been developed. The root cause of the generation of yaw motion in AUV due to the rudder angle and AUV forward velocity has been discussed in Section 2.4. This section also represents the development of the governing equation of yaw motion dynamics and the development of a Simulink model. Lastly, the development of AUV path-following tracking control models in the 2-D plane has been discussed in Section 2.5.

Chapter 3 details the results and discussions. Starting with a brief introduction, Section 3.2 has covered the CFD analysis for hull drag coefficients during heave motion, along with results from solving the governing equation. Section 3.3 has showcased propeller performance curves and has determined the AUV's speed limit through CFD analysis. In Section 3.4, side thrust force generation and yaw motion dynamics have been explored, concluding with Matlab-Simulink results. Section 3.5 has demonstrated simulation outcomes for various 2-D desired trajectories, highlighting robust path-following tracking capabilities in stagnant water as well as under the influence of various water currents.

Finally, in Chapter 4, the major findings and contributions of the work are summarized. The future scope of work of this study has also been presented in this chapter.

This page is left blank intentionally

CHAPTER 2

System Description and Modelling

Chapter 2 provides the detail system description and modelling of heave motion dynamics and control, propeller performance, yaw motion dynamics and control, and way-point tracking of the AUV.

2.1 Introduction

Autonomous Underwater Vehicles (AUVs) represent the cutting edge of technology in the field of marine robotics, enabling study and exploration in vast and sometimes difficult underwater habitats. Controlling the AUV's mobility is a crucial field of research as it affects the vehicle's capacity for autonomous navigation and mission execution. Attaining accurate and adaptive motion control is crucial for effective mission execution and research pursuits as AUVs continue to progress in terms of design and capabilities.

This study focuses on the intricate aspects of AUV motion control, addressing heave motion, which involves vertical displacement; propeller performance, a critical component influencing the AUV's propulsion and efficiency; yaw motion, representing rotation around the vertical axis and trajectory tracking, essential for guiding the AUV along predefined paths. Detailed system descriptions, encompassing mathematical models and numerical methodologies, have been presented in the following sections.

2.2 Heave Motion Dynamics and Control

AUVs represent a class of unmanned marine vehicles designed to navigate and perform tasks autonomously in vast and often challenging underwater environments. One critical aspect of AUV operation is the dynamic response to vertical motion, commonly referred to as heave motion. Heave motion involves the vertical displacement of the AUV within the water column. This dynamic vertical movement is intricately influenced by the delicate equilibrium between buoyancy and gravity forces acting on the AUV. Understanding the heave motion dynamics is fundamental for achieving stability, precise navigation, and successful mission execution in diverse aquatic settings.

Historically, control surfaces have been the primary means of managing the depth, yaw, roll, and pitch motion of AUVs. However, this study introduces a novel approach by proposing a four-ballast tank mechanism to control the depth, pitch, and roll motion of a model AUV. These four ballast tanks are strategically positioned at the AUV's four bottom corners, as illustrated in Fig. 2.2.1.
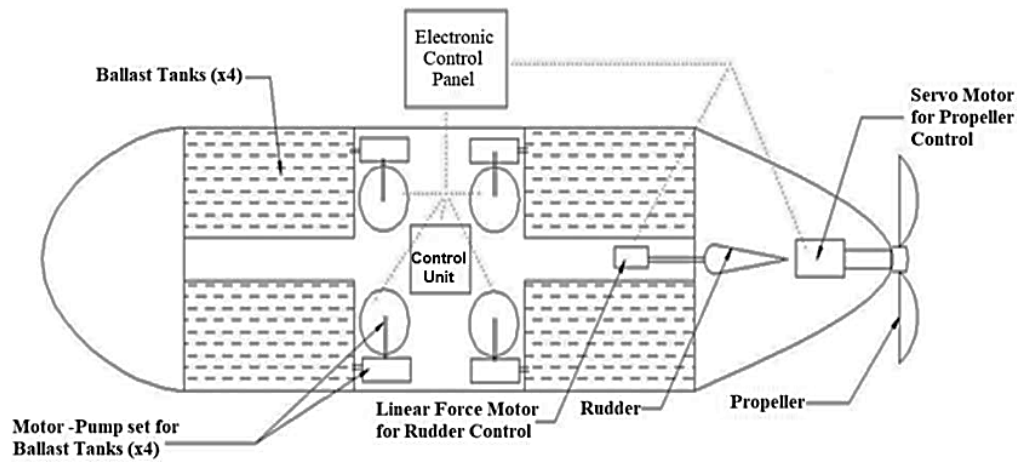
Fig. 2.2.1 Schematic diagram of AUV (plan view) (Ghosh and Mandal, 2019)

This innovative arrangement aims to reduce the reliance on traditional control surfaces by utilizing four motor-pump setups for ballast tank regulation. The primary strategy for controlling the AUV's depth involves manipulating the buoyancy force. Achieving equilibrium occurs when the buoyancy force equals the total weight of the AUV, allowing it to either float on the water's surface or remain fully submerged. Under fully submerged conditions, the AUV's depth can be adjusted at any position beneath the water surface by precisely operating the pumps that regulate the flow rate (Q) in and out of the ballast tanks. Initially, the ballast tanks are partially filled to ensure the AUV is fully immersed. Further filling decreases buoyancy, making the AUV heavier, causing it to sink, and vice versa. This approach offers a distinctive and potentially more efficient means of controlling the AUV's heave motion compared to conventional control surfaces.

The movement of an AUV can be decomposed into six distinct degrees of freedom, encompassing heave, sway, surge, pitch, roll, and yaw. However, in this section, the primary control target is the depth of the AUV. Therefore, only the heave motion of the AUV is considered in the mathematical modelling. To streamline the mathematical model for numerical simulations, several assumptions have been applied: (i) the motion of the AUV in surge, sway, roll, pitch, and yaw directions is neglected, (ii) the ballast tanks are filled with approximately 0.5 liters each (half of the total volume) of water to balance gravity, ensuring the AUV maintains neutral buoyancy, (iii) the body-fixed coordinate system of the AUV is positioned at its CG, aligning with the CG for the four ballast tanks. This alignment simplifies the coordinate system for mathematical representations, (iv) the flow rates (Q) governing the water entering and leaving the ballast tanks are equal in all four motor-pump setups, (v) due to the relatively small size of the AUV under consideration, the added mass effect is neglected, and (vi) disturbance underwater has been neglected. With these assumptions in place, the dynamics of heave motion for the AUV can be described by the following mathematical representation as:

$$m\ddot{z} = F_b - F_w - F_{hd} \tag{2.2.1}$$

Where m is the total mass of AUV, z is the depth, F_w is the AUV gravity force, F_b is the total buoyancy and F_{hd} is the hydrodynamics resistance.

Based on this idea, and assuming the ballast tanks have been topped off with a small amount of water to offset the AUV's gravity after diving, the pump might control the residual buoyancy by either adding or subtracting water from the tanks. As a result, the analysis could overlook the AUV's gravity. Taking into account the volume flow rate

of water entering and exiting the ballast tanks, which is represented by Q m³/s, the AUV's residual buoyancy is represented by F_{br}, which can be described as:

$$F_{br} = F_b - F_w = \rho g \int_0^t Q \, dt \tag{2.2.2}$$

Although it is recognized that the gravitational acceleration (g) value can fluctuate with position, for this study, the magnitude of this change is deemed inconsequential. As a result, it is assumed that the gravitational acceleration (g) is always 9.81 m/s². Here, the density of water is considered as 998.2 kg/m³.

The third term in Eq. (2.2.1), denoted as F_{hd}, corresponds to the hydrodynamic resistance. This force is intrinsically associated with the heave motion of the AUV and consistently opposes the direction of this motion, akin to a braking force. The hydrodynamic resistance (F_{hd}) serves to decelerate the AUV's heave motion, acting as a braking mechanism. Importantly, when the AUV is at rest with no heave motion, the hydrodynamic resistance force is zero. This characteristic aligns with the intuitive expectation that in the absence of motion, there is no opposing force exerted by the surrounding water. Consequently, the hydrodynamic resistance term captures the dynamic interplay between the AUV and its aquatic environment, reflecting the braking effect on heave motion during the vehicle's underwater operations. The expression of the force is given as

$$F_{hd} = \frac{1}{2} C_d \rho A_s \dot{z}^2 \tag{2.2.3}$$

Here, C_d is the coefficient of drag, A_s is the projected surface area of the AUV with $\dot{z}$ being the velocity of AUV during heave motion.

As heave motion encompasses both upward and downward movements of the AUV, Eq. (2.2.3) requires modification to account for the squared velocity. To accurately capture the resisting force during the vertical movement (z), the term $\dot{z}^2$ is replaced by

$\dot{z} \times |\dot{z}|$. This adjustment reflects the bidirectional nature of heave motion, acknowledging that the resisting force is contingent on the speed and direction of the AUV's vertical motion. By making this modification, the equation appropriately represents the hydrodynamic resistance in a manner that aligns with the nuanced dynamics of heave motion, providing a more comprehensive depiction of the forces acting on the AUV during both ascent and descent. So, the final equation for hydrodynamic force becomes,

$$F_{hd} = \frac{1}{2} C_d \rho A_s \dot{z} |\dot{z}| \tag{2.2.4}$$

After substituting the values from Eq. (2.2.2) and Eq. (2.2.4) into equation (2.2.1), the expression for the heave dynamics governing the heave motion of the AUV is obtained as follows:

$$m\ddot{z} = \rho g \int_0^t Q \, dt - \left(\frac{1}{2} C_d \rho A_s \dot{z} |\dot{z}| \right) \tag{2.2.5}$$

In the obtained dynamics equation for heave motion, where $\ddot{z}$ represents the acceleration of the AUV during heave motion, a sign convention has been rigorously applied to differentiate between upward and downward motions. Specifically, during the downward motion of the AUV, the velocity has been considered positive, whereas during the upward motion, the velocity has been considered negative. This sign convention is crucial for accurately characterizing the direction of the AUV's motion and ensures that the dynamics equation (Eq. 2.2.5) appropriately captures the system's response during both ascent and descent phases. By adhering to this sign convention, the mathematical representation provides a clear and consistent understanding of the acceleration dynamics governing the heave motion of the AUV. MATLAB Simulink has been used to implement the heave motion control system model, which has been

obtained from Eq. (2.2.5). The control diagram for the AUV heave motion is shown in Fig. 2.2.2. The pump is used as an actuator to drive the AUV to the appropriate depth. The expected depth (z_d) is fed into the depth controller. The controller constantly adjusts the AUV to attain the desired depth by measuring the AUV's depth using a depth sensor. It has been assumed that the pump's flow rate and input voltage have a linear connection, which is expressed as

$$Q = k_L c_i \tag{2.2.6}$$

Where, k_L is the proportional coefficient of the motor-pump set and c_i is the control voltage. In this case $k_L = 5.658 \times 10^{-6}$ m³/Volt.
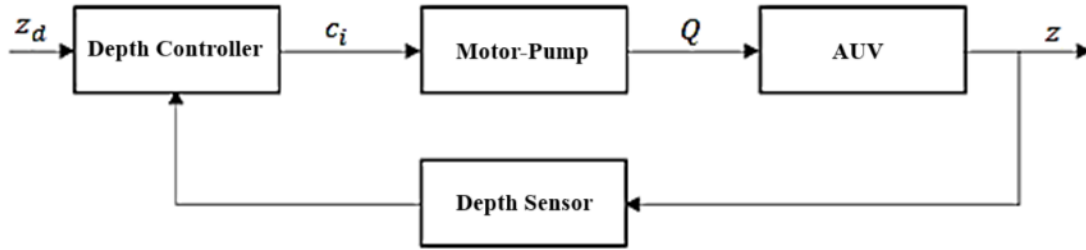
Fig. 2.2.2 Block diagram of AUV heave motion control

In the Simulink model, the controller takes the deviation between the expected and feedback signals as input and generates an output to mitigate the deviation. In depth control both PI and PID controllers have been used. The PI and PID control law for depth control in AUV is expressed in Eq. (2.2.7) and Eq. (2.2.8) respectively.

$$c_i = K_p e + K_i \int_0^t e \, dt \tag{2.2.7}$$

$$c_i = K_p e + K_i \int_0^t e \, dt + K_d \dot{e} \tag{2.2.8}$$

where K_p, K_i, and K_d are the controller gains of proportional, integral, and differential, respectively, and $e = (z_d - z)$ is the feedback error.

2.3 Propeller Performance Analysis

In the realm of marine propulsion, the propeller and its design wield significant influence. Furthermore, regarding power estimation, the interaction between an AUV's hull and propeller holds great importance. The primary goal when selecting a propeller is to achieve optimal rotational speed by providing maximum thrust and minimal torque. Additionally, propeller design encompasses maximum efficiency, reduced noise, and lighter weight. The true performance of these designed propellers remains unknown until subjected to experimental testing. However, conducting such experiments is not only costly and time-consuming but also poses a considerable challenge when assessing propellers behind the hull in the presence of a highly disturbed wake zone (Hayati et al., 2013). Gratefully, the swift progress in Computational Fluid Dynamics (CFD) technology allows for the numerical simulation of such studies, offering a close real-time prediction of actual propeller performance. The propeller performance is studied through open-water tests.

Given the maximum width of 0.2 m and height of 0.16 m of the AUV in this investigation, a four-bladed, right-hand, skewed Wageningen B-series propeller with an outer diameter of 0.16 m (i.e. radius (R) of 0.08 m) blade area ratio (A_E/A_O) set at 0.8 has been determined to be suitable (Barnitsas et al., 1981; Tran et al., 2019). Additional details regarding the propeller's geometry are provided in Table 2.3.1. Furthermore, a propeller model has been crafted using AutoCAD and SolidWorks software, visually depicted in Fig. 2.3.1 and Fig. 2.3.2.
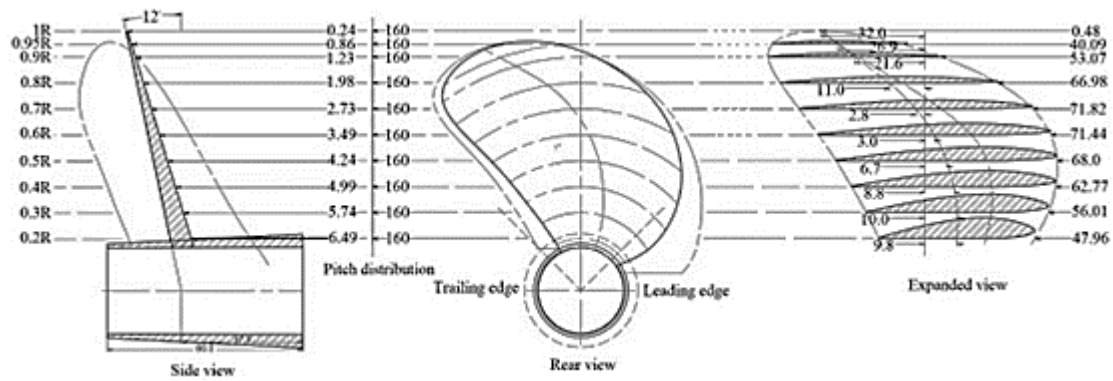
Fig. 2.3.1 Geometrical 2-D drawing of 4-bladed B-series propeller
(Ghosh and Mandal, 2021)

(a)   (b)
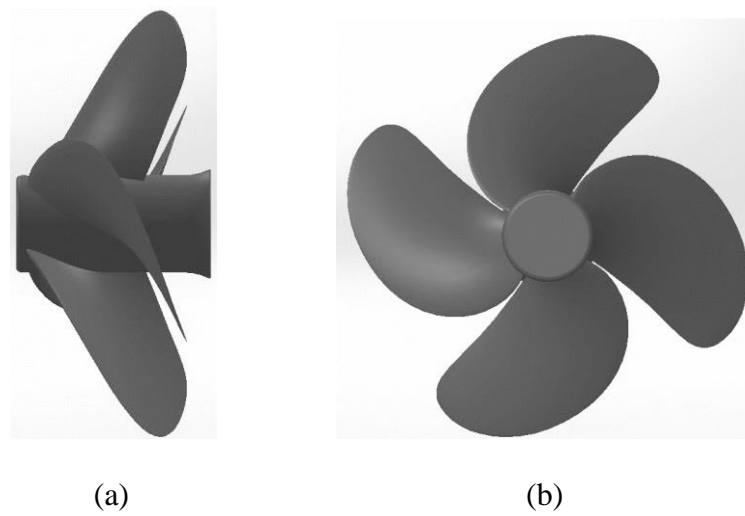
Fig. 2.3.2 Geometrical model of the propeller (a) side view, (b) front view
(Ghosh and Mandal, 2021)

Table 2.3.1 Important propeller parameters (Ghosh and Mandal, 2021)

Position from axis	Pitch-diameter ratio (*P/D*)	Skew (degree)	Chord-diameter ratio (*c/D*) in %	Blade thickness ratio (*t/D*) in %
1*R*	1	32.0	0.48	0.24
0.95*R*	1	26.9	40.09	0.86
0.9*R*	1	21.6	53.07	1.23
0.8*R*	1	11.0	66.98	1.98
0.7*R*	1	2.8	71.82	2.73
0.6*R*	1	-3.0	71.44	3.49
0.5*R*	1	-6.7	68.00	4.24
0.4*R*	1	-8.8	62.77	4.99
0.3*R*	1	-10.0	56.01	5.74
0.2*R*	1	-9.8	47.96	6.49

To estimate AUV hull drag, the 3-D model of the AUV has been employed for CFD analysis in Ansys-Fluent. This model AUV is 1 m in overall hull length. The computational analysis utilizes a rectangular enclosure, as depicted in Fig. 2.3.3. This computational domain has been intentionally enlarged to effectively capture the interaction between the hull and the fluid, as well as the development of the wake. In Fig. 2.3.3, the length of the AUV, excluding the propeller, is denoted as *L*.
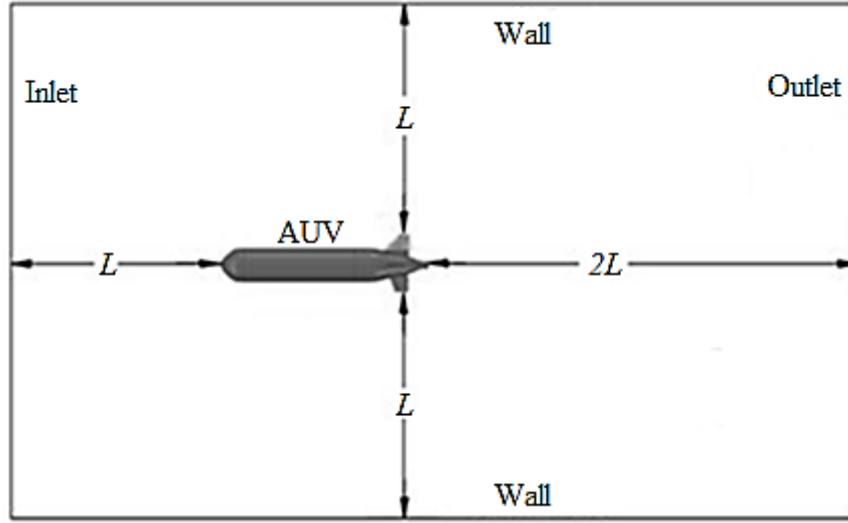
Fig. 2.3.3 Computational domain for hull drag estimation under submerged conditions (Ghosh and Mandal, 2021)

The continuity equation and Navier-Stokes equations (Ansys Release Note 10.0) are given as:

$$\frac{\partial(\rho u_i)}{\partial x_i} = 0 \tag{2.3.1}$$

$$\frac{\partial(\rho u_i)}{\partial t} + u_j \frac{\partial(\rho u_i)}{\partial x_j} = -\frac{\partial p_r}{\partial x_i} + \frac{\partial}{\partial x_j}\left((\mu + \mu_t)\frac{\partial u_i}{\partial x_j}\right) + \rho g_i + F_i \tag{2.3.2}$$

where, u_i is the velocity component in *x, y,* and *z* axis; ρ is the density of working fluid; p_r is the pressure; μ is the fluid dynamic viscosity; μ_t is the turbulent eddy viscosity; g_i is the gravitational acceleration; F_i represents the body forces.

In the current investigation, the estimation of AUV hull drag in submerged conditions relies on the application of the Shear-Stress Transport (SST) *k-ω* model. Developed by Menter in 1994, this model has since gained widespread use in AUV hull and propeller design studies, yielding satisfactory results for various researchers (Sousa et al., 2014; Karim et al., 2009). The transport equations governing the SST *k-ω* model (Ansys Release Note 10.0) are detailed as follows:

$$\frac{\partial(\rho k)}{\partial t} + \frac{\partial(\rho k u_i)}{\partial x_i} = \frac{\partial}{\partial x_i}\left(\Gamma_k \frac{\partial k}{\partial x_j}\right) + \widetilde{G_k} - Y_k + S_k \tag{2.3.3}$$

$$\frac{\partial(\rho \omega)}{\partial t} + \frac{\partial(\rho \omega u_i)}{\partial x_i} = \frac{\partial}{\partial x_i}\left(\Gamma_\omega \frac{\partial \omega}{\partial x_j}\right) + G_\omega - Y_\omega + S_\omega + D_\omega \tag{2.3.4}$$

In the above equations, G_ω is the generation of ω; $\widetilde{G_k}$ is the generation of turbulence kinetic energy due to mean velocity gradient; Γ_k and Γ_ω represent effective diffusivity of k and ω respectively; Y_k and Y_k represent the dissipation of k and ω due to turbulence; S_k and S_ω represents the used defined source terms; and D_ω is the cross-diffusion term. For numerical analysis, water has been taken as a working fluid having a dynamic viscosity (μ) of 0.001003 kg/m-s and density (ρ) of 998.2 kg/m^3.

Open-water test refers to the assessment of how a marine propeller operates in conditions where it is not influenced by the presence of a hull. During open-water testing, the propeller is evaluated in a towing tank or a controlled environment without the impact of a vessel's hull. This allows researchers and engineers to analyze the propeller's efficiency, thrust, torque, and other performance characteristics in isolation. Key parameters and performance metrics assessed during open-water propeller testing include the following:

(a) **Thrust Coefficient** (K_t)**:** It is the ratio of the thrust (T) produced by the propeller to the product of the density (ρ) of the water and the square of the propeller's rotational speed (n) as given in Eq. (2.3.5).

$$K_t = \frac{T}{\rho n^2 D^2} \qquad (2.3.5)$$

(b) Torque Coefficient (K_q): It is the ratio of the torque (Q) applied to the propeller shaft to the product of the density of the water and the cube of the propeller's rotational speed as given in Eq. (2.3.6).

$$K_q = \frac{Q}{\rho n^2 D^5} \qquad (2.3.6)$$

(c) Advance Ratio (J): It is the ratio of the forward speed (V_a) of the vessel to the product of the propeller's rotational speed and its diameter as given in Eq. (2.3.7).

$$J = \frac{V_a}{nD} \qquad (2.3.7)$$

(d) Efficiency (η): The efficiency of the propeller, often expressed as a percentage, is calculated by dividing the useful power (thrust times velocity) by the input power (torque times rotational speed) as given in Eq. (2.3.8).

$$\eta = \frac{1}{2\pi} \frac{K_t}{K_q} J \qquad (2.3.8)$$

For propeller performance assessment, a frame motion technique has been applied to induce rotation in the propeller. The computational domains pertaining to the propeller are illustrated in Fig. 2.3.4. The rotating domain is configured to rotate at a specific angular speed.

In this current investigation, the numerical analysis of the flow around the AUV hull and propeller has been conducted using the ANSYS-Fluent software platform. The pressure-velocity coupling has been implemented through a coupled scheme (Ghosh and Mandal, 2018). In terms of spatial discretization, the Least Squares Cell Based scheme (Ghosh and Mandal, 2018) has been employed, accompanied by the second-

order upwind method for discretizing the momentum and turbulent model. Detailed

boundary conditions are provided in Table 2.3.2.

Table 2.3.2 Boundary conditions for numerical analysis of AUV hull and propeller

Boundary	AUV	Propeller
Inlet	Velocity inlet	Velocity inlet
Outlet	Pressure outlet	Outflow
Body Surface	No-slip boundary	No-slip boundary
Wall	Free slip	Free slip
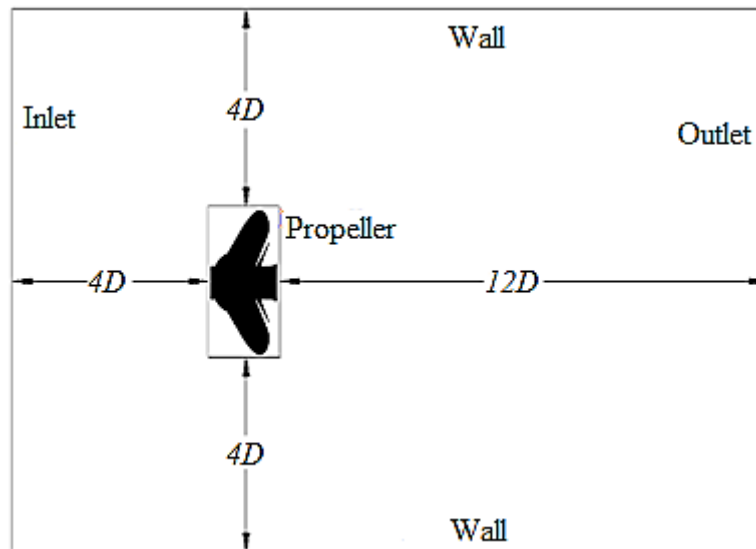
Fig. 2.3.4 Computational domain for open-water condition of propeller
(Ghosh and Mandal, 2021)

2.4 Yaw Motion Dynamics and Control

The Yaw motion dynamics of AUVs play a crucial role in their overall maneuverability and performance. Yaw refers to the rotation of the AUV around its vertical axis, which is perpendicular to the Earth's surface. Understanding and controlling yaw motion is essential for precise navigation, stability, and successful completion of underwater missions.

Yaw dynamics are influenced by various factors, including the vehicle's design, propulsion system, control algorithms, and environmental conditions. AUVs typically employ thrusters or control surfaces to generate yaw moments, allowing them to change their heading or orientation underwater. Accurate modeling and control of yaw dynamics are essential for achieving desired trajectories, optimizing energy consumption, and ensuring the AUV's ability to adapt to varying ocean currents and disturbances. Researchers and engineers focus on developing advanced control strategies and navigation algorithms to enhance the yaw motion capabilities of AUVs. This includes the integration of sensors for accurate position and orientation estimation, as well as the implementation of feedback control systems to maintain stability and achieve precise heading control.

The current investigation delves into the yaw motion dynamics of a novel small AUV model (Ghosh & Mandal, 2019). The central focus of this study is to scrutinize the effects of different orientations of the submarine rudder on the vessel's yaw dynamics. The yawing moment, a critical aspect of underwater maneuverability, is closely tied to pressure variations on the rudder. Consequently, understanding and quantifying these pressure variations for varying rudder angles become imperative.

A distinctive aspect of this research lies in its exploration of the relationship between yaw motion, rudder tilt angle, and the forward velocity of the submarine. Few

existing studies have thoroughly addressed the yaw control of AUVs with a specific emphasis on the interplay between forward movement and the resulting pressure changes on the rudder. This study bridges this gap in the literature by investigating the forces acting on the rudder due to pressure variations. Moreover, the study derives the available yawing moment as a function of both the tilt angle of the rudder and the forward velocity of the AUV.

The study focuses exclusively on the impact of the rudder on the motion of the AUV with the propeller assumed to have no effect due to its geometry. The rudder, as shown in Fig. 2.4.3b, is a trapezoidal shape with dimensions of 0.125 m at the bottom, 0.05 m at the top, and a thickness of 0.0125 m, which is an important parameter in the investigation. Among the four fin-like surfaces shown in Fig. 2.4.1, only the vertically positioned top one is movable and serves as the rudder, while the others remain fixed, contributing to stability.

The difference in water pressure occurs on the two sides of the rudder when it is tilted sidewise while the submarine is having forward velocity. It is due to the fact that the rudder while tilted at a particular angle (θ), renders an angle of attack equal to the angle of tilt (θ) with the free stream velocity of water particles. Water has been considered stagnant for the analysis thereby causing the free stream velocity of the water particles to be equal and opposite to the forward velocity (V_a) of the AUV. Such an angle of attack causes a difference in the overall pressure distribution on the two sides of the rudder thereby causing Lift-like side force, F_r to be acting on the same as shown in Fig. 2.4.2a. Here it has been considered that such side force on the rudder acts at the 'Centre of gravity', G of the planform area of the rudder surface as shown in Fig. 2.4.2a and Fig. 2.4.2b. Such a side force, F_r renders a yawing moment (M_{yaw}) about the CG of the AUV in the *x-y* plane as shown in Fig. 2.4.2a. The moment arm is also shown

in Fig. 2.4.2a and denoted as 'r'. The moment arm is determined by adding the distances 'a' from the CG to the tip of the base of the rudder and the distance of G from the tip of the base as shown in Fig. 2.4.1 and Fig. 2.4.2b. It may be noted that as the rudder is rotated about an axis passing through G, the angular position of the rudder does not change the value of 'c'. Also, for the present analysis, the CG of the AUV is a fixed point and the tip of the rudder is always a fixed point rendering the distance 'a' to be constant also. That necessarily means the moment arm 'r' is to be constant for the entire analysis and it is measured to be 0.513 m. So, the available yawing moment, M_{yaw} can be given by:

$$M_{yaw} = F_r \cdot r \qquad\qquad (2.4.1)$$

Where, F_r is the total side force on the rudder for any instance.
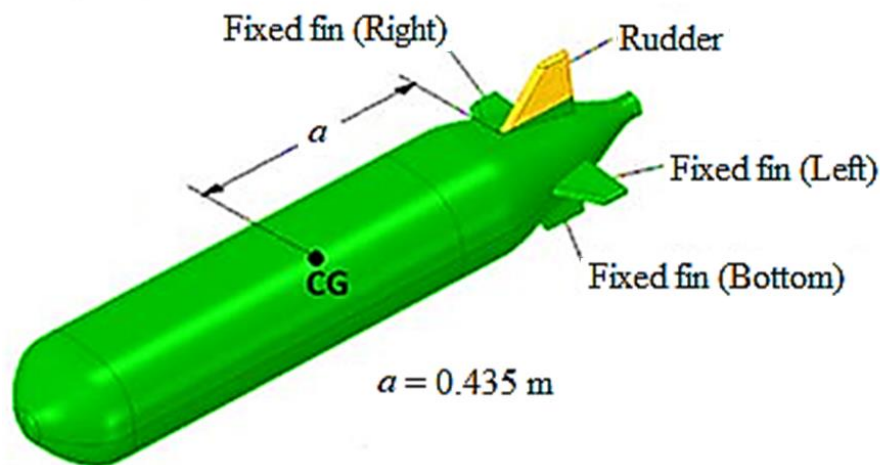
Fig. 2.4.1 3-D view of model AUV (Ghosh et al., 2023)

(a)   (b)
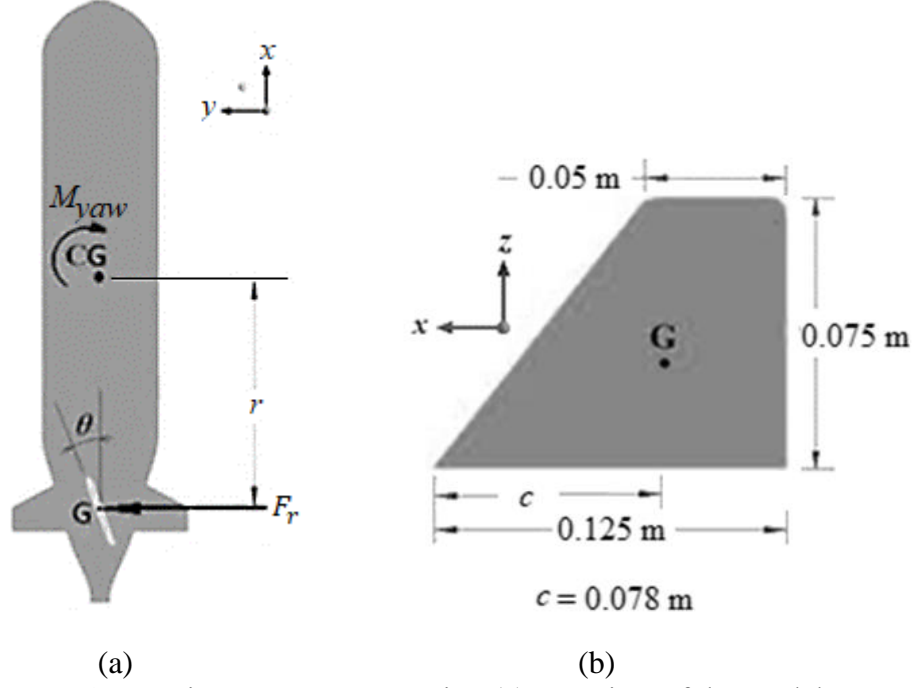
Fig. 2.4.2 Yawing moment generation (a) Top view of the model AUV. (b) Planform area of the rudder (Ghosh et al., 2023)

In this analysis, the forces on the rudder of the immersed submarine have been predicted at various rudder angles and different forward velocities using Ansys-Fluent platform. The Shear- Stress Transport (SST) *k-ω* model (Menter, 1994) has been used for the numerical analysis. This model, introduced in 1994, has garnered widespread acceptance and application in diverse simulation scenarios (Sousa et al., 2014). Its robustness and versatility make it a well-established choice for simulations involving fluid dynamics, allowing for a detailed and accurate examination of the forces exerted on the submarine's rudder under different operational conditions. The governing equations (Ansys Release Note 10.0) are given by:

$$\frac{\partial u_i}{\partial x_i} = 0 \tag{2.4.2}$$

$$\frac{\partial(\rho u_i)}{\partial t} + u_j \frac{\partial(\rho u_i)}{\partial x_j} = -\frac{\partial p}{\partial x_i} + \frac{\partial}{\partial x_j}\left((\mu + \mu_t)\frac{\partial u_i}{\partial x_j}\right) + \rho g_i + F_i \tag{2.4.3}$$

$$\frac{\partial(\rho k)}{\partial t} + \frac{\partial(\rho k u_i)}{\partial x_i} = \frac{\partial}{\partial x_i}\left(\Gamma_k \frac{\partial k}{\partial x_j}\right) + \widetilde{G_k} - Y_k + S_k \tag{2.4.4}$$

$$\frac{\partial(\rho\omega)}{\partial t} + \frac{\partial(\rho\omega u_i)}{\partial x_i} = \frac{\partial}{\partial x_i}\left(\Gamma_\omega \frac{\partial\omega}{\partial x_j}\right) + G_\omega - Y_\omega + S_\omega + D_\omega \tag{2.4.5}$$

Where, u_i is the velocity component along the *x, y, z-axis;* μ is the fluid viscosity*;* p is the pressure*;* ρ is the working fluid density; g is the gravitational acceleration; F_i is the body force; μ_t is the turbulent eddy viscosity; G_ω is the generation of specific turbulence dissipation rate; $\widetilde{G_k}$ is the generation of turbulence kinetic energy due to mean velocity gradient; Y_k is the effective diffusivity of turbulent kinetic energy; Y_ω is the effective diffusivity of turbulent dissipation rate; S_ω and S_k are the defined source terms of turbulent dissipation rate and turbulent kinetic energy respectively; Γ_k and Γ_ω are the effective diffusivity terms; D_ω is the cross-diffusion term.

The estimation of lift forces generated by the AUV's rudder is conducted through a meticulous analysis utilizing a 3-D model. The computational domain is strategically extended, encompassing a distance of *L* in front of the leading edge of the underwater hull form and *2L* behind the trailing edge, as visually represented in Fig. 2.4.3a. Here, *L* denotes the length of the AUV model. Furthermore, the domain both above and below the rudder and fixed fin is extended by a distance *L* for both scenarios, contributing to a comprehensive analysis.

In this study, water is considered as the working medium. The numerical analysis of fluid flow around the submarine hull and rudder employs a pressure-based solver, with a coupled system for pressure-velocity coupling (Ansys Release Note 10.0). To discretize the momentum and turbulent models, a Least Squares Cell-Based technique (Ansys Release Note 10.0) is applied in tandem with a second-order upwind method. The computational domain has been shown in Fig. 2.4.3. The specific boundary conditions are outlined in Table 2.4.1.
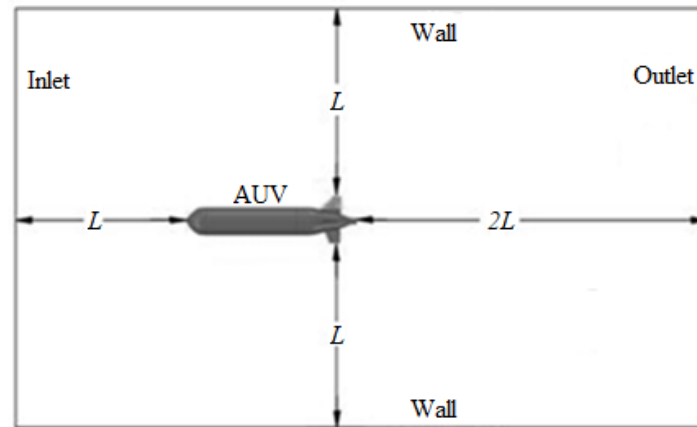
Fig. 2.4.3 Computational domain for yawing moment analysis (Ghosh et al., 2023)

Table 2.4.1 Boundary conditions for numerical analysis of yawing moment

Boundary	Boundary condition
Inlet	Velocity inlet
Outlet	Pressure outlet
Surface	No-slip boundary
Outer surface of Enclosure	Zero wall shear

Grid independence testing stands as a crucial aspect of validating the solution technique during CFD operations within the ANSYS-Fluent package. The selection of an appropriate mesh size is pivotal for computational accuracy but comes at the cost of increased computation time. To address this, a grid independence study is conducted using unstructured meshes with 0.43, 0.54, 0.71, 0.92, and 1.22 million elements, respectively.

The results of the grid independence study, as depicted in Fig. 2.4.4, reveal that the change in hull drag coefficient is minimal between 0.71 and 0.92 million elements. Consequently, 0.71 million elements are chosen for the numerical analysis, aligning with a hull drag coefficient of 0.143. This grid independence test ensures the selection

of an optimal mesh size for conducting the numerical simulation, striking a balance

between computational efficiency and reasonable accuracy.
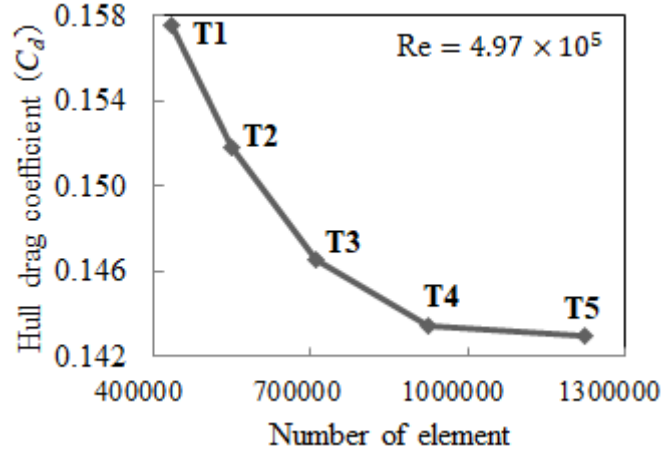
Fig. 2.4.4 Grid independence test for yawing moment analysis (Ghosh et al., 2023)

With the generation of the yawing moment (M_{yaw}), the AUV achieves a yaw motion

about the vertical axis. This yaw motion further generates hydrodynamic drag force on

the AUV hull surface which further generates a counter moment (M_d) to the AUV as

shown in Fig. 2.4.5.
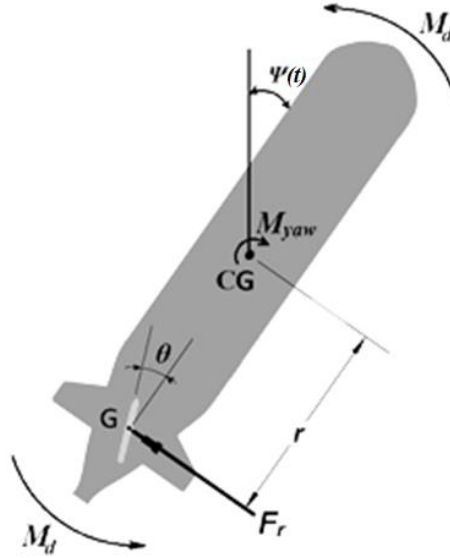
Fig. 2.4.5 Generation of counter moment (M_d) due to hydrodynamic drag

Considering the effect of sway motion and rudder motion, the governing equation of

yaw motion dynamics can be modelled as

$$I_z\ddot{\psi} = M_{yaw} - M_d + Y_v V_a + Y_r \dot{\psi} \qquad (2.4.6)$$

Where, I_z is the moment of inertia of the AUV about the yaw axis (z-axis), Y_v is the hydrodynamics coefficient due to sway velocity, Y_r is the hydrodynamics coefficient due to the rate of change of yaw angle. The expressions for Y_v and Y_r used in this study are given below (Johnson, 2001).

$$Y_v = -0.10700 \times \rho \times \frac{L^2}{2} \tag{2.4.7}$$

$$Y_r = 0.01187 \times \rho \times \frac{L^3}{2} \tag{2.4.8}$$

The system model for the yaw motion control has been developed in MATLAB Simulink using Eq. 2.4.6. The input to the system is the demand yaw angle (ψ_d) in the form of demand signals of various waveforms and the output of the system is the final yaw angle (ψ). A feedback system is incorporated using Proportional-Integral (PI) and Proportional-Integral-Derivative (PID) controllers whose parameters are tuned such that the yaw angle (ψ) closely follows the demand yaw angle (ψ_d) provided by the controller with minimal phase and amplitude lag. A schematic diagram of the closed-loop system is shown in Fig. 2.4.6. The ODE4 Runge-Kutta solver has been used for solving the governing equation of yaw motion dynamics.
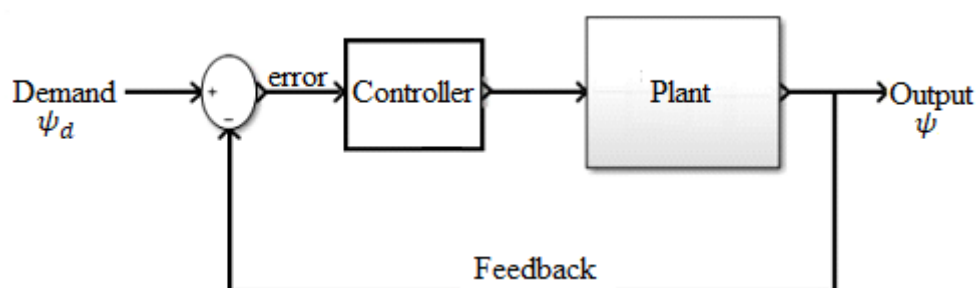

Fig. 2.4.6 Block diagram of yaw motion control

2.5 Trajectory Tracking of AUV

In the realm of AUVs, the ability to precisely navigate predefined routes is a fundamental requirement for achieving mission objectives. Way-point tracking stands at the forefront of this navigation paradigm, involving the development and implementation of sophisticated control algorithms that guide AUVs along designated waypoints with precision and efficiency. Way-points serve as critical reference locations within the underwater environment, defining the vehicle's path and ensuring it reaches specific destinations accurately. The study of way-point tracking in AUVs encompasses a fusion of disciplines, including control theory, marine robotics, and navigation algorithms. As AUVs continue to evolve as indispensable tools in scientific research, environmental monitoring, and industrial applications, understanding and optimizing way-point tracking algorithms become pivotal in enhancing their autonomy, reliability, and overall operational effectiveness. This introduction sets the stage for a comprehensive exploration of the principles, challenges, and advancements in the context of way-point tracking for Autonomous Underwater Vehicles.

In this section, the foundational aspects of AUV dynamics have been explored by examining the kinematic and dynamic equations governing its horizontal movement. AUVs, typically designed with symmetry, are explored with the body-fixed frame positioned at the center of gravity, maintaining neutral buoyancy. To conduct a comprehensive analysis of the AUV's motion, both the earth-fixed frame and the body-fixed frame have been considered, the latter being a dynamic coordinate system affixed to the AUV, as depicted in Fig. 2.5.1. This study adopts the T. Sname's (1950) notation to delineate various quantities, as outlined in Table 2.5.1. By establishing these fundamental parameters, the groundwork has been laid for a thorough investigation into

the intricate dynamics influencing an AUV's trajectory and response in underwater environments.
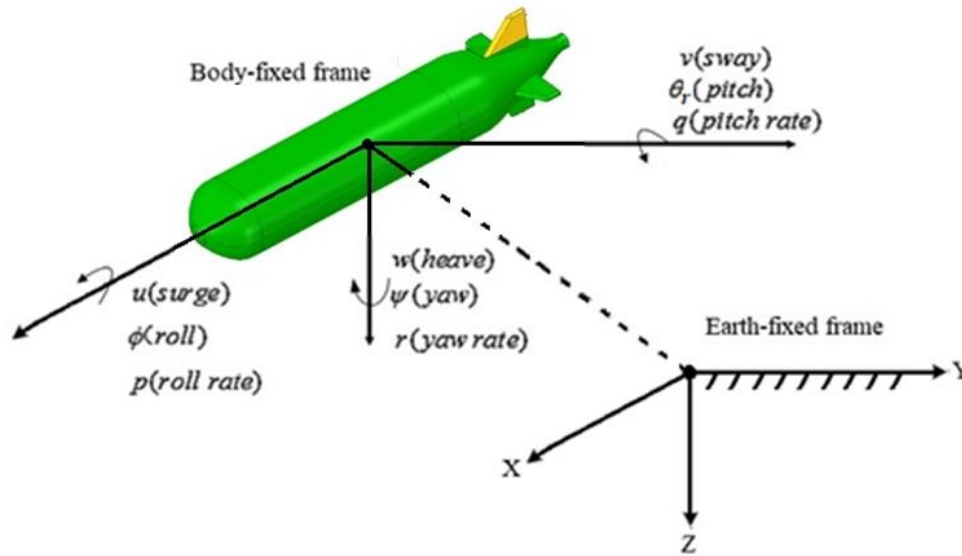
Fig. 2.5.1 Body-fixed frame & Earth-fixed frame for the AUV

Table 2.5.1 Notations used for AUV motion dynamics

DOF		Forces and Moments	Linear and Angular velocities	Positions and Euler angles
1	Motion in the *x*-direction (Surge)	X	u	x
2	Motion in the *y*-direction (Sway)	Y	v	y
3	Motion in the *z*-direction (Heave)	Z	w	z
4	Rotation about the *x*-axis (Roll)	K	p	φ
5	Rotation about the *y*-axis (Pitch)	M	q	θ_r
6	Rotation about the *z*-axis (Yaw)	N	r	ψ

Utilizing the Newton-Euler methodology, A. J. Healey (1995) formulated the six degree of freedom motion equations of AUV as follows:

$$X = m\big[\dot{u} - vr + wq - x_g(q^2 + r^2) + y_g(pq - \dot{r}) + z_g(pr + \dot{q})\big] \qquad (2.5.1)$$

$$Y = m\big[\dot{v} - wp + ur - y_g(p^2 + r^2) + x_g(pq + \dot{r}) + z_g(qr - \dot{p})\big] \qquad (2.5.2)$$

$$Z = m\big[\dot{w} - uq + vp - z_g(p^2 + r^2) + x_g(pq - \dot{q}) + y_g(qr + \dot{p})\big] \qquad (2.5.3)$$

$$K = I_x\dot{p} + (I_z - I_y)qr + I_{xy}(pr - \dot{q}) - I_{yz}(q^2 - r^2) - I_{xz}(pq - \dot{r}) + m\big[y_g(\dot{w} -$$

$$uq + vp) - z_g(\dot{v} + ur - wp)\big] \qquad (2.5.4)$$

$$M = I_y\dot{q} + (I_x - I_z)pr - I_{xy}(qr + \dot{p}) + I_{yz}(pq - \dot{r}) + I_{xz}(p^2 - r^2) - m\big[x_g(\dot{w} -$$

$$uq + vp) - z_g(\dot{u} - vr + wq)\big] \qquad (2.5.5)$$

$$N = I_z\dot{r} + (I_y - I_x)pq - I_{xy}(p^2 - q^2) - I_{yz}(pr + \dot{q}) + I_{xz}(qr - \dot{p}) + m\big[x_g(\dot{v} +$$

$$ur - wp) - y_g(\dot{u} - vr + wq)\big] \qquad (2.5.6)$$

Assuming (A. J. Healey, 1995) that (i) the centre of mass aligns with the body-fixed coordinate axis, (ii) there is a uniform mass distribution, (iii) hydrodynamic damping terms exceeding first order can be overlooked, (iv) variations in inertia are minor, (v) the heave, pitch, and roll modes are dismissible, and (vi) the speed u is also equated to the forward speed (V_a), the horizontal dynamics of the AUV can be represented as:

$$u = V_a \qquad (2.5.7)$$

$$m\dot{v} = -mV_a r + \Delta Y \qquad (2.5.8)$$

$$I_z\dot{r} = \Delta N \qquad (2.5.9)$$

Here, ΔY and ΔN are the forces influenced by the vehicle's dynamic parameters. By assuming "small" motions, the concept of 'hydrodynamic coefficients' emerges, correlating with distinct motion elements. The formula representing the transverse and rotational forces reads as follows:

$$\Delta Y = Y_{\dot{v}}\dot{v} + Y_v v + Y_{\dot{r}}\dot{r} + Y_r r \qquad (2.5.10)$$

$$\Delta N = N_{\dot{v}}\dot{v} + N_v v + N_{\dot{r}}\dot{r} + N_r r \tag{2.5.11}$$

Where, $Y_{\dot{v}} = $ added mass coefficient due to sway

$Y_{\dot{r}} = $ added mass coefficient due to yaw

$Y_v = $ sway force coefficient due to side slip

$Y_r = $ sway force coefficient due to yaw

$N_{\dot{v}} = $ coefficient of added mass moment of inertia arising from sway

$N_{\dot{r}} = $ coefficient of added mass moment of inertia arising from yaw

$N_v = $ sway moment coefficient due to side slip

$N_r = $ sway moment coefficient due to yaw

By integrating Eq. (2.5.8) & Eq. (2.5.9) with Eq. (2.5.10) and Eq. (2.5.11) respectively, the steering dynamics of the AUV has been derived in matrix form as:

$$\begin{bmatrix} m - Y_{\dot{v}} & -Y_{\dot{r}} & 0 \\ -N_{\dot{v}} & I_z - N_{\dot{r}} & 0 \\ 0 & 0 & 1 \end{bmatrix} \begin{bmatrix} \dot{v} \\ \dot{r} \\ \dot{\psi} \end{bmatrix} = \begin{bmatrix} Y_v & Y_r - mV_a & 0 \\ N_v & N_r & 0 \\ 0 & 1 & 0 \end{bmatrix} \begin{bmatrix} v \\ r \\ \psi \end{bmatrix} \tag{2.5.12}$$

Given the vehicle's symmetrical design and the proximity of the rudders to the center of the body, it has been assumed that the cross-coupling terms in the mass matrix are negligible. Consequently, the definitive dynamics (Eq. 2.5.12) of the vehicle are described as:

$$\begin{bmatrix} m - Y_{\dot{v}} & 0 & 0 \\ 0 & I_z - N_{\dot{r}} & 0 \\ 0 & 0 & 1 \end{bmatrix} \begin{bmatrix} \dot{v} \\ \dot{r} \\ \dot{\psi} \end{bmatrix} = \begin{bmatrix} Y_v & Y_r - mV_a & 0 \\ N_v & N_r & 0 \\ 0 & 1 & 0 \end{bmatrix} \begin{bmatrix} v \\ r \\ \psi \end{bmatrix} \tag{2.5.13}$$

The kinematic equations for an AUV navigating the horizontal plane can be articulated as:

$$\begin{bmatrix} \dot{X} \\ \dot{Y} \\ \dot{\psi} \end{bmatrix} = \begin{bmatrix} \cos\psi & -\sin\psi & 0 \\ \sin\psi & \cos\psi & 0 \\ 0 & 0 & 1 \end{bmatrix} \begin{bmatrix} u \\ v \\ r \end{bmatrix} + \begin{bmatrix} U_{cx} \\ U_{cy} \\ 0 \end{bmatrix} \tag{2.5.14}$$

Where, U_{cx} and U_{cy} are the current velocities in the associated direction.

Guidance for an AUV involves the continuous calculation of the desired location, speed, and even acceleration for the vessel, which the control system then utilizes (Molnar et al., 2007). Such guidance systems typically incorporate a waypoint generator based on human input. One approach to set up this system involves pre-storing desired waypoints, which then inform the AUV's trajectory. Alternatively, the system can integrate elements like weather routing, obstacle evasion, collision prevention, and mission strategizing (Breivik and Fossen, 2005). A straightforward way to guide the AUV is to provide a directional command that aligns the vehicle with the direct line between its current position and the target waypoint. When constructing waypoint guidance systems, it's crucial to differentiate between path-following tracking and maneuvering controls. Such systems rely on human-directed waypoint generators. After storing these commands in a database, they help shape the AUV's movement path. Systems for both trajectory and maneuvering can be developed for this objective. Position terminology and definitions can be referenced in Fig. 2.5.2.
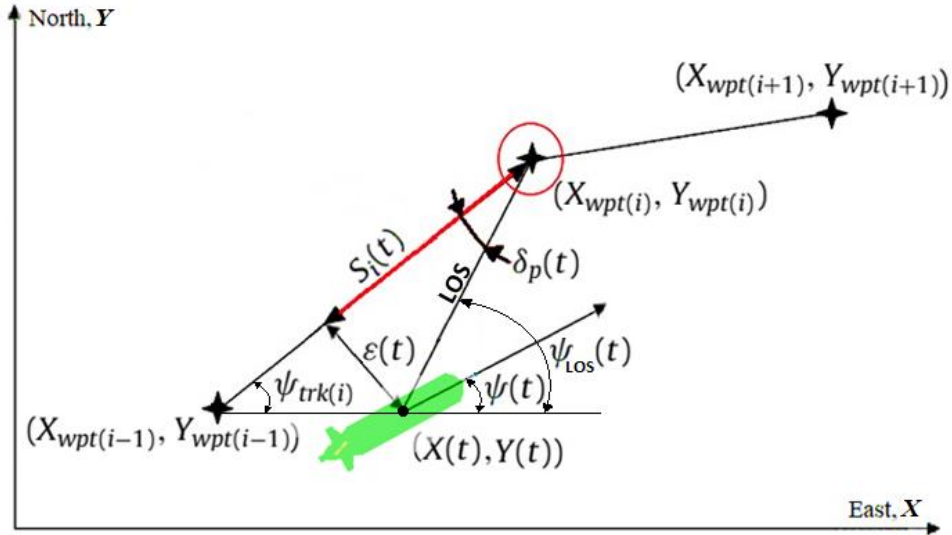
Fig. 2.5.2 Track geometry and Cross-Track Error (CTE) of the AUV

The fundamental guidance principles, based on the Line-of-Sight heading control method, are outlined as follows:

$$\psi(t)_{com}(los(i)) = \tan^{-1}\left(\frac{\tilde{Y}(t)_{wpt(i)}}{\tilde{X}(t)_{wpt(i)}}\right) \tag{2.5.15}$$

$$\tilde{Y}(t)_{wpt(i)} = Y_{wpt(i)} - Y(t) \tag{2.5.16}$$

$$\tilde{X}(t)_{wpt(i)} = X_{wpt(i)} - X(t) \tag{2.5.17}$$

In the 2-D plane, the AUV's path-following tracking control ensures it navigates along a pre-set course confined to a specific area. This set course often consists of segments connecting various waypoints. The control strategy is typically based on observable yaw angles and their rate of change. This study employs a sliding mode control strategy that incorporates both the cross-track error (CTE) and the line-of-sight (LOS) techniques. The cross-track error method consistently corrects the AUV's positioning based on its deviation, aiming to achieve the intended location. The cross-track error, denoted as $\varepsilon(t)$, represents the normal distance between the AUV's centre and its intended path, and its control goal is to minimize this distance.

The track angle and the overall path length between waypoints $(X_{wpt(i)}, Y_{wpt(i)})$ and $(X_{wpt(i-1)}, Y_{wpt(i-1)})$ are explicitly defined as follows:

$$\psi_{trk(i)} = \tan^{-1}\left(\frac{Y_{wpt(i)} - Y_{wpt(i-1)}}{X_{wpt(i)} - X_{wpt(i-1)}}\right) \tag{2.5.18}$$

$$L_i = \sqrt{(X_{wpt(i)} - X_{wpt(i-1)})^2 + (Y_{wpt(i)} - Y_{wpt(i-1)})^2} \tag{2.5.19}$$

For the i-th track segment, the cross-track heading error, denoted as CTE, is characterized as:

$$\tilde{\psi}(t)_{CTE(i)} = \psi_{trk(i)} - \psi(t) \tag{2.5.20}$$

It's important to note that the heading error $\tilde{\psi}(t)_{CTE(i)}$ should be normalized to fall within the range of $\pm\pi$. The projected distance of the i-th waypoint onto the track line, denoted as $S_i(t)$, can be characterized as:

$$S_i(t) = [\tilde{X}(t)_{wpt(i)}\left(X_{wpt(i)} - X_{wpt(i-1)}\right) + \tilde{Y}(t)_{wpt(i)}(Y_{wpt(i)} - Y_{wpt(i-1)})]/L_i$$

$$(2.5.21)$$

Hence, $S_i(t)$ varies within the range of 0 to 100 percent of L_i.

For the AUV to closely follow the set route, the control system on the 2-D plane must ensure that $\varepsilon(t)$ approaches 0. Based on the current position, the current path point, and the preceding path point, the cross-track error $\varepsilon(t)$ can be articulated as:

$$\varepsilon(t) = S_i(t) \tan\left(\delta_p(t)\right) \tag{2.5.22}$$

Here, $\delta_p(t)$ represents the angle formed between the line-of-sight directed at the next waypoint and the existing track line. The value of $\delta_p(t)$ needs to be adjusted to ensure it stays within the boundaries of $\pm\pi$. The equation is presented as follows:

$$\delta_p(t) = \tan^{-1}\left(\frac{Y_{wpt(i)} - Y_{wpt(i-1)}}{X_{wpt(i)} - X_{wpt(i-1)}}\right) - \tan^{-1}\left(\frac{\tilde{Y}(t)_{wpt(i)}}{\tilde{X}(t)_{wpt(i)}}\right) \tag{2.5.23}$$

Regarding the cross-track definition, a sliding surface can be articulated using the derivatives of the errors, presented as:

$$\dot{\varepsilon} = u \sin\left(\tilde{\psi}(t)_{CTE(i)}\right) \tag{2.5.24a}$$

$$\ddot{\varepsilon} = u\left(r(t) + \dot{\gamma}(t)\right)\cos\left(\tilde{\psi}(t)_{CTE(i)}\right) \tag{2.5.24b}$$

$$\dddot{\varepsilon} = u\left(\dot{r}(t) + \dot{\gamma}(t)\right)\cos\left(\tilde{\psi}(t)_{CTE(i)}\right) - u\left(r(t) + \dot{\gamma}(t)\right)^2 \sin\left(\tilde{\psi}(t)_{CTE(i)}\right)$$

$$(2.5.24c)$$

We postulate that $\dot{\gamma}$ and $\ddot{\gamma}$ are minimal and hence can be disregarded, especially when contrasted with the angular velocity of the yaw angle. The cross-track error-based sliding mode controller's sliding surface can be structured in the shape of a second-order polynomial as:

$$\sigma(t) = \ddot{\varepsilon}(t) + \lambda_1\dot{\varepsilon}(t) + \lambda_2\varepsilon(t) \tag{2.5.25}$$

The formulation of Eq. (2.5.19) and the condition for achieving error reduction can be articulated as follows:

$$\dot{\sigma}(t) = \dddot{\varepsilon}(t) + \lambda_1\ddot{\varepsilon}(t) + \lambda_2\dot{\varepsilon}(t) = -\tanh\left(\frac{\sigma}{\phi}\right) \qquad (2.5.26)$$

To determine the control input, the heading dynamics of the AUV are streamlined by excluding the side slip dynamics, and this can be depicted as:

$$\dot{r}(t) = ar(t) + b\delta_r(t) \qquad (2.5.27)$$

$$\dot{\psi}(t) = r(t) \qquad (2.5.28)$$

By integrating Eq. (2.5.26) with Eq. (2.5.24), Eq. (2.5.27) and Eq. (2.5.28), the subsequent expression has been obtained as:

$$\dot{\sigma}(t) = u\big(ar(t) + b\delta_r(t)\big)\cos\big(\tilde{\psi}(t)_{CTE(i)}\big) - u\big(r(t)\big)^2\sin\big(\tilde{\psi}(t)_{CTE(i)}\big) +$$

$$\lambda_1 u r(t)\cos\big(\tilde{\psi}(t)_{CTE(i)}\big) + \lambda_2 u\sin\big(\tilde{\psi}(t)_{CTE(i)}\big) \qquad (2.5.29)$$

Reformulating Eq. (2.5.25), the sliding surface $\sigma(t)$ can be presented as:

$$\sigma(t) = u r(t)\cos\big(\tilde{\psi}(t)_{CTE(i)}\big) + \lambda_1 u\sin\big(\tilde{\psi}(t)_{CTE(i)}\big) + \lambda_2\varepsilon(t) \qquad (2.5.30)$$

Utilizing Eq. (2.5.26) and Eq. (2.5.29) the rudder input can be represented as:

$$\delta_r(t) = \left[\big(u(r(t))^2\sin\big(\tilde{\psi}(t)_{CTE(i)}\big)\big) - \big(a u r(t)\cos\big(\tilde{\psi}(t)_{CTE(i)}\big)\big) - \right.$$

$$\left.\big(\lambda_1 u r(t)\cos\big(\tilde{\psi}(t)_{CTE(i)}\big)\big) - \big(\lambda_2 u\sin\big(\tilde{\psi}(t)_{CTE(i)}\big)\big) - \big(\tanh\left(\frac{\sigma}{\phi}\right)\big)\right] \times$$

$$\left[b u\cos\big(\tilde{\psi}(t)_{CTE(i)}\big)\right]^{-1} \qquad (2.5.31)$$

When heading error, $\tilde{\psi}(t)_{CTE(i)}$ goes beyond 90^0, AUV is likely to traverse the track in a direction contrary to what's intended. To avoid this scenario in real-world applications, a 40° threshold has been established, beyond which the system transitions to line-of-sight (LOS) control.

The heading guidance can be established as:

$$\psi(t)_{LOS(i)} = \tan^{-1}\left(\frac{\tilde{Y}(t)_{wpt(i)}}{\tilde{X}(t)_{wpt(i)}}\right) \tag{2.5.32}$$

And the error in the line of sight can be articulated as:

$$\tilde{\psi}(t)_{LOS(i)} = \psi(t)_{LOS(i)} - \psi(t) \tag{2.5.33}$$

The application of the LOS controller becomes evident in two scenarios: i) at the onset of the mission, if the AUV's initial heading deviates more than 40° from the first waypoint, and ii) when the angular difference between consecutive track lines surpasses 40°. As soon as the cross-track heading error falls below 40°, the AUV switches to the CTE controller.

CHAPTER 3

Results and Discussions

Chapter 3 provides the discussions on the findings of heave motion dynamics and control, propeller performance, yaw motion dynamics and control, and way-point tracking of the AUV.

3.1 Introduction

In the realm of marine robotics, the advancement of control mechanisms for AUVs is the focus of this project through a multidimensional approach. Comprising heave motion control, yaw motion control, propeller performance test for maximum speed, and trajectory tracking, AUV autonomy and efficiency are sought to be enhanced. Robust control strategies are developed to ensure stability, precise navigation, and adaptability to dynamic underwater environments. Section 3.2 emphasizes on heave motion control addressing vertical displacement, crucial for maintaining equilibrium and executing maneuvers at varying depths. A pivotal role is played by propeller selection and performance analysis, presented in section 3.3, aiming for maximum speed and energy efficiency to propel the AUV through underwater realms. Section 3.4 emphasizes the findings of yaw motion control. The regulation of yaw motion is delved into, enhancing the rotational dynamics of the AUV for improved heading changes and maneuverability. Finally, section 3.5 pointed to the trajectory tracking of AUV. The trajectory tracking endeavors focus on guiding the AUV along predefined paths with accuracy, facilitating complex missions and scientific exploration. As the results and discussion are delved into, the comprehensive approach undertaken in this project is seen to hold promise for transforming AUV capabilities and advancing underwater technology.

3.2 Heave Motion Dynamics and Control

The heave motion of AUVs plays a pivotal role in their operational capabilities and adaptability to underwater environments. Heave motion involves the vertical displacement of the AUV within the water column, and its significance lies in maintaining equilibrium and stability during various underwater missions. Traditionally, control surfaces have been key in managing AUV motions, including

depth, yaw, roll, and pitch. This study introduces innovation with a four-ballast tank mechanism strategically positioned at the AUV's four corners, reducing reliance on conventional controls (Fig. 2.2.1). The dynamics of heave motion have been presented in Eq. (2.2.5) and MATLAB-Simulink platform has been used for solving this equation.

In the process of solving Eq. (2.2.5), a challenge arises concerning the unknown value of the drag coefficient (C_d). To address this, numerical analysis is employed to predict the C_d value during the heave motion of the AUV. Specifically, a numerical investigation of the flow around the AUV hull during heave motion is conducted utilizing the ANSYS-Fluent software platform. The pressure-velocity coupling in this study is achieved through a coupled scheme. Spatial discretization is implemented using the Least Squares Cell-based scheme, complemented by a second-order upwind method for both the momentum and turbulent models. Fig. 3.2.1 depicts the computational domains and various boundary conditions employed in the simulations.

Various inflow velocities were designated as the boundary conditions at the inlet. The outlet boundary condition is set with zero relative pressure. Free-slip boundary conditions were applied to the lateral walls, and a no-slip boundary condition was implemented on the hull surface. Details about the domain parameters are outlined in Table 3.2.1.
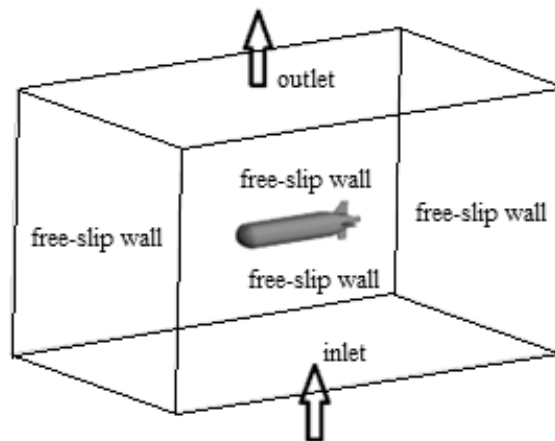

Fig. 3.2.1 Computational domain of heave motion analysis

**Table 3.2.1** Domain parameters for numerical simulations

Parameters	Settings
Type	Fluid
Material	Water
Reference Pressure	1 atm
Density of Fluid	998.2 kg/m3
Viscosity of Fluid	0.001003 kg/m-s
Model of Turbulence	k-ε
Turbulent Wall Function	Scalable

Considering that the prevailing research (Barnitsas et al., 1981; Martinez-Calle et al., 2002; Nakisa et al., 2010) has predominantly favored unstructured grids for their CFD analysis models, the computational model in this study similarly utilizes unstructured grids, as depicted in Fig. 3.2.2.
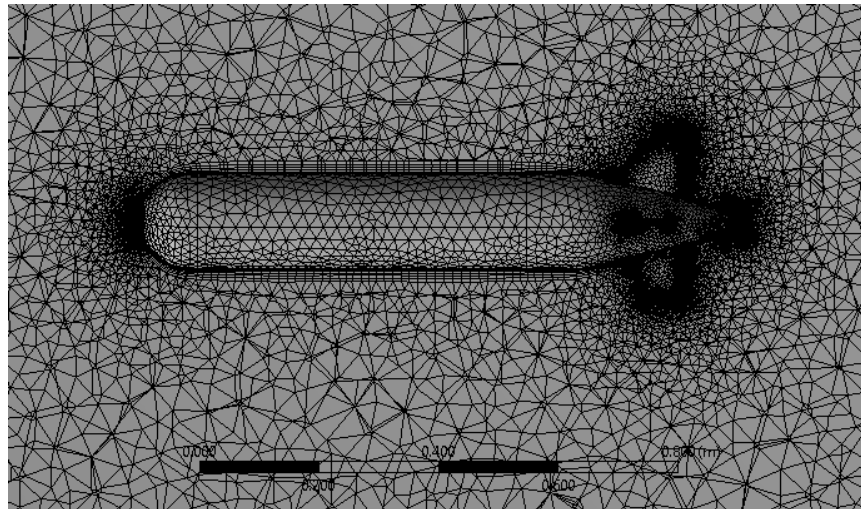

Fig. 3.2.2 Unstructured mesh view of AUV hull

When performing numerical analyses through the Ansys-Fluent platform, assessing grid independence stands as a crucial phase. Computational time increases with a higher element count, making a grid independence test crucial to determine an optimal element count for accurate results without unnecessary computational load. Assessing the drag coefficient in heave motion for a fully submerged AUV involved using different grid sizes. Mesh refinements were applied in various zones for numerical accuracy. The

results in Fig. 3.2.3 demonstrate that test 3 (0.71 million elements) offers the most

suitable conditions, ensuring precise numerical simulations for drag coefficient

analysis.
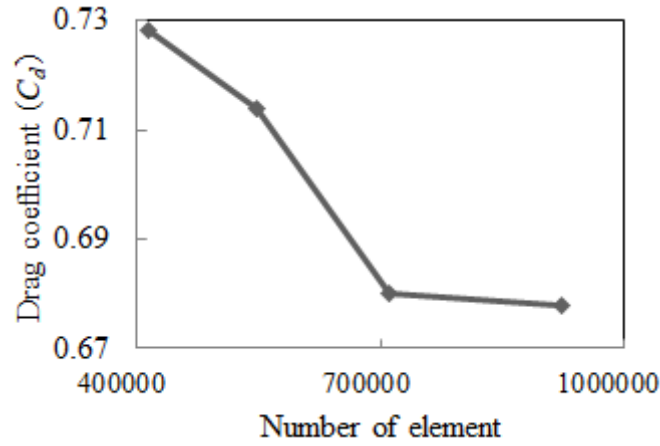
Fig. 3.2.3 Grid independence study of heave motion analysis

Figure 3.2.4 displays the relationship between the computational hull resistance

coefficient and the Reynolds number, which is based on the hull length.
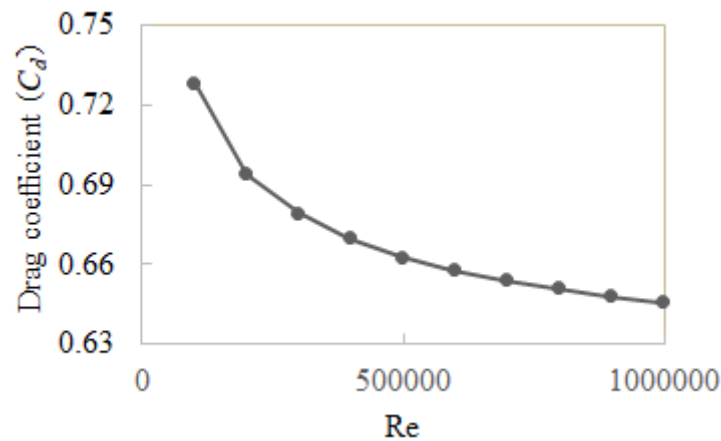
Fig. 3.2.4 Variation of C_d with Re during heave motion

After having determined the value of the drag coefficient (C_d) in heave motion, the

governing equation (Eq. 2.2.5) of heave motion has been solved in MATLAB-simulink.

Here, the Ordinary Differential Equation (ODE4) Runge-Kutta solver has been

implemented. In the calculations, it has been assumed that the water in the ballast tank

has not been compressed. Additionally, changes in the density of water and air with

temperature have been ignored. The main designed parameters of the proposed AUV

are shown in Table 3.2.2.

Table 3.2.2 Design parameters of AUV for heave motion

Parameters	Value
Ballast tank volume	4 L
Water density (ρ)	998.2 kg/m^3
Total mass of AUV (m)	18 kg
Projected surface area of AUV (A_s)	0.139 m^2
Proportional coefficient of motor-pump (k_L)	5.658×10^{-6} m^3/V
Drag coefficient of AUV in heave motion (C_d)	0.68

PI and PID controllers have been used to investigate the AUV's heave motion

dynamics. The depth control performance can be compared when the AUV system

depicted in Fig. 2.2.2 is taken into consideration as a controlled plant. Before the

simulation, every controller was fine-tuned to ensure the validity of the comparison

results. Table 3.2.3 contains a list of the control parameters.

Table 3.2.3 Controller parameters of AUV for heave motion

| Type of controller	Controller parameter
PI	$K_p = 0.00189, K_i = 3.306 \times 10^{-5}$
PID	$K_p = 6.643 \times 10^{-4}, K_i = 2.581 \times 10^{-5}, K_d = 3.145 \times 10^{-3}$

In order to evaluate the effectiveness of the depth controllers that were designed,

numerical simulations are used to apply three step signals with varying intended depths,

assuming that the AUV has already submerged in water to a depth of thirty meters. For

the first 250 s, the targeted depths are set to 25 m, 20 m, and 10 m, respectively, before

going back to 30 m. A 500-second simulation lasts for each. Fig. 3.2.5 shows the

response of depth control curves of the AUV system with PI and PID controllers. These

curves show that the PID controller is superior to the PI controller overall. The figure

illustrates how the PI controller's curves oscillate around the intended depths after
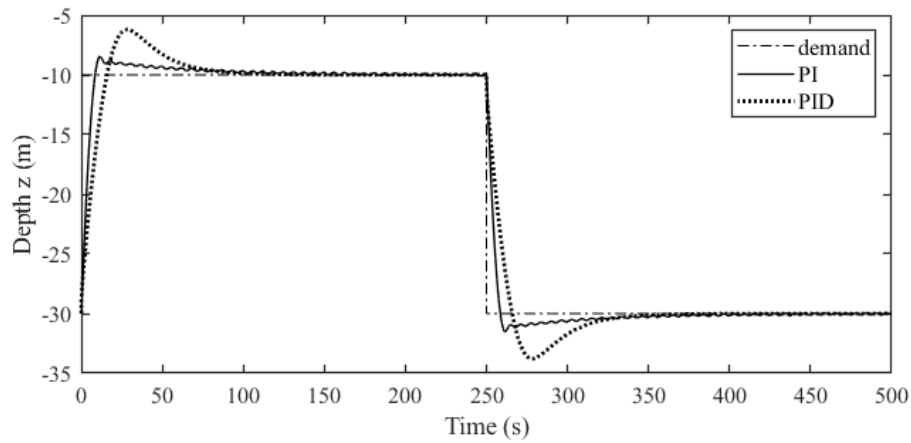
reaching them. This is because the PI controller is unable to stabilize the AUV system's

higher-order dynamics in this simulation.
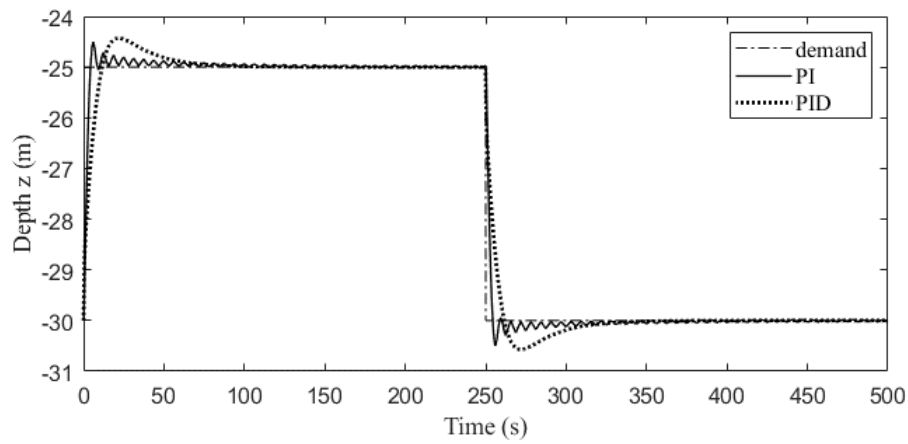

(a)
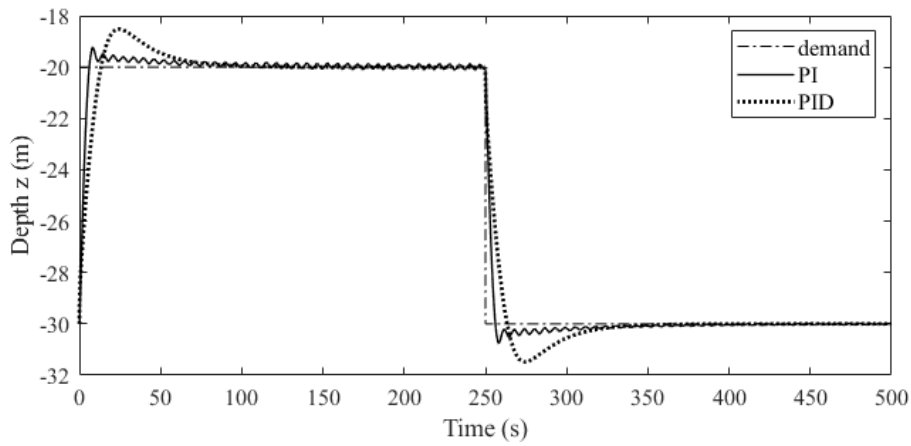
(b)

(c)

Fig. 3.2.5 Response curves for depth control with different controllers. (a) $z_d = -25$ m. (b) $z_d = -20$ m. (c) $z_d = -10$ m.

Moreover, PI controller's steady-state error increases with target distance. The

reason is it is simpler for the AUV to flow upward (towards buoyant force) as the depth

lowers. In contrast, the curves of the PID controller achieve the target depth without steady-state errors. The output of the PI and PID controllers, which correspond to the three target depths in Fig. 3.2.5, is displayed in Fig. 3.2.6.
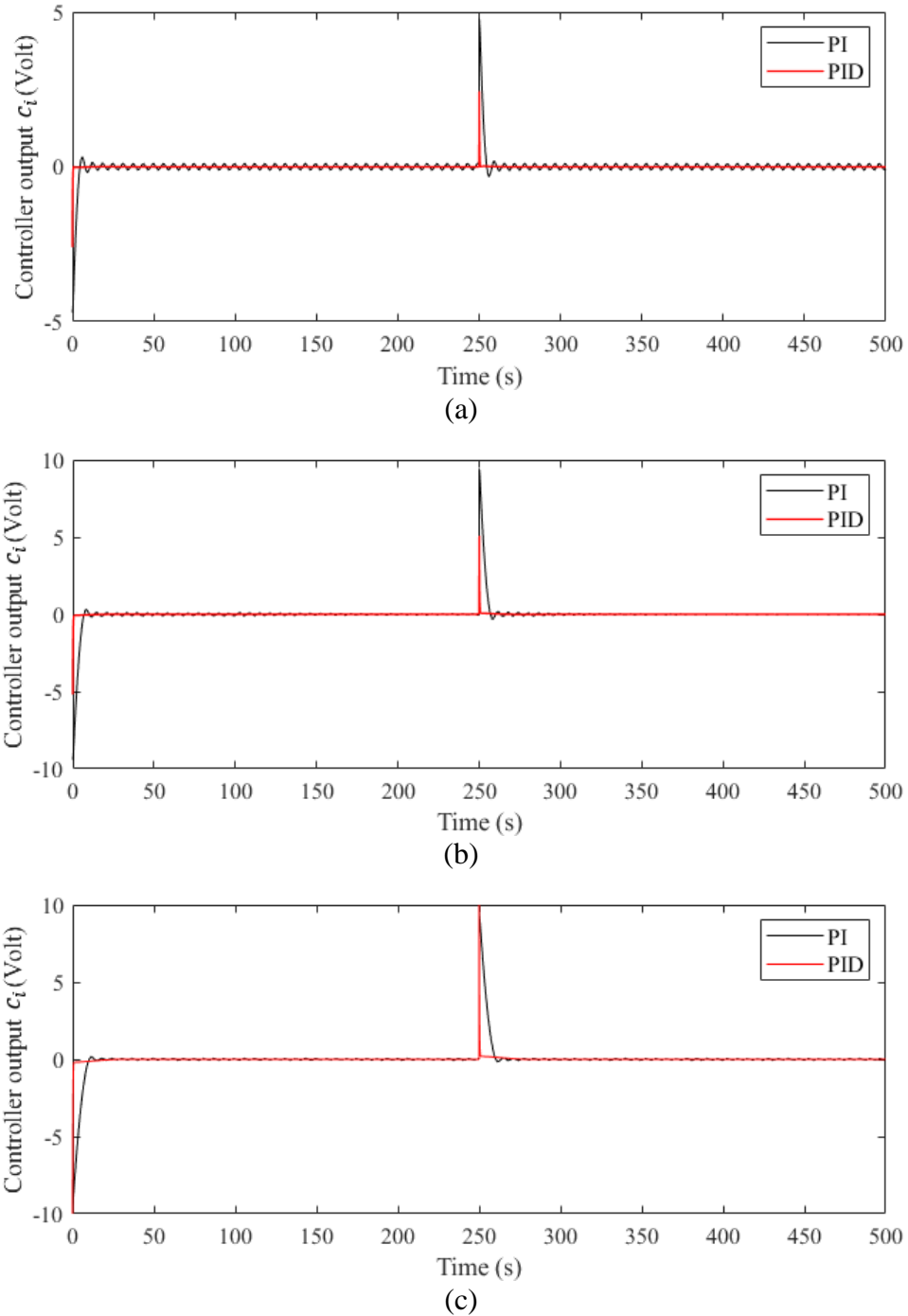
Fig. 3.2.6 Controller outputs for various target depths (a) $z_d = -25$ m. (b) $z_d = -20$ m. (c) $z_d = -10$ m.

The PID controller's enhanced performance in comparison to the PI controller is clearly attributed to its more assertive output. Table 3.2.4 illustrates the unique response characteristics of the simulation, providing additional points for comparison.

Table 3.2.4 Response parameters of controllers

Controller	Target Distance (m)	Rise Time (s)	5% Settling Time (s)	Steady-State Error (m)	Max. Overshoot (%)
	5	4	19	±0.6	2.5
PI	10	7	21	±1.4	7.8
	20	9	30	±0.78	7.78
	5	12	49	0	11.40
PID	10	14	54	0	14.92
	20	15	60	0	18.91

3.3 Propeller Performance Analysis

The propeller of an AUV holds paramount importance in determining the vehicle's overall performance and functionality. As a critical component of the propulsion system, the propeller directly influences the AUV's speed, maneuverability, and energy efficiency. The true performance of these designed propellers remains unknown until subjected to experimental testing. However, conducting such experiments is not only costly but also time-consuming (Hayati et al., 2013). Gratefully, the swift progress in CFD technology allows for the numerical simulation of such studies, offering a close real-time prediction of actual propeller performance. Given the maximum width and height of the AUV in this investigation, a four-bladed, right-hand, skewed B-series propeller with an outer diameter (D) of 0.16 m and an area ratio (A_E/A_O) set at 0.8 has been deemed appropriate. Additional details regarding the propeller's geometry are provided in Chapter 2, Table 2.3.1. Furthermore, a modified model of the propeller has been crafted using AutoCAD and SolidWorks software, visually depicted in Chapter 2 (Fig. 2.2.1 and Fig. 2.2.2).

Here, the numerical analysis of the flow around the AUV hull and propeller has been conducted using the ANSYS-Fluent software platform. The pressure-velocity coupling is implemented through a coupled scheme. Spatial discretization employs the Least Squares Cell-based scheme, complemented by a second-order upwind method for discretizing both the momentum and turbulent models. This choice of discretization methods is essential for accurately capturing the complex flow dynamics around the hull and propeller. Details regarding the domain parameter and boundary conditions have been provided in Table 3.3.1, Table 3.3.2, Fig. 3.3.1, and Fig. 3.3.2, outlining the prescribed specifications at the domain boundaries to simulate realistic environmental conditions and ensure the fidelity of the numerical simulations. These choices

collectively contribute to the accuracy and reliability of the CFD analysis in investigating the fluid behavior around the AUV hull and propeller.

Table 3.3.1 Boundary conditions for numerical analysis of AUV hull drag and propeller performance.

Boundary	AUV	Propeller
Inlet	Velocity inlet	Velocity inlet
Outlet	Pressure outlet	Outflow
Body Surface	No-slip boundary	No-slip boundary
Side walls	Free slip boundary	Free slip boundary

Table 3.3.2 Domain parameters for numerical analysis of AUV hull drag and open-water test

| Parameters	Settings
Type	Fluid
Material	Water
Reference Pressure	1 atm
Density of Fluid	998.2 kg/m^3
Viscosity of Fluid	0.001003 kg/m-s
Model of Turbulence	SST k-ω
Turbulent Wall Function	Scalable
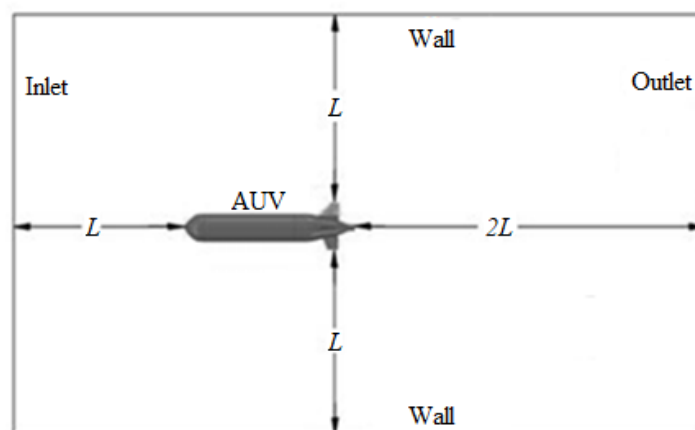
Fig. 3.3.1 Computational domain for hull drag estimation (Ghosh and Mandal, 2021)
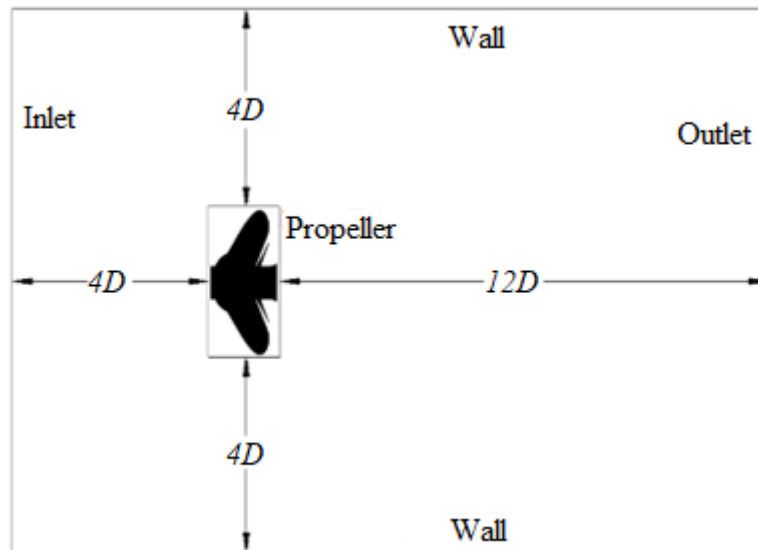
Fig. 3.3.2 Computational domain for open-water test of propeller
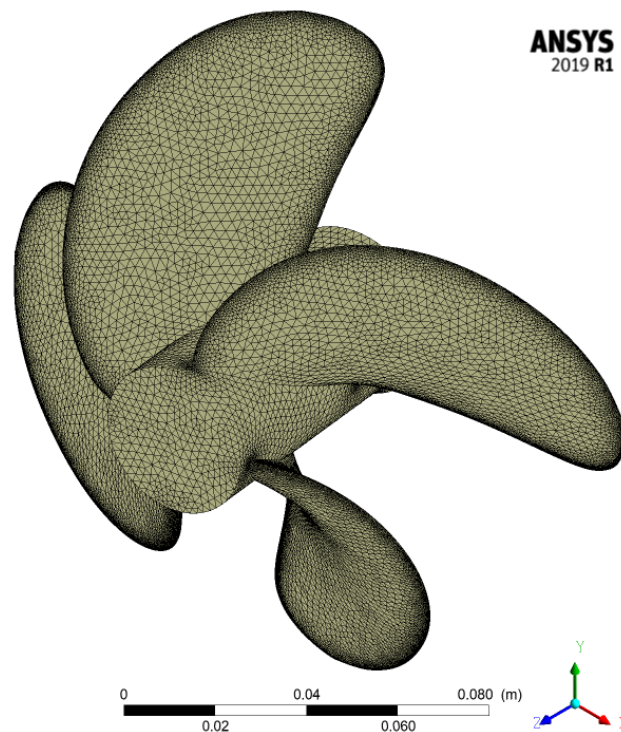(Ghosh and Mandal, 2021)

Given that the majority of research (Barnitsas et al.,1981; Martinez-Calle et al. 2002; Nakisa et al.,2010) have adopted unstructured grids for their CFD analysis models, the computational model in this study also employs unstructured grids, as illustrated in Fig. 3.3.3 and Fig. 3.3.4.
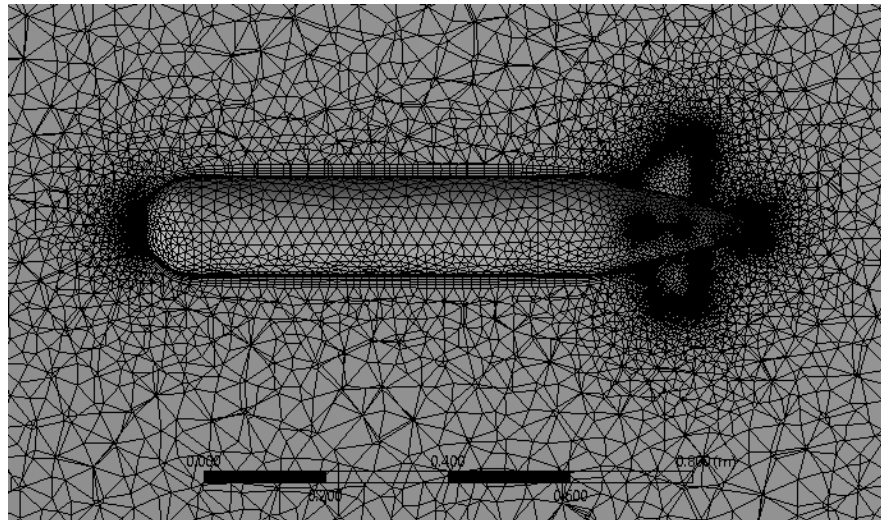
**Fig. 3.3.3** Unstructured mesh view of AUV hull
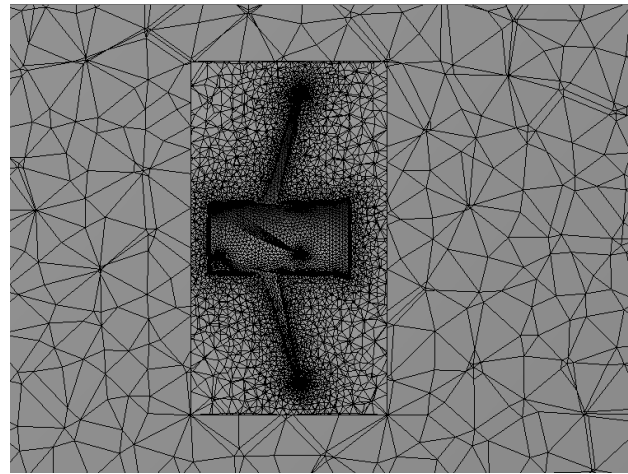
(a)

(b)

Fig. 3.3.4 Unstructured mesh of propeller (a) computational domain; (b) propeller

When performing numerical analyses through the Ansys-Fluent platform, assessing grid independence stands as a crucial phase. The computational time increases with a higher number of elements. The grid independence test aids in determining an appropriate number of elements for numerical analysis, ensuring accuracy in test results without unnecessary computational burden. In the assessment of hull drag for a fully

submerged 3-D AUV and the performance analysis of a 3-D propeller, different grid

sizes were employed to solve the fluid flow around the hull and propeller. To enhance

numerical accuracy, refinements were applied at various zones during mesh generation.

Figure 3.3.5 and Fig. 3.3.6 present the results of the grid independence study.
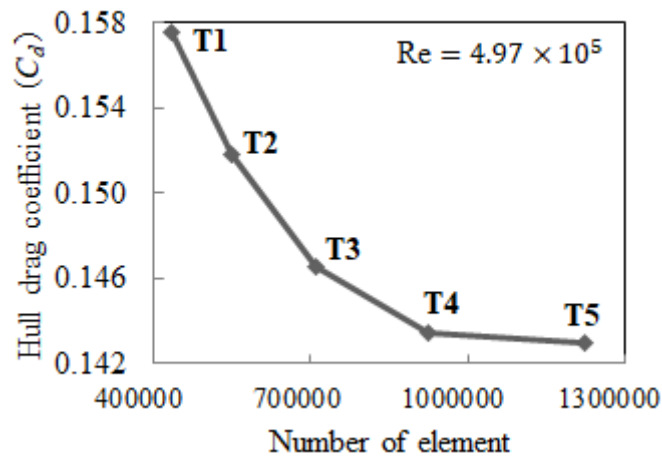
Fig. 3.3.5 Grid independence study of AUV hull drag (Ghosh et al., 2023)
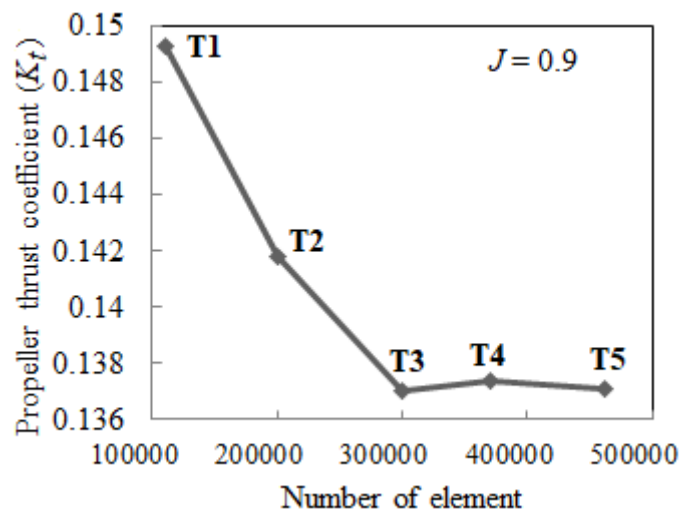
**Fig. 3.3.6** Grid independence study of propeller performance

It has been observed that for AUV hull analysis, test 4 provides the most suitable

conditions, ensuring accurate numerical simulations for hull drag analysis. Similarly,

for propeller performance analysis, test 3 emerged as the most suitable, as the

differences in drag coefficient (C_d) for the hull between test 4 and test 5 and thrust

coefficient (K_t) for the propeller between test 3 and test 4 or test 5 were found to be negligible. For investigation of propeller performance in open-water conditions and hull drag in submerged conditions, the thrust generated by propeller and hull resistance have been studied.

A numerical analysis of open-water performance has been conducted using ANSYS-Fluent on the designed propeller in the present study. Each test iteration has been repeated three times. A direct comparison has been conducted between the numerical results and the experimental findings obtained by Bernitsas et al. (1981) to validate the present numerical model. The validation process involves computing thrust coefficient (K_t), torque coefficient (K_q), and efficiency (η) which are then graphically represented in Fig. 3.3.7 to provide a comprehensive overview of the overall behavior of the AUV propeller model. Throughout the simulations, the propeller's rotational speed has been held constant at 850 rpm, while the flow velocity has been systematically adjusted to achieve an advance ratio (J) ranging from 0 to 0.875. The comparative results are visually depicted in Fig. 3.3.7.
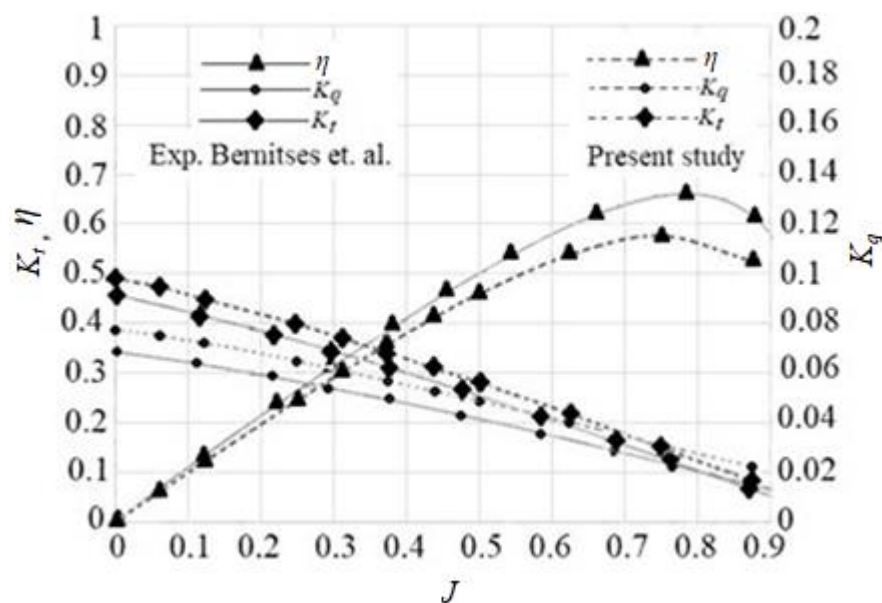

Fig. 3.3.7 Propeller performance: open-water test results (Ghosh and Mandal, 2021)

Upon comparing the present study with the experimental results of Bernitsas et al. (1981), a marginal disparity has been identified between the two sets of data. The maximum difference observed is 6.52% for thrust coefficients (K_t) and 7.5% for torque coefficients (K_q). Despite these slight variations, the overall consistency between the numerical and experimental results attests to the accuracy of the numerical simulations.

Six distinct cases have been systematically investigated and analyzed, yielding pressure distributions on the propeller blade. Figures 3.3.8a through Fig. 3.3.8f display the pressure distribution on the suction side and pressure side of the propeller across different advance ratios (J). These figures elucidate the trend of decreasing pressure on the blade face with a rise in advance ratio (J) while maintaining a constant propeller speed at 850 rpm. Particularly noteworthy is the highest-pressure value observed at the blade leading edge on the pressure side of the propeller, as it represents the initial point of contact with water.

(a)

(b)

(c)

(d)

(e)

(f)
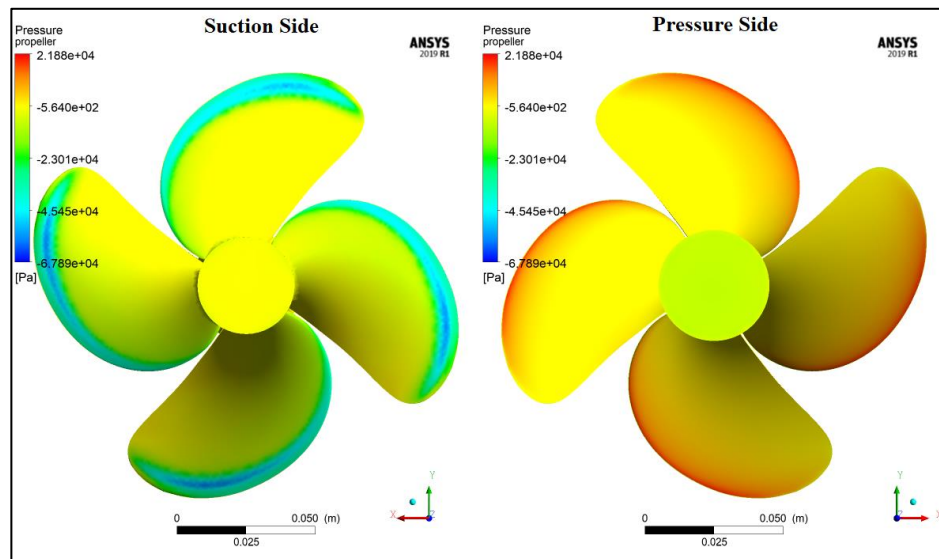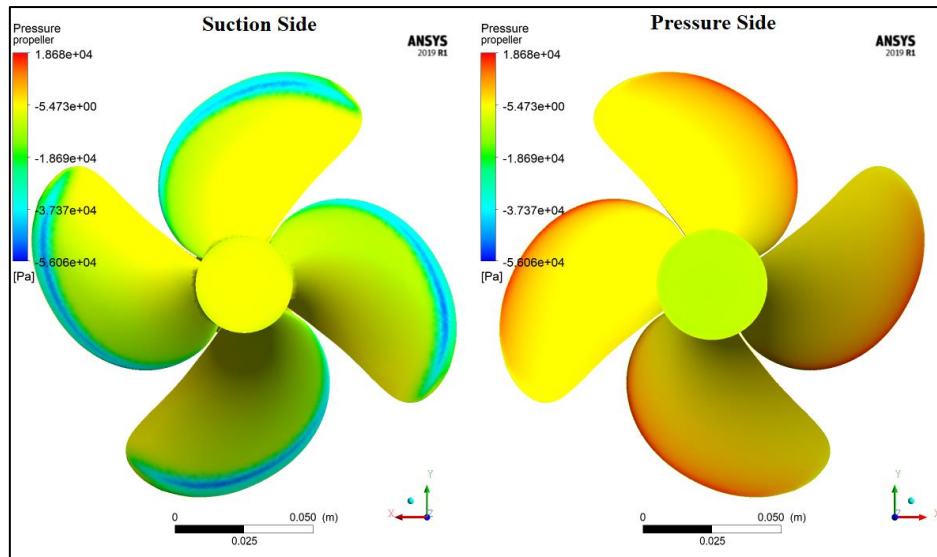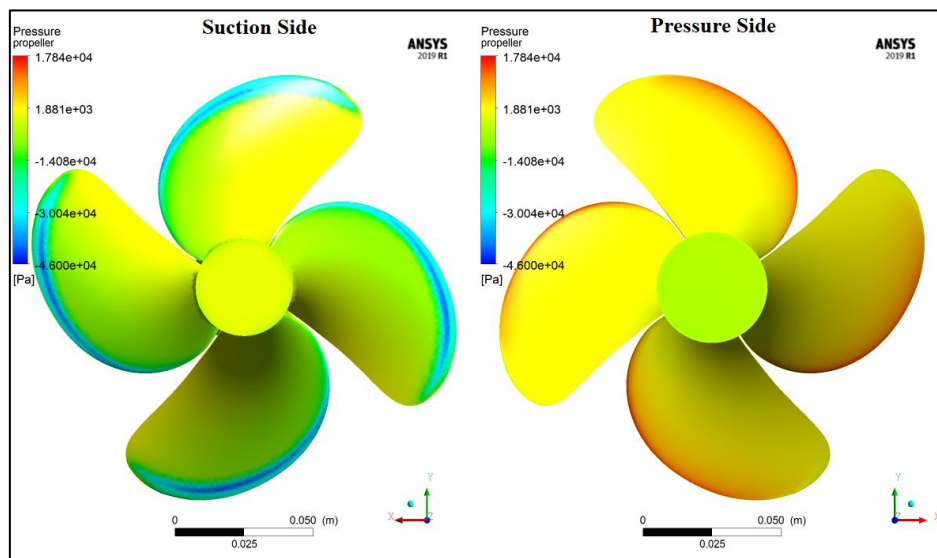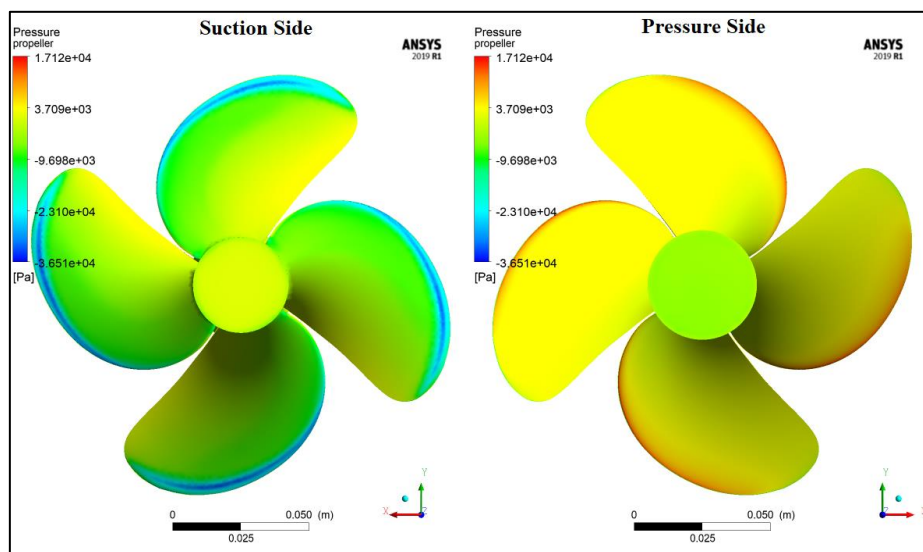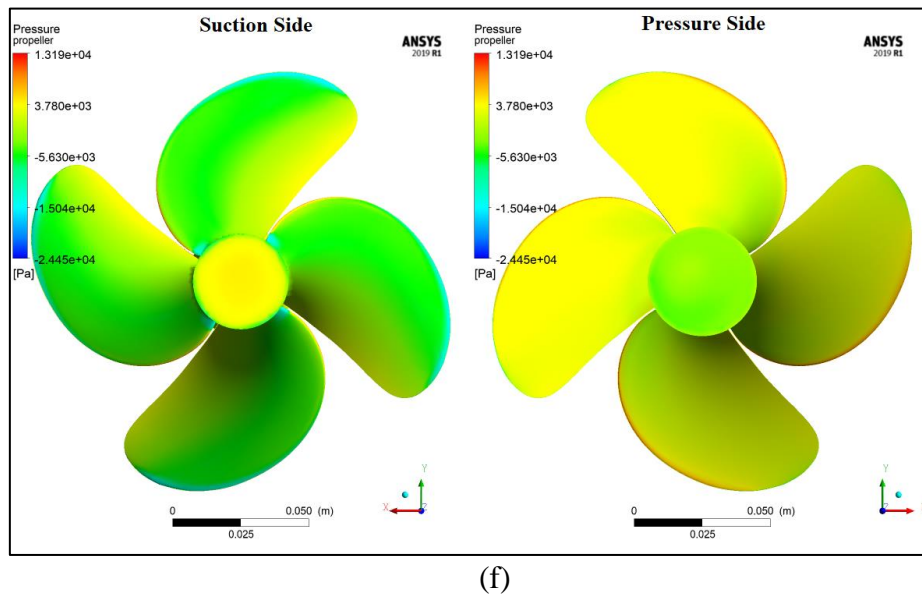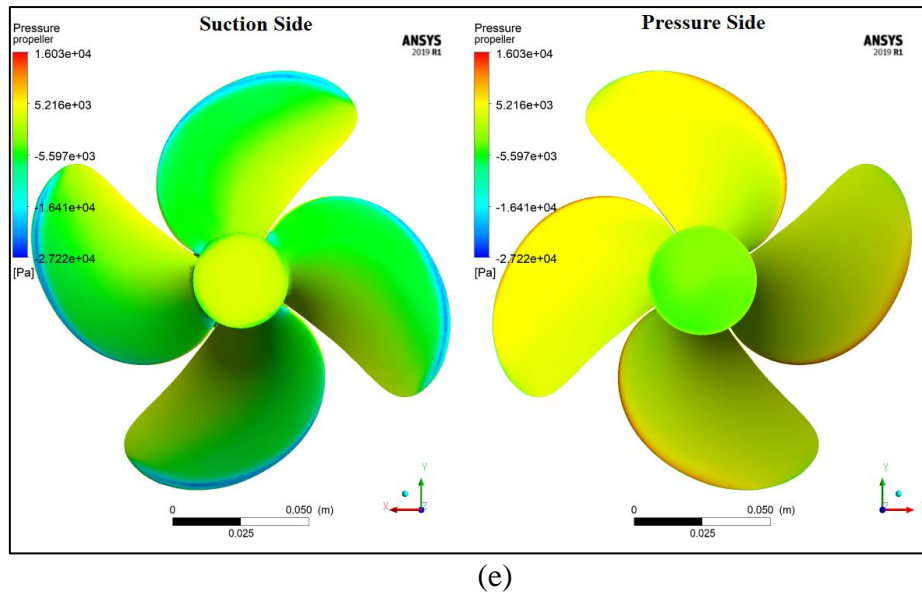
Fig. 3.3.8 Pressure distribution around propeller at various advance ratios (a) *J* = 0.125; (b) *J* = 0.25; (c) *J* = 0.375; (d) *J* = 0.5; (e) *J* = 0.625; (f) *J* = 0.75

The graphical representation depicting the distribution of the pressure coefficient (C_p) across a propeller is presented in Fig. 3.3.9. This visualization provides insights into how the pressure varies along different sections of the propeller, typically from the suction side to the pressure side.

Numerical analysis of AUV's hull drag has also been performed using the ANSYS-Fluent software platform. This involves utilizing numerical methods to simulate and

analyze the fluid flow around the AUV hull. The AUV hull has been subjected to multiple test iterations, and each test has been repeated three times to ensure the reliability and accuracy of the numerical simulations. This approach allows for a comprehensive examination of the hydrodynamic forces acting on the AUV hull.
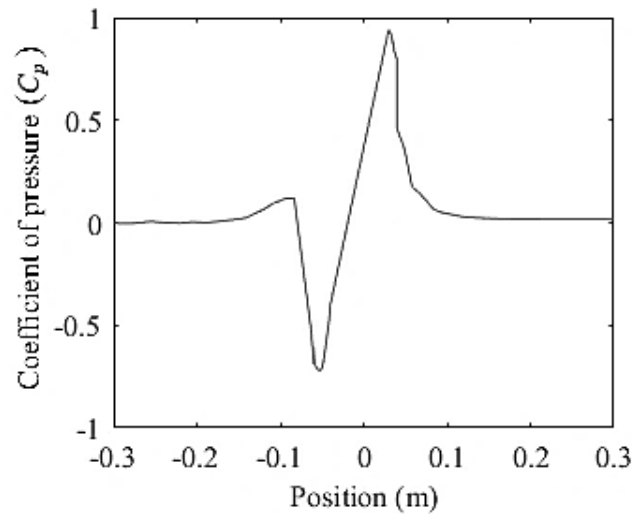
Fig. 3.3.9 Variation of pressure coefficient (C_p) across propeller at $J = 0.5$ (Ghosh and Mandal, 2021)

In this context, the flow velocity has been systematically modulated to attain a range of advance ratios (J) from 0 to 1. The resulting variation of drag force with advance ratio (J) has been graphically represented in Fig. 3.3.10, illustrating the relationship between these parameters across the specified range.
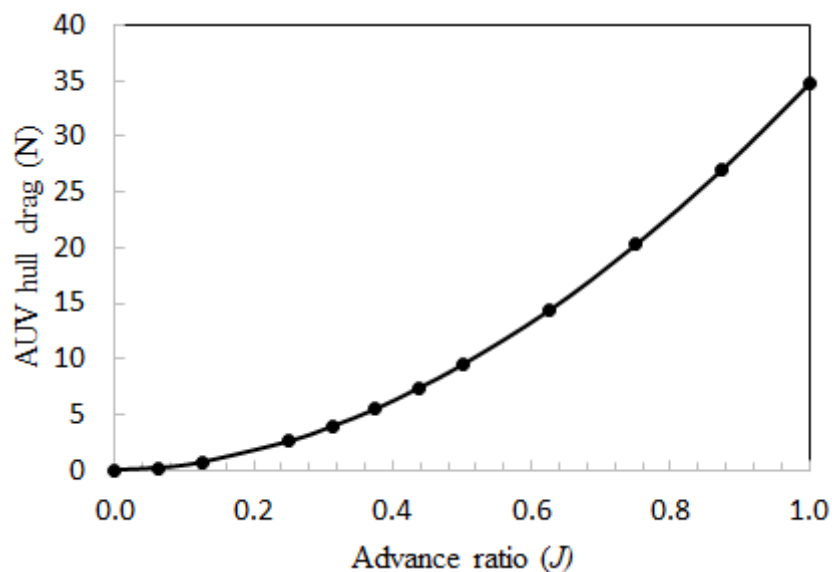
Fig. 3.3.10 Variation of AUV hull drag force with advance ratio (J)

Observing Fig. 3.3.10, it is evident that as the advance ratio increases, there is a corresponding increase in drag force. This visual insight helps in understanding how changes in the advance ratio impact the drag force acting on the AUV under consideration. Figure 3.3.11 displays the relationship between the computational hull drag coefficient (C_d) and the Reynolds number (Re) during forward motion.
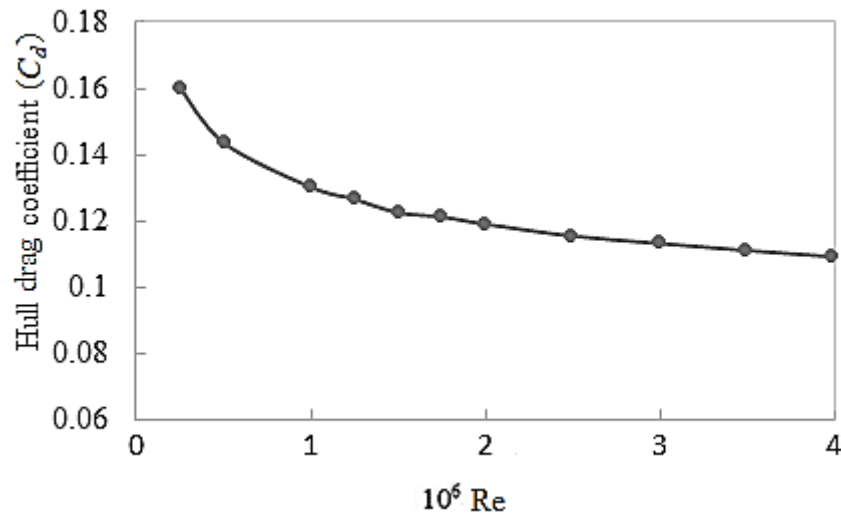
Fig. 3.3.11 Variation of AUV hull drag coefficient (C_d) with Reynolds number (Re) during forward motion

The variation of the pressure coefficient (C_p) along line 'A' (as depicted in Fig. 3.3.12) is visually presented in Fig. 3.3.13. This graph illustrates that the pressure loss increases along line 'A', and the coefficient of pressure (C_p) remains relatively constant with changes in the advance ratio (J). Additionally, Fig. 3.3.13 highlights the impact of the fixed fin and rudder located at the tail side of the AUV, showcasing abrupt changes in pressure that consequently affect the pressure distribution. The analysis of the AUV hull indicates that with an increase in the AUV speed, there is a concurrent rise in the drag experienced by the hull.
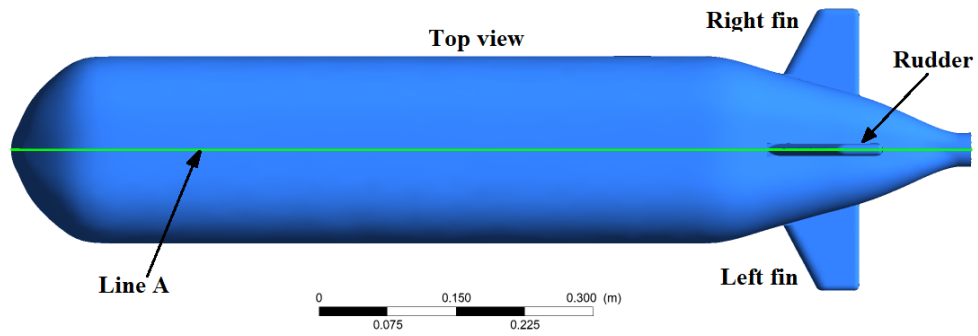
Fig. 3.3.12 Projected line on AUV hull for calculation of C_p
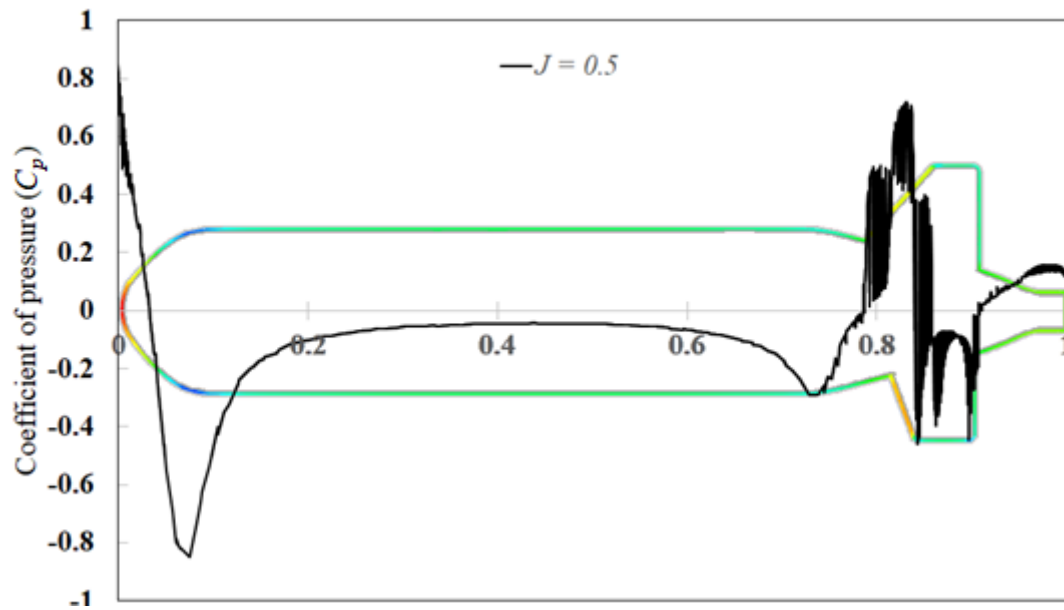
Fig. 3.3.13 Variation of coefficient of pressure (C_p) around AUV hull

According to the data presented in Fig. 3.3.14, it is observed that around the advance ratio (J) of 0.9, the hull drag of the AUV exceeds the thrust generated by the propeller when the propeller is operating at its maximum speed of 850 rpm. This observation implies that the AUV reaches its maximum limiting speed (2.5 m/s) when the advance ratio (J) is approximately 0.9, aligning well with the specified requirements for this particular AUV model.
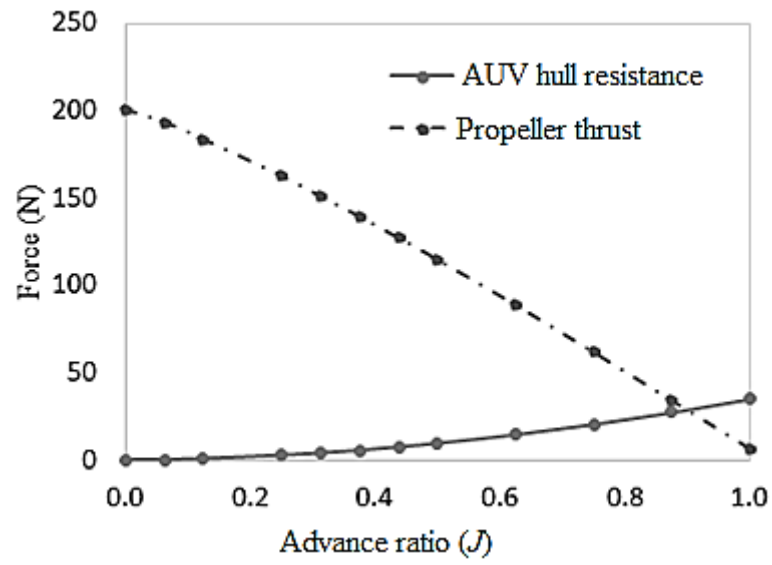
Fig. 3.3.14 AUV hull resistance and propeller thrust (Ghosh and Mandal, 2021)

3.4 Yaw Motion Dynamics and Control

The significance of yaw motion in AUVs is crucial for their efficient functionality and adaptability within underwater environments. Yaw motion empowers these vehicles to dynamically alter their orientation and heading, providing essential directional control for navigating intricate terrains and circumventing obstacles. The precise control of this yaw motion is played by the rudder.

The analysis of the rudder's performance involves systematically tilting it at various angles of attack (θ) ranging from 0^0 to 17^0, while simultaneously varying the forward velocity (v) of the AUV. The analysis has been carried out in the ANSYS-Fluent software platform in a 3-D environment. This analysis employs the same computational domain and boundary conditions as detailed in section 3.3, with the exception of the boundary condition at the rudder angle (θ). Figures 3.4.1 to 3.4.6 showcase the pressure variations across the AUV model for different combinations of θ and v. The velocities utilized in this study are associated with the advance ratio (J), as indicated in Table 3.4.1 below.

Table 3.4.1 Inlet velocities corresponding to advance ratio

J	0.00	0.06	0.13	0.25	0.31	0.38	0.44	0.50	0.63	0.75	0.88
v (m/s)	0.00	0.14	0.29	0.57	0.70	0.86	1.00	1.13	1.43	1.70	1.99

Taking Fig. 3.4.1a as an example, it illustrates the pressure distribution over the entire AUV model for $\theta = 5^0$ and $v = 1.0$ m/s. In Fig. 3.4.1b, the specific focus is on illustrating the discrepancy in pressure distribution between the two sides of the rudder. The observed pressure difference on each side of the rudder gives rise to a side force (F_r), quantified at 0.538 N, and a corresponding yawing moment (M_{yaw}) of 0.234 N-m.

(a)

(b)
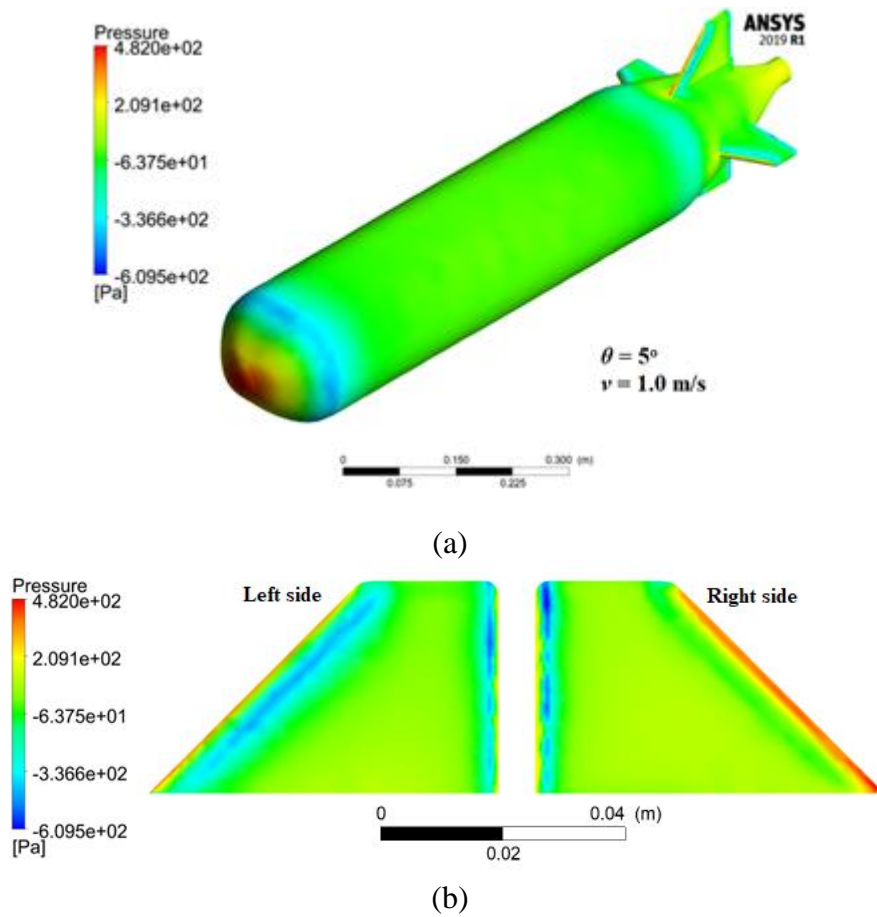
Fig. 3.4.1 Pressure distribution for $\theta = 5^0$ and $v = 1.0$ m/s. (a) AUV hull, (b) rudder (Ghosh et al., 2023)

Similarly, Fig. 3.4.2 illustrates pressure distributions for $\theta = 5^0$ and $v = 2.5$ m/s. Here, the legend reveals increased overall pressure values with an elevated forward velocity. This increase correlates with a higher F_r and M_{yaw}, measured at 3.505 N and 1.526 N-m, respectively.

(a)

(b)
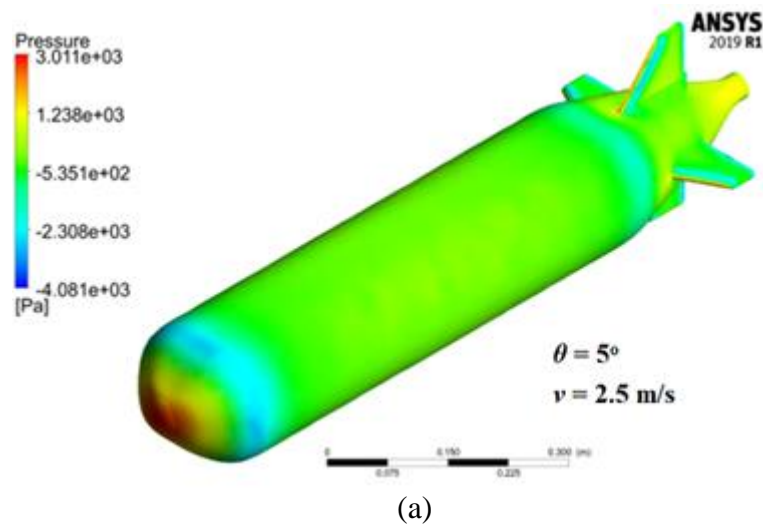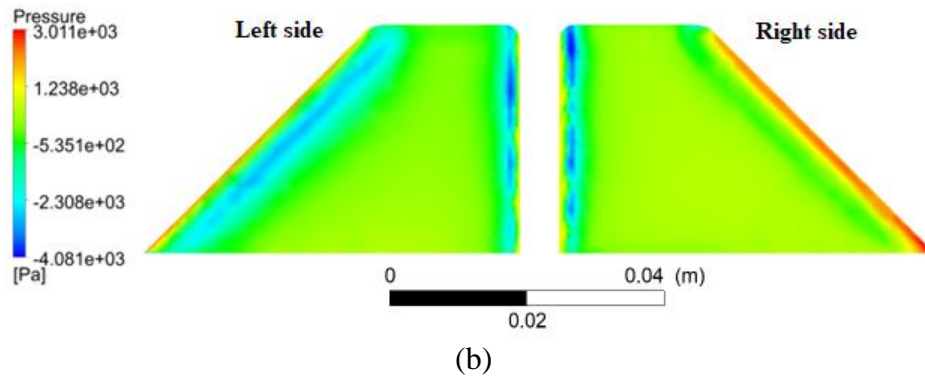
Fig. 3.4.2 Pressure distribution for $\theta = 5^0$ and $v = 2.5$ m/s. (a) AUV hull, (b) rudder (Ghosh et al., 2023)

Figures 3.4.3 and Fig. 3.4.4 extend the analysis to $\theta = 10^0$, with velocity (v) maintained at 1.0 m/s and 2.5 m/s. The resulting F_r values are 0.853 N and 5.419 N, accompanied by M_{yaw} values of 0.371 N-m and 2.36 N-m, respectively. It is evident from the figures that with the increase in the value of θ from 5^0 to 10^0, the side force and the corresponding yawing moment also increase.

(a)

(b)
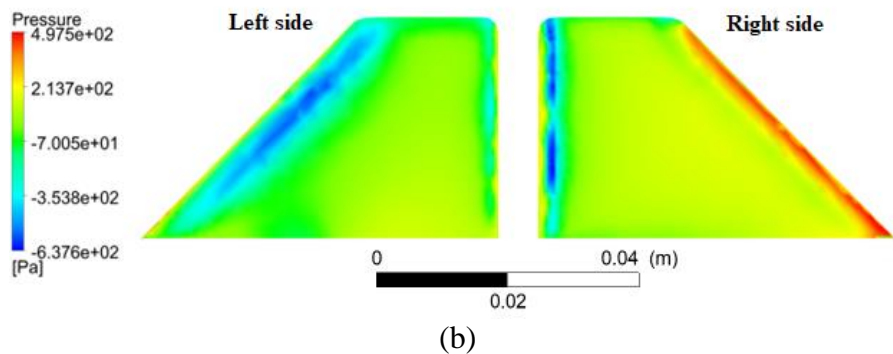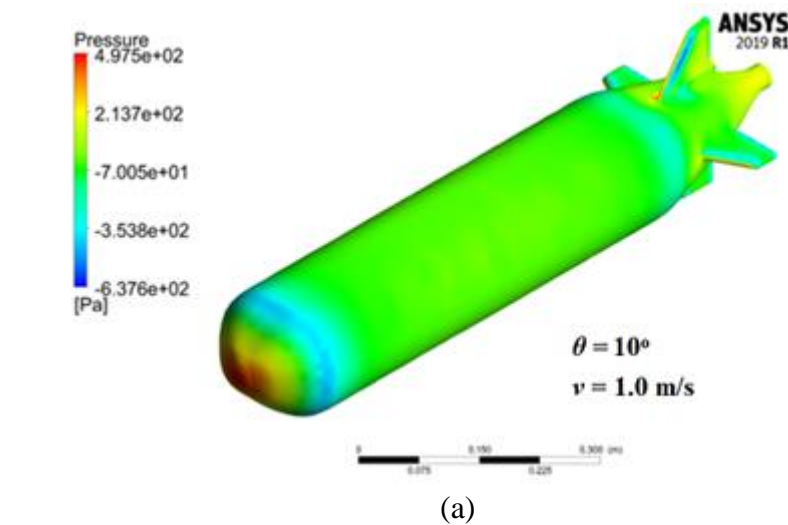
Fig. 3.4.3 Pressure distribution for $\theta = 10^0$ and $v = 1$ m/s (a) AUV hull, (b) rudder (Ghosh et al., 2023)

(a)

(b)
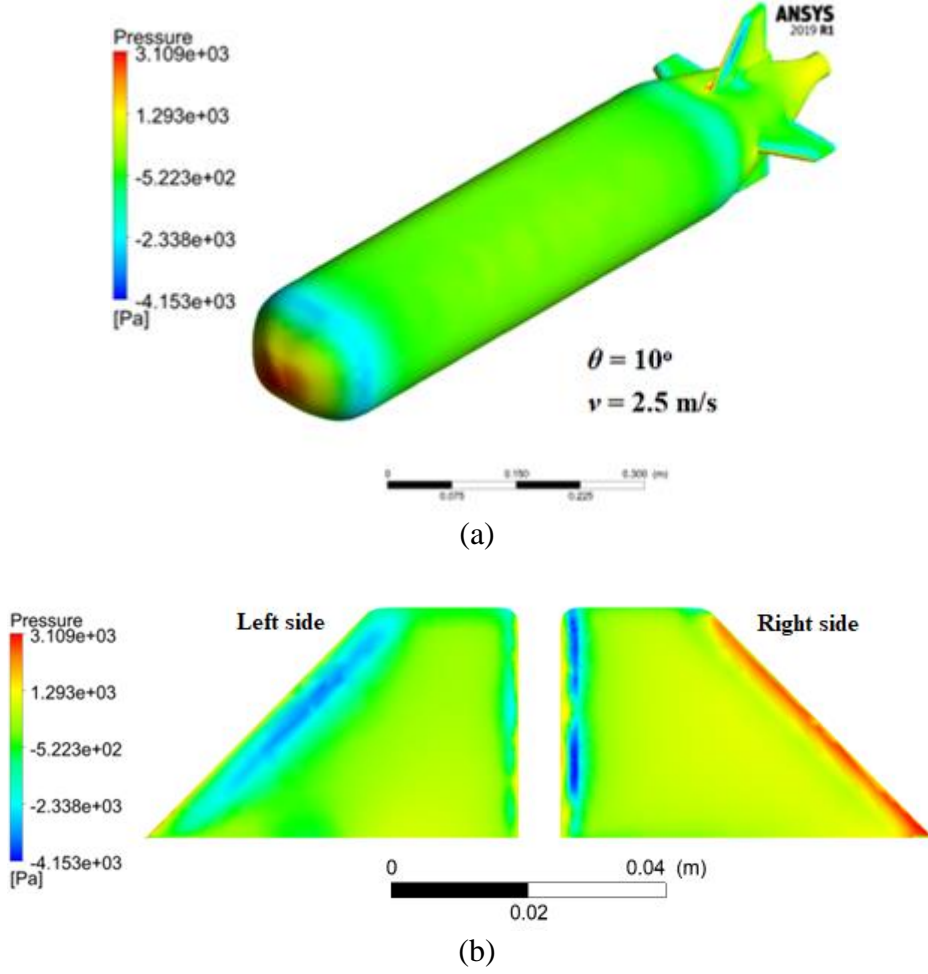
Fig. 3.4.4 Pressure distribution for $\theta = 10^0$ and $v = 2.5$ m/s (a) AUV hull, (b) rudder (Ghosh et al., 2023)

The analysis extends to a diverse range of θ and v combinations, and the resulting available yawing moments (M_{yaw}) are systematically plotted against θ for different values of v in Fig. 3.4.5. The plotted curves reveal a discernible trend: M_{yaw} increases with the tilt angle θ up to a certain point, beyond which it begins to decline. This critical angle signifies the stalling angle of the rudder, where the Lift-like side force F_r starts to diminish, consequently leading to a reduction in M_{yaw}.

The influence of forward velocity (v) on M_{yaw} is evident in the curves, showcasing those higher velocities result in increased Lift-like side force F_r and, consequently, heightened M_{yaw} values. Furthermore, the stalling angle exhibits a decreasing trend with higher forward velocities. For instance, at a forward velocity of 2.0 m/s, stalling

occurs around a tilt angle of approximately 15^0, while at a higher velocity of 3.5 m/s, it

decreases to around 13^0. Consequently, it is inferred that the operational range for the

tilt angle of the rudder should be maintained at less than approximately 11^0 to prevent

stalling.
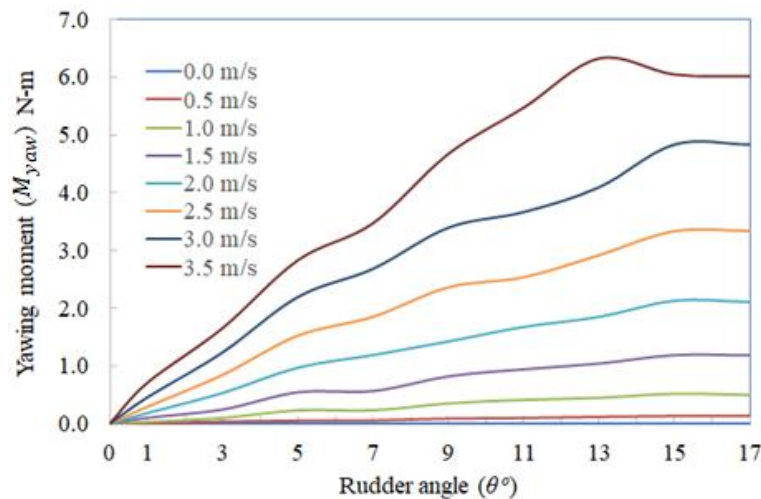
Fig. 3.4.5 Variation of yawing moment with rudder angle and forward velocity
(Ghosh et al., 2023)

Upon the generation of the yawing moment (M_{yaw}), the AUV undergoes yaw

motion around the vertical axis (z-axis in Fig. 3.4.6). This yaw motion induces

hydrodynamic drag forces on the AUV hull surface, accompanied by a resisting

moment (M_d) acting in opposition to the yaw motion. Here, the yaw angle is denoted

by the symbol 'ψ'.
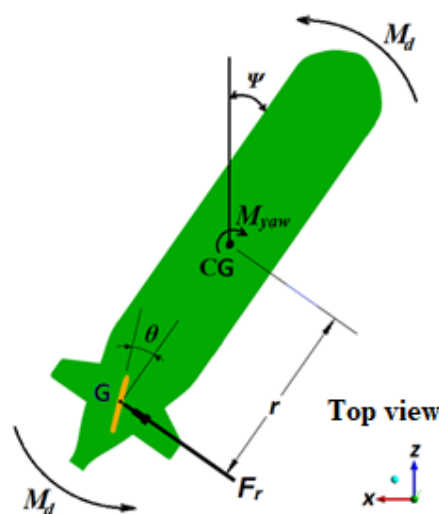
Fig. 3.4.6 Generation of resisting moment (M_d) by hydrodynamics drag

Since the resisting moment (M_d) is contingent upon the angular velocity ($\dot{\psi}$) of the AUV around the vertical axis, understanding the relationship between the resisting moment and angular velocity is crucial for precise yaw motion control. To establish this relationship, a CFD analysis is conducted, wherein the resisting moment (M_d) is calculated by providing various angular velocities ($\dot{\psi}$) (ranging from 0 to 1 rad/s) as input to the AUV. Figure 3.4.7 illustrates the pressure distribution on the AUV hull at different angular velocities ($\dot{\psi}$).

(a)

(b)

(c)
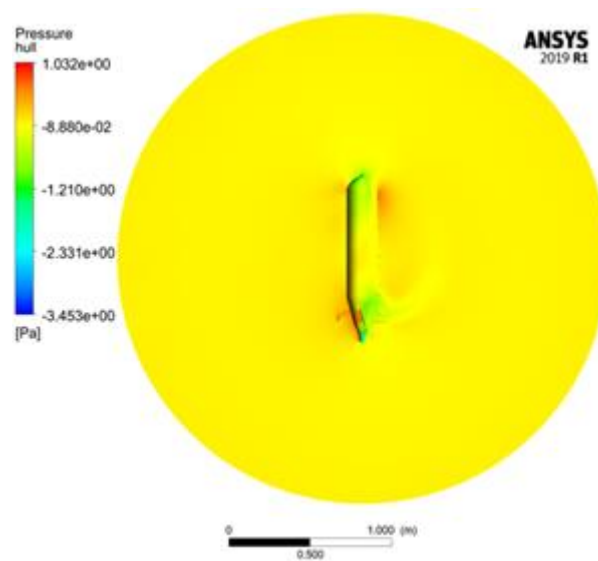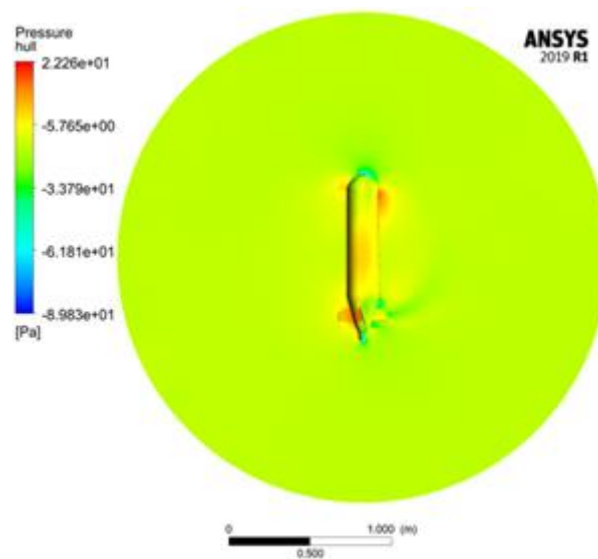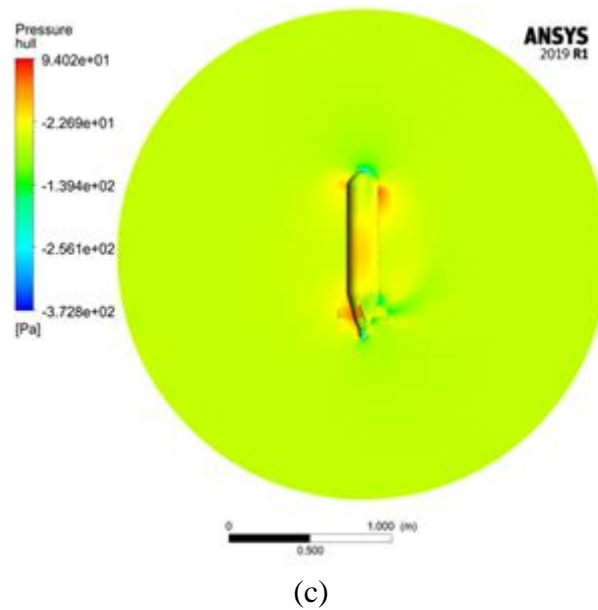
Fig. 3.4.7 Pressure distribution on AUV hull in turning (a) $\dot{\psi} = 0.1$ rad/s, (b) $\dot{\psi} = 0.5$ rad/s, (c) $\dot{\psi} = 1.0$ rad/s

   The observations from Fig. 3.4.7 reveal that as the angular velocity increases, there is a corresponding rise in pressure on the AUV hull, attributed to increased hydrodynamic drag. This augmentation in pressure results in an increase in the resisting moment (M_d). The graphical representation of the relationship between the resisting moment and the angular velocity of the AUV is depicted in Fig. 3.4.8. This graphical representation serves to elucidate the direct correlation between angular velocity and the resisting moment, providing a visual understanding of the hydrodynamic forces influencing the AUV's yaw motion.
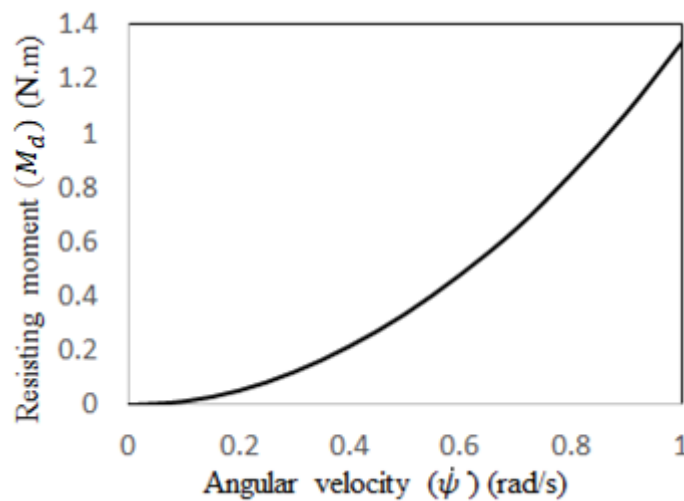
Fig. 3.4.8 Variation of resisting moment (M_d) with angular velocity ($\dot{\psi}$)

Having established the relationships between yawing moment (M_{yaw}) and rudder angle (θ), as well as the resisting moment (M_d) and angular velocity ($\dot{\psi}$) through CFD analysis, the governing equation (Eq. 2.4.6) has been solved for controlling the yaw motion of the AUV. A system model has been developed in MATLAB-Simulink using Eq. 2.4.6, and a corresponding transfer function has been created for the feedback control system. The Proportional-Integral (PI) and Proportional-Integral-Derivative (PID) controllers have been implemented, with the proportional gain denoted as K_p and the integral gain as K_i. These controller values have been fine-tuned to ensure that the output closely follows the demand waveform. Different demand input types in yaw motion control have been accommodated based on the specific needs (viz stability, control, energy efficiency, etc.) of the AUV mission. The results, obtained under various input conditions, have been discussed below.

A. *Constant demand*

An input with a constant demand of magnitude 1 rad has been introduced to test the performance of PI and PID controllers. The PI-Controller, with a gain K_p set at 2.606 and $K_i = 0.286$, has been optimized to closely emulate the input with minimal oscillations, leading the steady-state error towards zero. Simultaneously, the PID-Controller, having gains of $K_p = 18.034, K_i = 7.984$ and $K_d = 8.483$ has been adjusted using various step signals. Results are depicted in Fig. 3.4.9, from a 30-second simulation. The results reveal that the PI-Controller maintains an error percentage of around 19%. Post-initial rise, tapering to around 2% in the 20 sec. The PID-Controller, despite a prominent initial peak, showed a faster decline in oscillations, achieving an error of less than 1% within 5 sec and nearing 0% within 10 sec of the simulation.
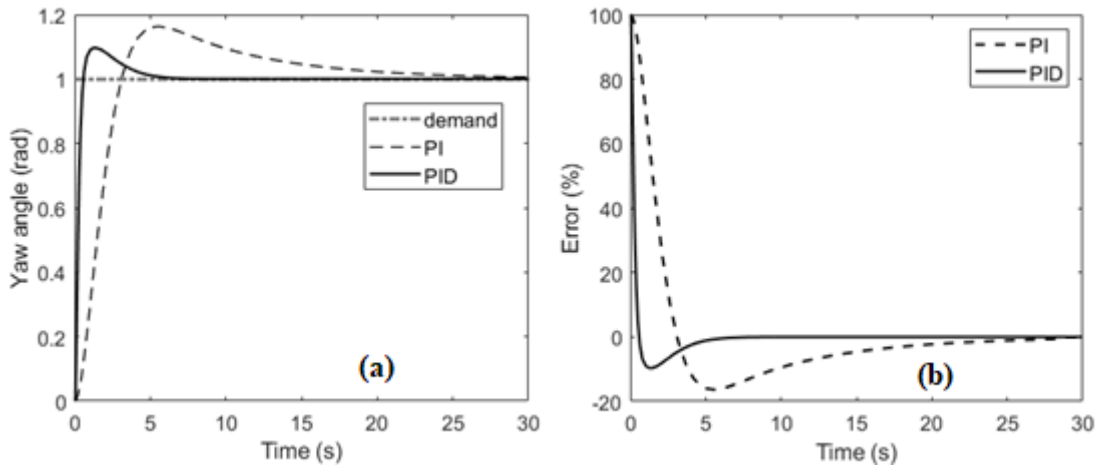
Fig. 3.4.9 Constant demand (a) PI and PID responses, (b) error comparison

B. *Square demand*

In a 50-second test, depicted in Fig. 3.4.10a, a square demand with a frequency of 0.25 Hz has been presented to test the performance of PI and PID controllers. the PI-Controller has been finely tuned with a gain, $K_p = 3.548$ and $K_i = 0.045$, achieving a response that closely mirrors the input with little oscillations. For the PID-Controller, based on the same demand, the optimal gain values have been tuned as $K_p = 18.034, K_i = 7.984$ and $K_d = 8.483$. Figure 3.4.10b shows that the PI-Controller maintains an error of around ±30% and reduces to 5% in 8s at each cycle. On the other hand, the PID-Controller shows a faster decline in oscillation with a reduced overshoot and achieving an error of less than 1% within 8 sec at each cycle.
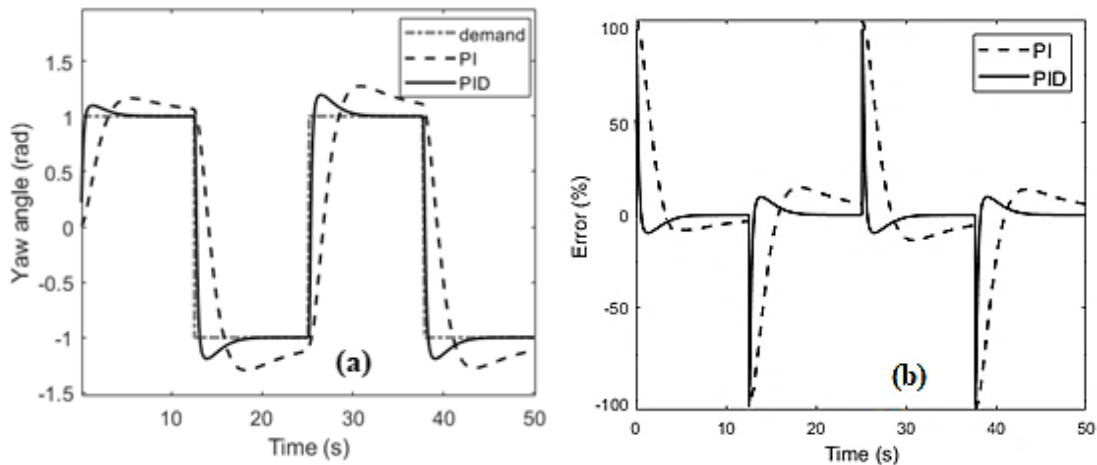
Fig. 3.4.10 Square demand (a) PI and PID responses, (b) error comparison

C. *Trapezoidal demand*

The performances of PI and PID Controllers are presented under a trapezoidal demand frequency of 0.05Hz, shown in Fig. 3.4.11. An amplitude of 1 rad has been considered as demand. The gain settings are $K_p = 2.609$, $K_i = 0.2867$ for the PI-Controller and $K_p = 18.034$, $K_i = 7.984$ and $K_d = 8.483$ for PID-Controller. The error margin for the PI system extends to $\pm80\%$, whereas the PID system restricts it to $\pm10\%$.
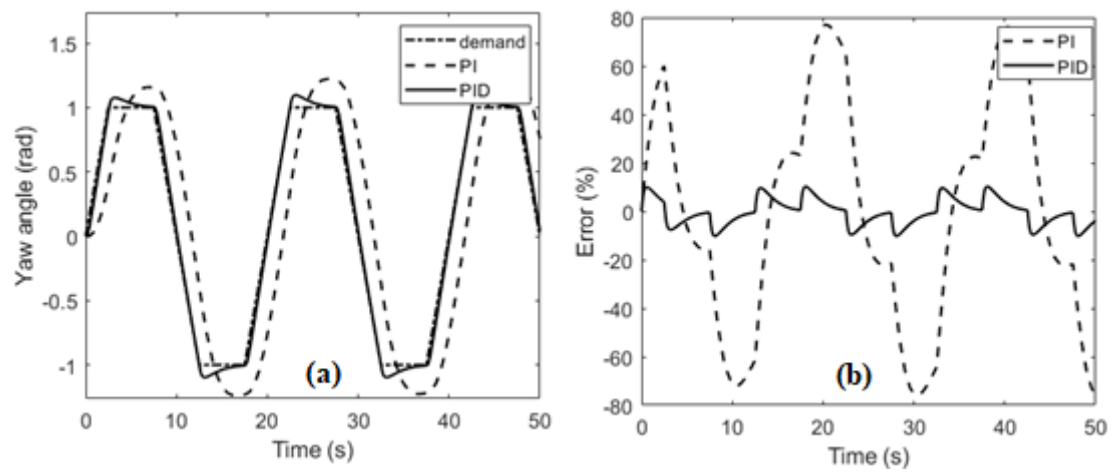
Fig. 3.4.11 Trapezoidal demand (a) PI and PID responses, (b) error comparison

Among the three input demands, the trapezoidal demand is the most practical choice since the rudder cannot be abruptly shifted from 1 to -1, but rather requires a gradual adjustment. The results from Fig. 3.4.11 indicate that, for the trapezoidal demand, the PID controller outperforms the PI controller, maintaining an error percentage at one-fourth of the PI controller's error.

3.5 Trajectory Tracking of AUV

The AUV's path-tracking performance has been studied by examining its convergence to four distinct 2-D trajectories: linear, linear with sharp turns, curved, and circular trajectories. Four different water environment conditions have been taken into consideration for each of the four trajectories in order to comprehensively evaluate the AUV performance. The first readings for all the cases have been taken for absolutely static water environment. Subsequent readings have then been obtained under dynamic water conditions, reflecting scenarios with varying water flow dynamics. The fluctuations in water flow across these conditions have been shown in Fig. 3.5.1a-c. In this context, perturbations along the positive *x*-axis and positive *y*-axis have been referred to as the "longitudinal current" and "lateral current" respectively. Here positive *x*-direction is taken eastward, and positive *y*-direction is taken northward. Figure 3.5.1a illustrates water current solely along the longitudinal direction, with a sinusoidal velocity variation in the *x*-direction being described by

$$U_{cx} = 0.5 + 0.4\sin(2\pi f t) \tag{3.5.1}$$

Conversely, Figure 3.5.1b depicts water current solely along the lateral direction, with a velocity variation in the *y*-direction represented by

$$U_{cy} = 0.5 + 0.2\sin(2\pi f t) \tag{3.5.2}$$

Here, the frequency (f) of 0.2 Hz has been taken for generation of perturbations in each direction.

Lastly, Fig. 3.5.1c showcases a blend of water current perturbations along both the longitudinal and lateral directions and the velocities in the *x* and *y*-directions are given by Eq. (3.5.1) and Eq. (3.5.2) respectively.
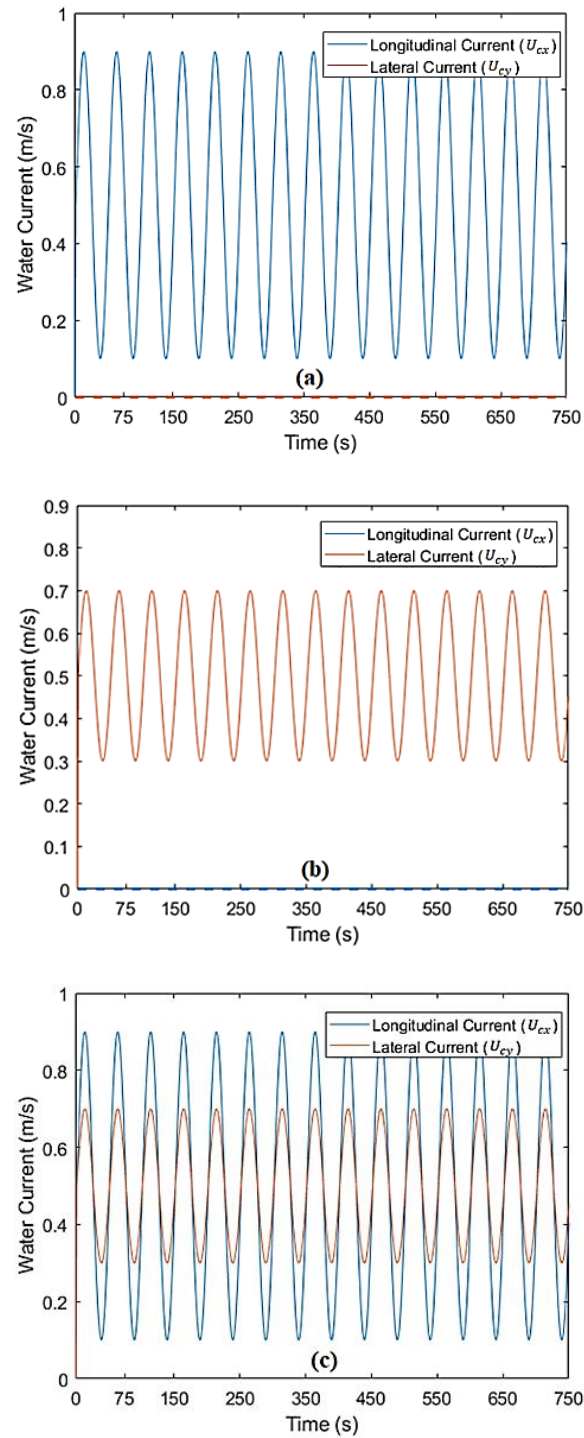
Fig. 3.5.1 Water flow conditions having water current along (a) longitudinal direction, (b) lateral direction, (c) both longitudinal and lateral direction

In order to quantitatively assess the accuracy of the trajectory tracking, local error at a particular point of the demand trajectory is taken to be the perpendicular distance between the demand trajectory and the AUV's actual position. A co-ordinate *'s'* is defined along the trajectory with the starting point being designated as the initial point

$(s = 0)$ and the total trajectory path length is denoted as 'S_T'. Local errors have been taken at various points having different 's' co-ordinate values. Summation of all such errors over the entire trajectory path should give the overall error throughout the entire trajectory. However, as the errors can be both positive and negative, a direct summation would give incorrect value of such overall error. In order to overcome this problem, Root Mean Square (RMS) value of all such local errors is required to be taken. This Root Mean Square Error (RMSE) value would provide a correct quantitative assessment of the error in trajectory tracking. Calculation of such RMSE value would obviously require a large number of local error values for which the demand trajectory has been divided into very small segments, each measuring $\delta s = 0.001$ mm in length. Local error values have been taken at mid-points of each of such segments and RMSE value is calculated accordingly. The segments are small enough so that their lengths can be considered to be negligibly small. It has been checked that reduction of the segmental length below 0.001 mm does not notably affect the RMSE value. Hence, a segmental length of 0.001 mm is adopted for this study. RMSE values have been obtained for each and every combination of demand trajectory and water environment. Further the RMSE values have been normalized with respect to corresponding total demand trajectory lengths in order to get dimensionless RMSE coefficient (ε_{cr}) values for all the cases. The RMSE co-efficient values serve as valuable indicators of error across the entire trajectory for different water environment scenarios.

A. *Linear trajectory*

Simulations have been conducted to demonstrate the efficiency of the controller when the AUV adhered to a straight demand trajectory given by

$$y = x \tag{3.5.3}$$

The demand trajectory initiates at the coordinate (0,0), then following the relation given in Eq. (3.5.3) it ends at (50,50). Thus, it spans a total length (S_T) of 70.71 m. In the simulation, the AUV is positioned at point (0, –5) with its heading directed northward. Figure 3.5.2 illustrates both the obtained and demand trajectory curves of the AUV for various conditions of water environment and it is evident that the tracking performance of the AUV is satisfactory. Tracking errors at different points along the trajectory length has been shown in Fig. 3.5.3 for various water conditions. The positions of these points have been denoted in dimensionless form normalizing with respect to S_T and has been denoted as s/S_T. In Fig. 3.5.3 the tracking errors for various point have been plotted against s/S_T. The RMSE coefficient (ε_{cr}) values have been calculated accordingly for each water condition cases and listed in Table 3.5.2.
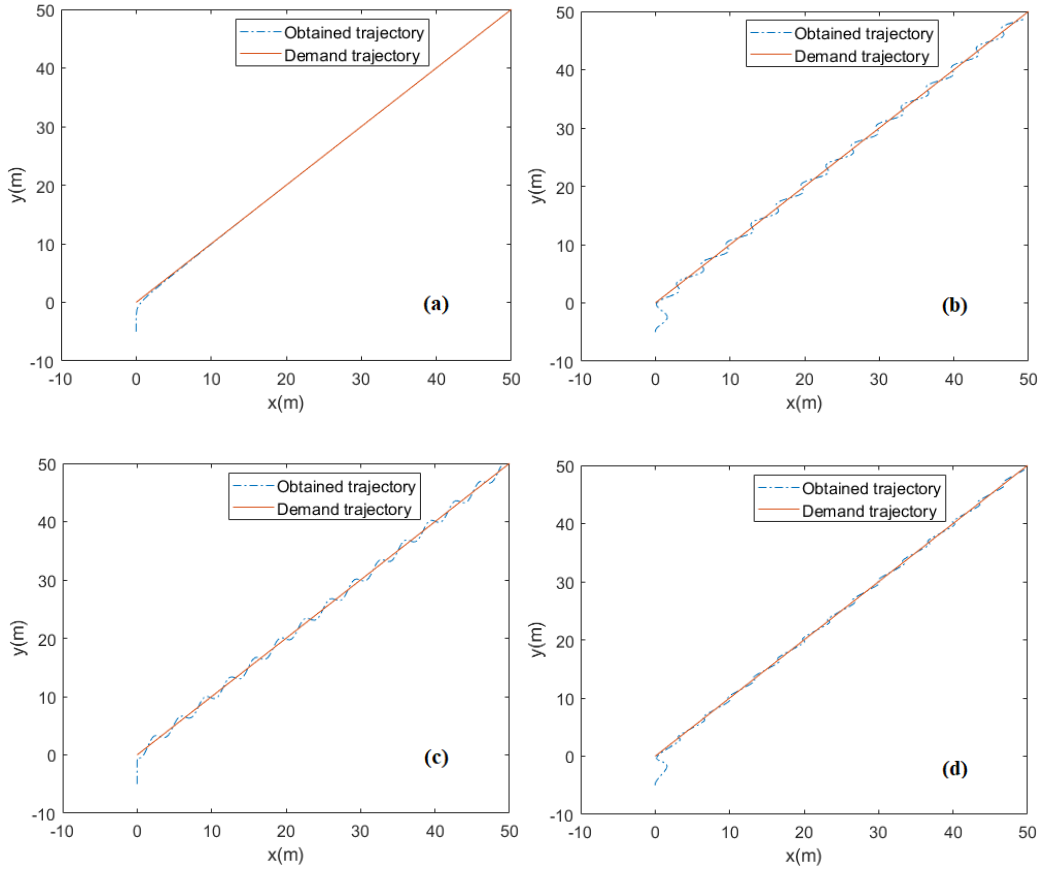
Fig. 3.5.2 Linear trajectory tracking under the influence of (a) stagnant water, (b) longitudinal current, (c) lateral current, (d) combined longitudinal and lateral current.
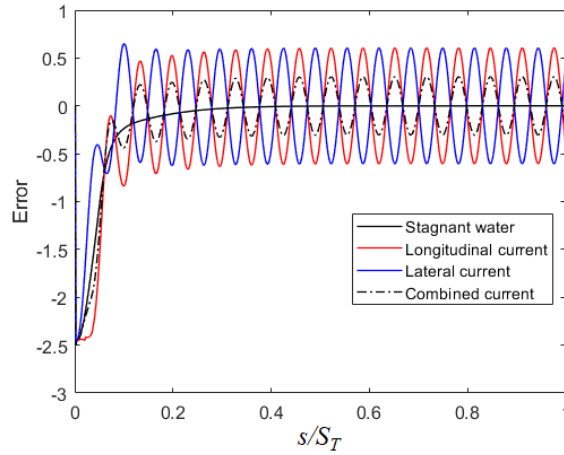
Fig. 3.5.3 Tracking error plots for linear trajectory under various water conditions

B. *Linear trajectory with sharp turns*

Simulations for tracking four consecutive linear trajectories having sharp turns have been carried out to further validate the system. The demand curved trajectory is defined in terms of waypoints in 2-D space as given in Table 3.5.1. Starting from the point (25, –35), the demand trajectory progresses through waypoints 1, 2, 3, and 4, ending at waypoint 5. The total demand trajectory length (S_T) for this case is 404.85 m.

Table 3.5.1 Coordinate of waypoints in 2-D space

Starting point	Waypoint 1	Waypoint 2	Waypoint 3	Waypoint 4	Waypoint 5
$(25, -35)$	$(40, -40)$	$(150, -40)$	$(150, 60)$	$(40, 60)$	$(100, 0)$

From Fig. 3.5.4 it is evident that the AUV initiates its mission at point (25, -35) with an initial heading towards north. The LOS control is engaged until the cross-track heading error drops below 40 degrees, at which point the CTE control is activated. The use of LOS control becomes apparent at every turn. Upon examining the trajectories, it becomes evident that the tracking performance is satisfactory. Figure 3.5.5 displays the tracking errors at different points that have been plotted against s/S_T. The RMSE coefficient (ε_{cr}) values corresponding to each water environment conditions have been calculated and listed in Table 3.5.2.

Fig. 3.5.4 Linear trajectory tracking with sharp turns under the influence of (a) stagnant water, (b) longitudinal current, (c) lateral current, (d) combined longitudinal and lateral current.
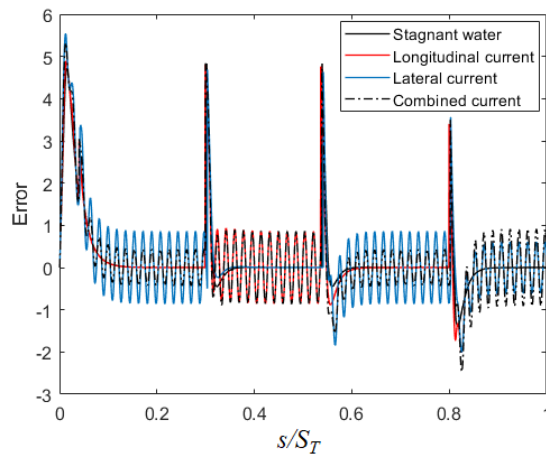
Fig. 3.5.5 Tracking error plots for linear trajectory having sharp turns under various water conditions

C. *Curved trajectory*

Simulations for tracking a curved path is carried out to further validate the system.

The demand curved path is defined as follows:

$$y = 5\sin(2\pi f_1 x) \hspace{4cm} (3.5.4)$$

Here, the frequency (f_1) of 0.005 Hz has been taken for the generation of curved trajectory. The starting point of the demand trajectory is located at the point (0,0). Following Eq. (3.5.4) the demand trajectory ends at the point (500,0) making a total demand trajectory length (S_T) of 11352 m. Initially, the AUV is positioned at point (–5, –6) with its heading directed northward. Figure 3.5.6 illustrates both the obtained and demand trajectory curves of the AUV for various water environment conditions. Upon examining the Fig. 3.5.6, it becomes evident that the tracking performance is satisfactory. The tracking errors at various positions have been plotted against s/S_T as depicted in Fig. 3.5.7. The RMSE coefficient (ε_{cr}) values corresponding to each water environment conditions have been calculated and listed in Table 3.5.2.
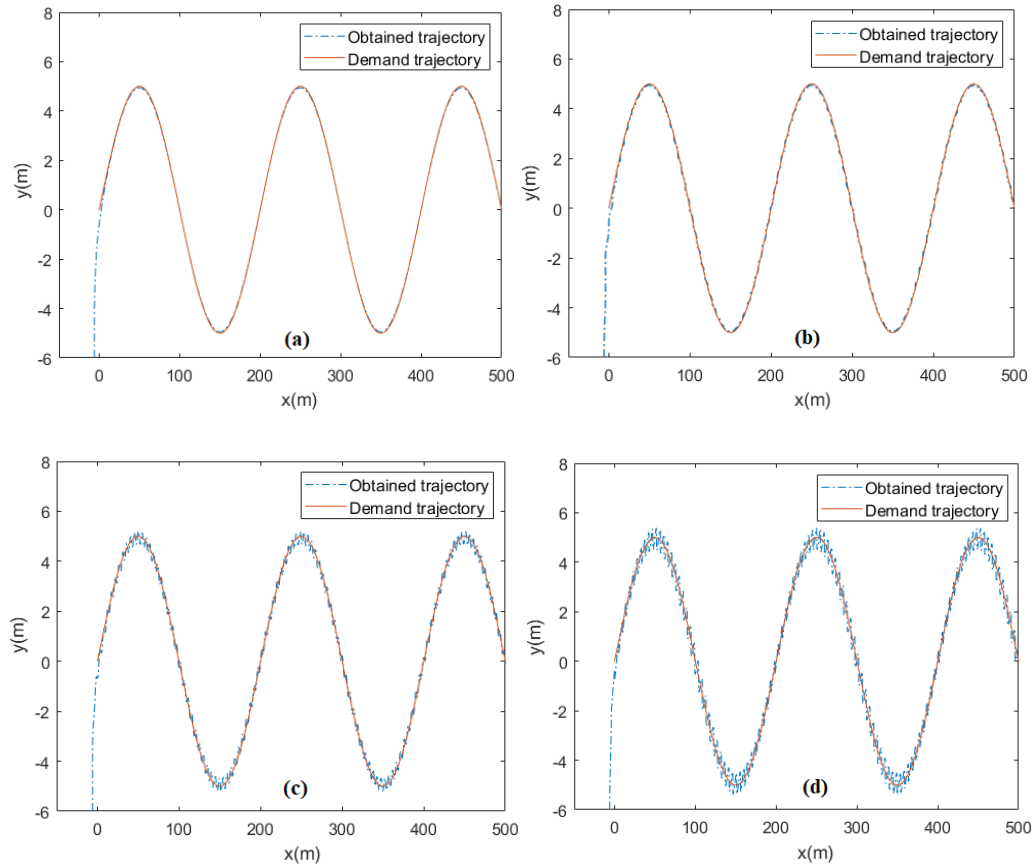
Fig. 3.5.6 Curved trajectory tracking under the influence of (a) stagnant water, (b) longitudinal current, (c) lateral current, (d) combined longitudinal and lateral current

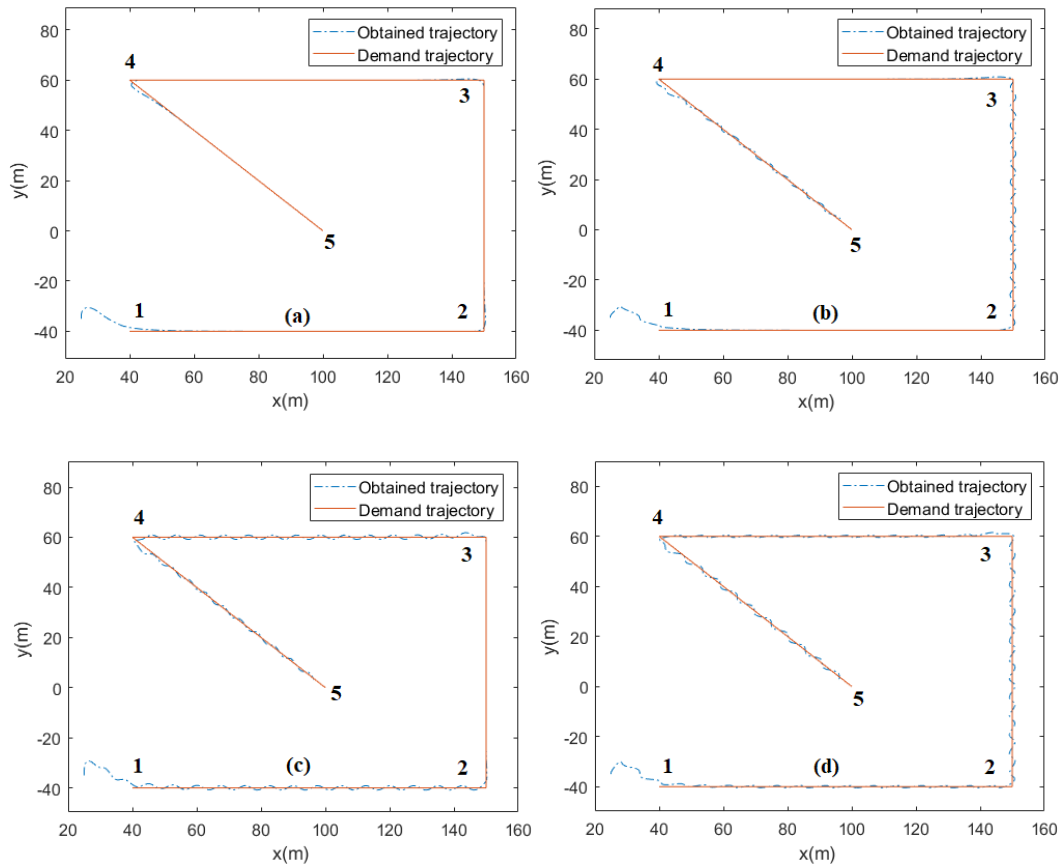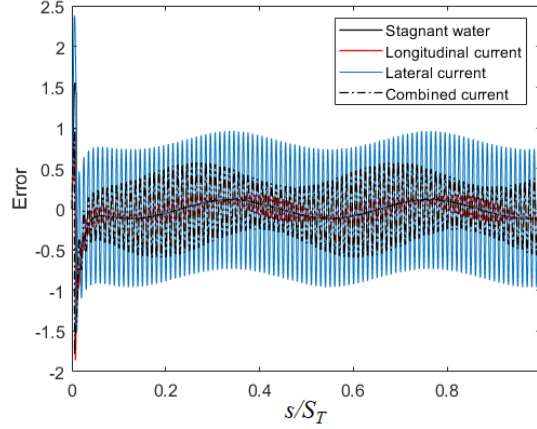**Fig. 3.5.7** Tracking error plots for curved trajectory under various water conditions

D. *Circular trajectory*

Simulations for tracking a circular path have been carried out to further validate the system. The equation used for generation of demand circular trajectory is defined as,

$$x^2 + y^2 = 40^2 \tag{3.5.5}$$

with its center point positioned at (0,0) and having a radius of 40 m. The circular trajectory begins at (40,0). Following Eq. (3.5.5), the trajectory ends at same point describing a full circular path of total demand trajectory length (S_T) of 251.3 m. In this simulation, the AUV is positioned at point (40, –50) with its heading directed northward. Figure 3.5.8 illustrates both the obtained and demand trajectory curves of the AUV for various conditions of water environment. Examining both trajectories, it becomes evident that the tracking performance is satisfactory. The tracking errors at different positions along the trajectory length under different water conditions have been plotted against s/S_T as shown in Fig. 3.5.9. The RMSE coefficient ε_{cr} values have been calculated accordingly for each water condition and listed in Table 3.5.2.
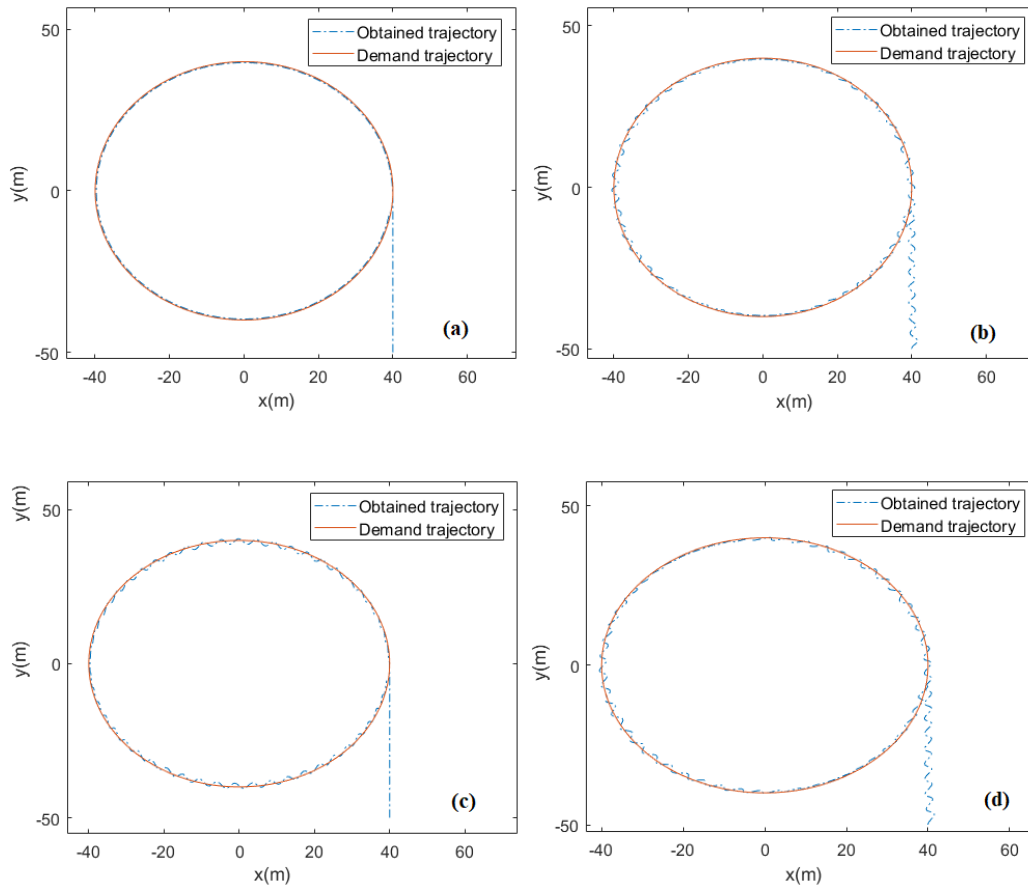
Fig. 3.5.8 Circular trajectory tracking with sharp turns under the influence of (a) stagnant water, (b) longitudinal current, (c) lateral current, (d) combined longitudinal and lateral current.
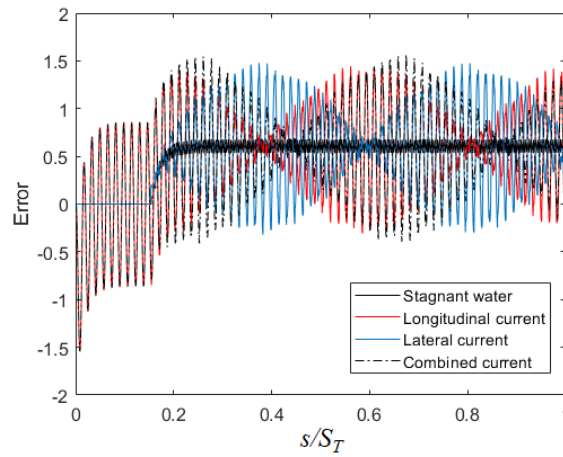
Fig. 3.5.9 Tracking error plots for circular trajectory under various water conditions

Analyzing the RMSE coefficient (ε_{cr}) values as shown in Table 3.5.2, it has been observed that in stagnant water, where external perturbations are absent, the AUV demonstrates better accuracy in tracking the demand trajectories, reflected in lower ε_{cr}

85

values across all trajectory types. However, trajectory having sharp turns exhibits higher ε_{cr} values compared to linear trajectory. This suggests that the AUV faces challenges in maintaining accuracy when navigating through trajectories with abrupt changes in direction. Furthermore, the presence of water flow perturbations amplifies trajectory tracking errors with longitudinal, lateral, and combined perturbations leading to increased ε_{cr} values across different trajectory types.

Table 3.5.2 RMSE coefficients (ε_{cr}) for various water conditions and trajectories

Water condition Trajectory type	Stagnant water	Longitudinal current	Lateral current	Combined current
Linear trajectory	0.453	0.672	0.544	0.520
Linear trajectory with sharp turns	0.876	0.998	1.060	1.079
Curved trajectory	0.154	0.179	0.625	0.545
Circular trajectory	0.547	0.712	0.667	0.737

The stability analysis has been conducted for checking the robustness of the controllers by providing sudden underwater disturbance. This analysis has been conducted on two trajectory types: a linear trajectory having sharp turns and a circular trajectory. For the linear trajectory with sharp turns, as shown in Fig. 3.5.10a, a sudden disturbance has been introduced in water at point A (80, –40) and point B (150, 0) on the demand trajectory. This disturbance is caused by a longitudinal current (U_{cx}) and a lateral current (U_{cy}) with magnitude of 5 m/s and 2 m/s respectively. Similar to this, a sudden disturbance has also been introduced on the demand circular trajectory at point C (10, 40) and point D (–5, –40) trajectory as shown in Fig. 3.5.10b. In this case the disturbance is caused by a longitudinal current (U_{cx}) and a lateral current (U_{cy}) with magnitude of 2 m/s and 4 m/s respectively. Observing Fig. 3.5.10a and 3.5.10b, it becomes evident that despite the abrupt change of water condition, the AUV initially

deviates from demand path but swiftly recovers and returns to the intended trajectory.

This indicates the stability of the controllers in response to unexpected disturbances.
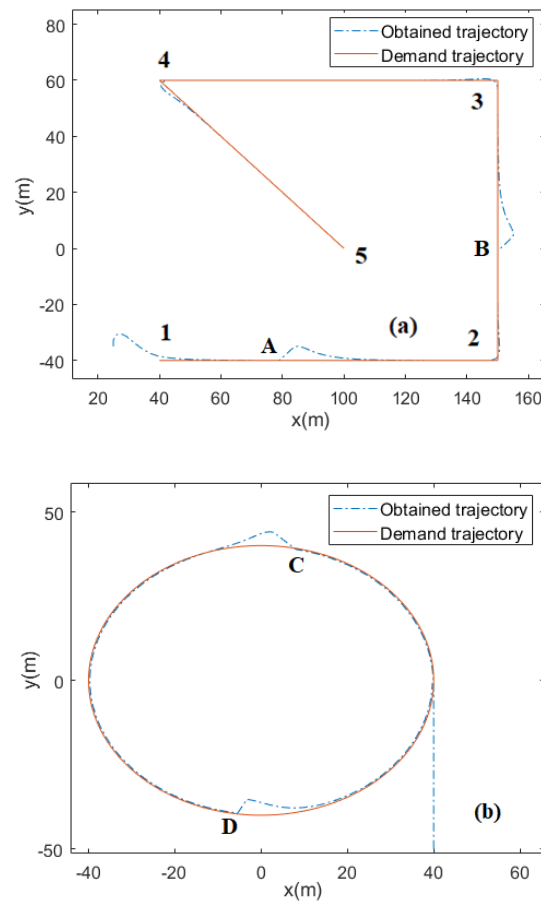
Fig. 3.5.10 Stability analysis of controllers for (a) trajectory with sharp turns, (b) circular trajectory

This page is left blank intentionally

CHAPTER 4

Conclusions and Future Scope

Chapter 4 distils the core of the project, delving into the conclusions drawn from the research findings. It outlines the future prospects for potential extensions and advancements in the project, suggesting avenues for further exploration.

4.1 Conclusions

The complex field of controller design for an AUV has been explored in this dissertation, which also presents a unique four-ballast tank mechanism to enhance manoeuvrability. Through the use of four motor-pump configurations, this novel method seeks to reduce dependence on conventional control surfaces for ballast tank adjustment. Key components of AUV motion control, such as heave motion, propeller performance, yaw motion, and trajectory tracking for guided navigation along predetermined courses, are the main emphasis of the study.

The system description and modelling of heave motion dynamics has been covered in detail in Section 2.2. A strategy utilising two methodologies has been employed to tackle the problem of an unknown AUV drag coefficient. Using MATLAB-Simulink, a governing equation for the dynamics of heave motion has been developed and solved. Concurrently, the unknown value of hull drag coefficient has been estimated in Section 3.2 by employing Ansys-Fluent for a thorough CFD investigation, yielding a reasonable result that has been integrated into the governing formula. The implementation and evaluation of two depth controllers, PID and PI, demonstrate the advantage of the PID controller in managing higher-order dynamics and guaranteeing stability during heave motion.

The choice of an appropriate propeller and an analysis of its performance on open water have been covered in Section 2.3. Based on AUV dimensions, a four-bladed B-series propeller has been selected. In Section 3.3, the numerical analysis of propeller's performance has been evaluated using ANSYS-Fluent and the accuracy of the numerical results is confirmed by comparing it to experimental findings of Bernitsas et al. (1981). The examination of AUV hull drag in forward motion indicates that the craft

achieves its top speed limit of 2.5 m/s at an advance ratio (J) of roughly 0.9, which is in compliance with the requirements.

The link between yaw motion, rudder tilt angle, and forward velocity has been examined in Section 2.4, along with the system description and modelling of yaw motion dynamics. Comprehensive analysis using ANSYS-Fluent takes into account different tilt degrees (θ) and forward velocities (v) in Section 3.4. The identification of critical angles for rudder stalling highlights the necessity of keeping the tilt angle below around 11^0 degrees in order to avoid stalling. In order to develop the governing equation of yaw motion dynamics, the generated yawing moment is subjected to additional analysis. PID controllers, which outperform PI controllers in this regard, have been implemented in MATLAB Simulink.

Section 2.5 tackles the interconnected difficulties of planar path-following tracking control within the 2-D plane. More precise path-following tracking control has been ensured by the kinematic and dynamic model establishment, cross-track-error design, and line-of-sight guidance design. Section 3.5 presents simulation outcomes featuring various 2-D desired trajectories, illustrating the robustness and effective path-following tracking capabilities of the proposed controllers.

4.2 Future Scope of Work

The future works of the present investigation are enumerated as follows:

- Optimizing the hull shape of the AUV would address limitations in hull drag, particularly at higher advance ratios.
- Fine-tuning the heave motion dynamics model by accounting for real-world factors and exploring alternative control algorithms beyond PID would enhance depth controller accuracy.
- Refining the propeller's geometry or exploring alternative designs would improve thrust generation and overall efficiency.

- Considering additional factors such as underwater currents in yaw motion dynamics and exploring advanced control algorithms for rudder tilt optimization would further enhance performance.

- Enhancing path-following tracking control with sophisticated algorithms, adaptive techniques, or machine learning approaches would improve precision and robustness.

- Expanding trajectory testing to include three-dimensional paths would provide a more realistic evaluation of the AUV's capabilities.

- Integrating developed control systems into an AUV prototype and conducting field tests would offer valuable insights.

REFERENCES

Alam, K., Ray, T., & Anavatti, S. G. (2015). Design optimization of an unmanned underwater vehicle using low-and high-fidelity models. IEEE Transactions on Systems, Man, and Cybernetics: Systems, 47(11), 2794-2808.

Allotta, B., Pugi, L., Bartolini, F., Ridolfi, A., Costanzi, R., Monni, N., & Gelli, J. (2015). Preliminary design and fast prototyping of an autonomous underwater vehicle propulsion system. Proceedings of the Institution of Mechanical Engineers, Part M: Journal of Engineering for the Maritime Environment, 229(3), 248-272.

ANSYS Workbench Products ReleaseNotes 10.0.

Bandyopadhyay, P. R. (2005). Trends in biorobotic autonomous undersea vehicles. IEEE Journal of Oceanic Engineering, 30(1), 109-139.

Barnitsas, M. M., Ray, D., & Kinley, P. (1981). KT, KQ and efficiency curves for the Wageningen B-series propellers. University of Michigan.

Binns, S. D., Gibbs, T. & Eddy, R., (2011). A Vision for an MXV and UXV Enabled Future Host Submarine (SSH). Proc. of RINA Warship 2011: Naval Submarines and UUVs, Bath, UK, June 2011.

Blidberg, D. R. (2001, May). The development of autonomous underwater vehicles (AUV); a brief summary. In Ieee Icra (Vol. 4, No. 1, pp. 122-129).

Bradley, A. M., Feezor, M. D., Singh, H., & Sorrell, F. Y. (2001). Power systems for autonomous underwater vehicles. IEEE Journal of oceanic Engineering, 26(4), 526-538.

Carlton, J. S. (2011). Marine Propellers and Propulsion. Butterworth-Heinemann.

Chase, N. and P. M. Carrica (2013). Submarine propeller computations and application to selfpropulsion of DARPA Suboff, Ocean Engineering 60, pp. 68–80.

Chen, C. W., Kouh, J. S., & Tsai, J. F. (2013). Maneuvering modeling and simulation of AUV dynamic systems with Euler-Rodriguez quaternion method. China Ocean Engineering, 27, 403-416.

Das, S., & Mandal, P. (2023). Heave Motion Control of an Autonomous Underwater Vehicle Having Four Ballast Tanks. Journal of Material Science and Mechanical Engineering, 10(2), 112-117.

de Sousa, J. V. N., de Macêdo, A. R. L., de Amorim Junior, W. F., & de Lima, A. G. B. (2014). Numerical analysis of turbulent fluid flow and drag coefficient for optimizing the AUV hull design. Open journal of fluid dynamics, 4(03), 263.

Farrell, J. A., Pang, S., & Li, W. (2005). Chemical plume tracing via an autonomous underwater vehicle. IEEE Journal of Oceanic Engineering, 30(2), 428-442.

Fossen, T.I. (1994). Guidance and control of ocean vehicles. John Wiley & Sons Ltd.

Gao, X. W. and T. G. Davies (2002). Boundary Element Programming in Mechanics. Cambridge University Press, New York.

Ghassemi, H. (2003). Hydrodynamic characteristics of marine propeller in steady and unsteady wake flows. Journal of Science and Technology of AmirKabir 14(54), 81-98.

Ghosh, P., & Mandal, P. (2018). Pressure and Shear Stress Distribution over External Hull of an Autonomous Underwater Vehicle. Journal of Basic and Applied Engineering Research, 5(5), 452-456.

Ghosh, P., & Mandal, P. (2019). Numerical study of depth control of an innovative underwater vehicle having four ballast tanks. International Journal of Emerging Technologies and Innovative Research, 6(5), 123-126.

Ghosh, P., & Mandal, P. (2021, December). Numerical Analysis of Open-Water Propeller Performance and Submarine Hull Drag. In Conference on Fluid Mechanics and Fluid Power (pp. 159-164). Singapore: Springer Nature Singapore.

Ghosh, P., Das, A., & Mandal, P. (2023). Analysis of Available Yawing Moment of an Autonomous Underwater Vehicle Model in Simulation Frame. Journal of Graphic Era University, 191-206.

Gohil, P. P. and R. P. Saini (2016). Numerical Study of Cavitation in Francis Turbine of a Small Hydro Power Plant. Journal of Applied Fluid Mechanics 9(1), 357-365.

Gross, A., A. Kremheller and H.F. Fasel (2011). Simulation of Flow over Suboff Bare Hull Model. AIAA Aerospace Sciences Meeting, Orlando, Florida.

Hagen, P. E., Storkersen, N., Vestgard, K., & Kartvedt, P. (2003, September). The HUGIN 1000 autonomous underwater vehicle for military applications. In Oceans 2003. Celebrating the Past... Teaming Toward the Future (IEEE Cat. No. 03CH37492) (Vol. 2, pp. 1141-1145). IEEE.

Hai, H., Zexing, Z., Jiyong, L., Qirong, T., Wanli, Z., & Wang, G. (2019). Investigation on the mechanical design and manipulation hydrodynamics for a small sized, single body and streamlined I-AUV. Ocean Engineering, 186, 106106.

Hayati, A. N., S. M. Hashemi and M. Shams (2013). A study on the behind-hull Performance of marine propellers astern autonomous underwater vehicles at diverse Angles of attack. Ocean Engineering 59, 152-163.

Healey, A.J., 1995. Dynamics of Marine Vehicles (ME-4823). Class Notes, Naval Postgraduate School, Monterey, CA.

Ji, B., X. W. Luo, Y. L. Wu, S. H. Liu, H. Y. Xu and A. Oshima (2010). Numerical Investigation of Unsteady Cavitating Turbulent Flow Around a Full Scale Marine Propeller. Journal of Hydrodynamics 22(5), 747–752.

Johnson, J. (2001). Parameter Identification of the ARIES AUV (Doctoral dissertation, MS Thesis Naval Postgraduate School, Monterey, CA).

Karim, M. M., Rahman, M. M., and Alim, M. A. (n.d.) (2009). Computation of Turbulent Viscous Flow around Submarine Hull Using Unstructured Grid, 1–18.

Kenny, A. J., Cato, I., Desprez, M., Fader, G., Schüttenhelm, R. T. E., & Side, J. (2003). An overview of seabed-mapping technologies in the context of marine habitat classification. ICES Journal of Marine Science, 60(2), 411-418.

Kim, J., Kim, K., Choi, H. S., Seong, W., & Lee, K. Y. (2002). Estimation of hydrodynamic coefficients for an AUV using nonlinear observers. IEEE journal of oceanic engineering, 27(4), 830-840.

Kinnas, S. A. and C. Y. Hsin (1992). Boundary element method for the analysis of the unsteady flow around extreme propeller geometry. AIAA Journal 30(3), 688-696.

Kormushev, P., & Caldwell, D. G. (2013, September). Towards improved AUV control through learning of periodic signals. In 2013 OCEANS-San Diego (pp. 1-4). IEEE.

Marti´nez-Calle, J. N., Balbona-Calvo, L., Gonza´lez-Pe´rez, J., & Blanco-Marigorta, E. (2002, January). An open water numerical model for a marine propeller: A comparison with experimental data. In Fluids Engineering Division Summer Meeting (Vol. 36169, pp. 807-813).

Menter, F. R. (1994). Two-equation eddy-viscosity turbulence models for engineering applications. AIAA Journal, 32(8): 1598–1605.

Menter, F. R. (1994). Two-equation eddy-viscosity turbulence models for engineering applications. AIAA journal, 32(8), 1598-1605.

Molnar, L., Omerdic, E. and Toal, D., 2007. Guidance, navigation and control system for the Tethra unmanned underwater vehicle. International Journal of Control, 80(7), pp.1050-1076.

Nakisa, M., Abbasi, M. J., & Amini, A. M. (2010, December). Assessment of marine propeller hydrodnamic performance in open water via CFD. In Proceedings of The 7th International Conference on Marine Technology (MARTEC 2010).

Nan, Z., S. Hongcui, and Y. Huizhi (2005). Numerical simulation of flow around submarine under full surface and submerged conditions. In 5th Osaka Colloquium on Advanced Research on Ship Viscous Flow and Hull Form Design by EFD and CFD Approaches.

Nemati Hayati, A., Hashemi, S. M., and Shams, M. (2013). A study on the behind-hull performance of marine propellers astern autonomous underwater vehicles at diverse angles of attack. Ocean Engineering, 59: 152–163.

Nor, A. M., Abdullah, S. S., Aras, M. S. M., & Rashid, A. (2012). Neural Network Predictive Control (NNPC) of a Deep Submergence Rescue Vehicle (DSRV). In 4th International Conference on Underwater System Technology: Theory and Applications 2012, 24-29.

Ohkusu, M. (1996). Advances in Marine Hydrodynamics, Computational Mechanics (5)., 279-322.

Phillips, A. B., Turnock, S. R., & Furlong, M. (2010). The use of computational fluid dynamics to aid cost-effective hydrodynamic design of autonomous underwater vehicles. Proceedings of the Institution of Mechanical Engineers, Part M: Journal of Engineering for the Maritime Environment, 224(4), 239-254.

Purton, I. M., Andrews, D. J., Mistry, A. & Kay, P., (2013b). Integrating Smart Unmanned Underwater Vehicle Networks with a Host Vessel. Proc. of IMarEST Engine As A Weapon V, Bristol, UK, July 2013.

Raman, N. S., Briscoe, J. D., & Grivel, T. (2002, June). Lithium-ion batteries for autonomous underwater vehicles. In Proceedings of the 2002 Workshop on Autonomous Underwater Vehicles. (pp. 45-49). IEEE.

Ridao, P., Carreras, M., Ribas, D., & Garcia, R. (2010). Visual inspection of hydroelectric dams using an autonomous underwater vehicle. Journal of Field Robotics, 27(6), 759-778.

Sahoo, A., Dwivedy, S. K., & Robi, P. S. (2019). Advancements in the field of autonomous underwater vehicle. Ocean Engineering, 181, 145-160.

Shome, S. N., Nandy, S., Pal, D., Das, S. K., Vadali, S. R. K., Basu, J., & Ghosh, S. (2012). Development of modular shallow water AUV: Issues & trial results. Journal of The Institution of Engineers (India): Series C, 93(3), 217-228.

Sname, T., 1950. Nomenclature for treating the motion of a submerged body through a fluid. The Society of Naval Architects and Marine Engineers, Technical and Research Bulletin, (1950), pp.1-5.

Supriyanka, J., Parveen, S., & Babu, N. (2011). The Development of Controller for Buoyancy Engine for Use in Autonomous Underwater Vehicle (AUV). International Journal of Computer Science Issues, Special Issue, ICVCI-201, 1(1), 52-57.

Tanakitkorn, K., Wilson, P. A., Turnock, S. R., & Phillips, A. B. (2017). Depth control for an over-actuated, hover-capable autonomous underwater vehicle with experimental verification. Mechatronics, 41, 67-81.

Taskar, B., K. K. Yum, S. Steen and E. Pedersen (2016). The effect of waves on engine-propeller dynamics and propulsion performance of ships. Ocean Engineering 122, 262-277.

Tran, M., Binns, J., Chai, S., Forrest, A. L., & Nguyen, H. (2019). A practical approach to the dynamic modelling of an underwater vehicle propeller in all four quadrants of operation. Proceedings of the Institution of Mechanical Engineers, Part M: Journal of Engineering for the Maritime Environment, 233(1), 333-344.

Turnock, S.R. and A. M. Wright (2000). Directly coupled fluid structural model of a ship rudder behind a propeller. Marine Structures 13(1), 53-72.

Victor Nunes de Sousa, J., Roberto Lins de Macêdo, A., Ferreira de Amorim Junior, W., and Gilson Barbosa de Lima, A. (2014). Numerical Analysis of Turbulent Fluid Flow and Drag Coefficient for Optimizing the AUV Hull Design. Open Journal of Fluid Dynamics, 04(03): 263–277.

Watanabe, T., T. Kawamura, Y. Takekoshi, M. Maeda and S. H. Rhee (2003). Simulation of steady and unsteady cavitation on a marine propeller using a RANS CFD code. In Proceedings of Fifth International Symposium on Cavitation, Osaka, Japan, 1-4.

Watson, S. A., & Green, P. N. (2014). Depth control for micro-autonomous underwater vehicles (µAUVs): Simulation and experimentation. International Journal of Advanced Robotic Systems, 11(3), 31.

Wei, A., Zheng, R., & Guo, J. (2018, August). AUV Vertical Motion Control Based on Kalman Filtering. In 2018 WRC Symposium on Advanced Robotics and Automation (WRC SARA) (pp. 334-339). IEEE.

Whitcomb, L.L. (2000). Underwater robotics: Out of the research laboratory and into the field. In Proceedings of the 2000 ICRA. Millennium Conference (Vol. 1, pp. 709-716). IEEE.

Wynn, R. B., Huvenne, V. A., Le Bas, T. P., Murton, B. J., Connelly, D. P., Bett, B. J., & Hunt, J. E. (2014). Autonomous Underwater Vehicles (AUVs): Their past, present and future contributions to the advancement of marine geoscience. Marine geology, 352, 451-468.

Yu, X., Dickey, T., Bellingham, J., Manov, D., & Streitlien, K. (2002). The application of autonomous underwater vehicles for interdisciplinary measurements in Massachusetts and Cape Cod Bays. Continental Shelf Research, 22(15), 2225-2245.

Zhang, N. and S. L. Zhang (2014). Numerical Simulation of Hull/Propeller Interaction of Submarine in Submergence and Near Surface Conditions. Journal of Hydrodynamics 26(1), 50-56.

Zhang, Z. R. (2010). Verification and Validation for RANS Simulation of KCS Container Ship without/with Propeller. Journal Hydrodynamics 22(5), 932–939.

Zheng, H., & Wu, J. (2015, June). Data collection and event detection in the deep sea with delay minimization. In 2015 12th Annual IEEE International Conference on Sensing, Communication, and Networking (SECON) (pp. 354-362). IEEE.

Engineering Research Express

PAPER

AUV way-point tracking at constant velocity: cross-track error (CTE) and line-of-sight (LOS) guidance

Pritam Ghosh[1,2] and Pranibesh Mandal[1]

1   Department of Mechanical Engineering, Jadavpur University, Kolkata 700032, India
2   Department of Mechanical Engineering, Heritage Institute of Technology, Kolkata 700107, India

E-mail: pghosh_me@yahoo.com

Abstract

This paper addresses the integrated challenges of path-following and tracking control for an under-actuated Autonomous Underwater Vehicle (AUV) in the two-dimensional (2D) plane. Four distinct 2D trajectories: linear, linear with sharp turns, curved, and circular trajectories have been considered in this study. The proposed path-following control algorithm leverages AUV kinematic and dynamic models, incorporating the Cross-Track Error (CTE) method and Line-of-Sight (LOS) technique to determine the desired orientation. Stability analysis has been performed to evaluate the robustness of the controllers against sudden underwater disturbances. Additionally, perturbation has been introduced in simulations to mimic real-world conditions more accurately. The simulations confirm the controllers' proficiency in accurately tracking these various trajectories from a given starting point.

1. Introduction

The ocean spans about 66.67% of the earth's surface, housing vast resources. Yet, our exploration of its depths remains relatively limited. Historically, the sea, as one of the four pivotal human development arenas, has been a significant strategic point of contention among global powers. In recent times, maritime dominance or 'thalassocracy' has gained increased focus from numerous countries. The ocean's influence is complex and has many facets, affecting both the ecological balance and the intricacies of human society. As land resources diminish, the significance of the ocean to national interests grows more, making it a global focal point. As we progressed into the 21st century, coastal nations have increased their focus on marine science and technology, adjusted their military strategies, and strengthened their efforts for maritime rights. As a result, marine advancement has emerged as a crucial area of study and is poised to be a significant global battleground in the 21st century [1–3].

The idea of making AUVs that can move on their own, started several decades ago, with the idea of constructing robotic entities capable of autonomous navigation beneath the ocean's surface. An AUV is a powerful tool for marine activities. Unlike tethered vehicles, AUVs can navigate independently in three-dimensional water spaces using their own power, based on pre-set mission parameters. They boast features like long-range capability, intelligence, stealth, agility, and cost-effectiveness. In military contexts, AUVs play roles in surveys, mine detection and removal, submarine warfare, maritime alerts, blockading routes, or ports, attacking enemy vessels or submarines, targeting the enemy's communication infrastructure, and facilitating underwater communication relays. In civilian applications, they assist in exploring and tapping marine resources, tracking marine environmental changes, studying underwater topography, advancing deep-sea technology, inspecting underwater structures, and aiding in ocean rescue and salvage operations [4–6].

In recent decades, advancements in AUV technology have consistently provided scientists with sophisticated tools for tasks such as ocean exploration, extensive surveys, tracking underwater pipelines, scientific sampling, maintaining and constructing maps, as well as military search and rescue operations, among others [7–10]. AUVs bring many benefits, but they also come with intricate control challenges. This complexity arises because

NUMERICAL STUDY OF DEPTH CONTROL OF AN INNOVATIVE UNDERWATER VEHICLE HAVING FOUR BALLAST TANKS

[1]Pritam Ghosh, [2]Pranibesh Mandal

[1]Research Scholar, [2]Assistant Professor
Mechanical Engineering Department
Jadavpur University, Kolkata, India

Abstract:Underwater vehicle has been an active area of research for a long time. Design and control of such underwater vehicle is very much challenging. Here an innovative design of underwater vehicle has been proposed with an innovative placement of four ballast tanks. The dynamics behavior of heave motion has been obtained by solving the governing equation using Matlab-Simulink frame. Open loop depth control has also been achieved by proper control of water flow in and out of the ballast tanks.

***Index Terms*–Underwater vehicle, Diving Dynamics, Ballast tanks**

I. INTRODUCTION

Research on unmanned systems has gained notable development in the last few decades. Beginning with operation in the air these unmanned systems are continuously showing new possibilities on the ground and even underwater. With the first prototype in 1980s Unmanned Underwater Vehicle (UUV) started to spread its amazement in many areas in our daily life viz. in military field [1]; for proper utilization of oceanic resources, mapping as well as predicting underwater optical properties and visibility [2,3]; chemical pluming tracing [4] and many other applications. With the advancement of autonomous underwater vehicles, various shapes and sizes of AUVs have been developed. In most cases, the hull shapes have been of torpedo-like with streamlined body [5] and also smaller in size [6,7]. Design of "small size" AUV is a real challenge from various aspects viz. external hull shape design [8,9], pressure and shear stress distribution over external hull [10]. Besides, control of autonomous underwater vehicles is also a big challenge while executing operation under dangerous environments. Among various control-related problems, depth control plays an important role. For example, when seabed mapping is being done, it is required to keep the AUV at a constant depth from sea level. Many researchers have been working on depth controlling method of Unmanned Underwater Vehicles (UUV) and different techniques of depth control method has been studied. In 2017 Sayedet. al. [11] worked on different depth controlling methods of Unmanned Underwater Vehicle (UUV). In this work various depth control techniques viz. discrete quasi-sliding mode control, adaptive fuzzy logic and hybrid PID control system have been analysed in details and finally it has been found that for depth control the hybrid fuzzy PID control method can said to be the most suitable technique in UUV application. Based on several assumptions on the motion of submarine basically the diving dynamics has been derived. Among them main restriction has been imposed on pitch angle in diving plane which has been assumed to be small and another assumption is that the pitch motion dynamics could be described as a linear equation. These assumptions calls for many modelling errors making itinapplicable for practical cases. In 2005, Ji-Hong Li and Pan-Mook Lee [12]worked on this problem and found out a solution for eliminating these above said hindrance by considering the submarine to take any pitch angle. Besides,the diving dynamics of submarine has been taken as SISO system where the input has been taken as stern plane angle and the depth of the submarine as the output. Finally it has been found that the proposed scheme is more effective than existing method.

Till date for controlling the depth, yaw, roll and pitch motion mainly the control surfaces has been used. The novelty of the present study is that, herefour ballast tank mechanism has been proposedfor controlling of depth, pitch and roll motion of a model submarine. The four ballast tanks can be placed at the four bottom corners of the submarine as show in Fig. 1. Such an innovative placement of these ballast tanks would reduce the number of control surfaces of the submarine. In this present study only the depth control and diving dynamics have been studied for predicting the dynamics of the submarine model with the pitch and rolling motion studies being kept as future scope of work.Main principal for controlling depth of a submarine is to play with the buoyancy force. When the buoyancy force will be equal to the total weight of the submarine, the submarine will be in equilibrium and it will float either on water surface or it will float under fully submerged condition. Now when it is floating under fully submerged condition the submarine can be placed anywhere under water irrespective of the depth from free surface of water. That can be done by properly operating the pumps used for controlling the flow rate in and out of the ballast tanks. In this study four different depths has been obtained by controlling the overall weight of the submarine by controlling the pump activity for filling up or emptying the ballast tanks.

Pressure and Shear Stress Distribution over External Hull of an Autonomous Underwater Vehicle

Pritam Ghosh[1] and Pranibesh Mandal[2]

[1,2]Jadavpur University
E-mail: [1]pghosh_me@yahoo.com, [2]m.pran11@gmail.com

Abstract—*Under water vehicle design has been on the cards for long. Primary aspect of such vehicle design lies in proper geometrical design of the outer hull thereby providing minimum possible hull drag. However it is the pressure and shear stress distribution around the hull surface which dictates the hull drag and other forces applied on the hull. CFD analysis has been a useful tool to determine the same. The present work focuses on determination of such pressure and shear stress distribution over a 3D submarine hull geometry in simulation frame using ANSYS software platform.*

1. INTRODUCTION

The growing use of unmanned systems operating in air, on ground even under water are continually demonstrating new possibilities that can assist us in many ways in our daily life. The popularity of unmanned aerial vehicles which was initiated by US Department of Defense in 2005 and till date there are over 1000 UAS models being developed over 50 countries. In 2014 Cai et. al.[1] presented a brief overview on recent advances of small-scale unmanned aerial vehicles from three perspectives viz. platform, key elements and scientific research. A detailed survey has been conducted on 132 small-scale unmanned aerial vehicle models available worldwide. The small-scale unmanned aerial vehicles are classified into three categories bases on their collected data namely small-tactical, miniature, and micro. They have also presented the evolvement of key elements of a small-scale unmanned aerial vehicle including onboard processing units, navigation sensors, mission-oriented sensors, communication modules, and ground control station. An unmanned underwater vehicle is playing a vital role mainly in oceanic exploration, industrial and defense applications.

The HUGIN 1000 autonomous underwater vehicles (AUVs) has achieved great success in the civilian survey industry over past six years. Hagen et. al. [2] at San Diego, USA, has been presented a detail military applications of the HUGIN 1000 AUV. The HUGIN 1000 AUV has been developed jointly by the Norwegian Defense Research Establishment (FFI) and Kongsberg Simrad. Primary applications of HUGIN 1000 include mine countermeasures, rapid environmental assessment, anti-submarine warfare (ASW).

Yu et. al. [3] studied on ODYSSEY autonomous underwater vehicle which was deployed in September 1998 in Massachusetts and Cape Cod Bays for coastal optical and biological research. They also given the demonstration on AUVs which can be effectively used to study important coastal problems such as, concurrently measure bio-optical and physical properties and their interaction with physical process in coastal regions for ecosystem protection, proper utilization of oceanic resources, mapping and predicting underwater optical properties and visibility etc.

However the design of underwater vehicle is a complex and computationally expensive exercise and a big challenge too. To design of an underwater vehicle has long been an active area of research. While designing a submarine one needs to focus on various hydrodynamic parameters which play very significant role in submarine motion under water. Since under submerged condition energy is limited, so it is obvious that minimum resistance on the outer surface of the submarine is very necessary to attain and thus appropriate design of hull is an important criteria. Use of water channels have been a conventional method of finding an optimal hull shape in order to minimize the drag under water thereby reducing the engine power requirement. Recently with the development of the computational techniques costly water channel experimentations can be simulated in the computational domain. Submarine hull shape design using such computational methods have been also emerged now-a-days. In 2008 Karim et. al. [4] has presented a paper on numerical computation of viscous drag for axisymmetric underwater vehicles. In that paper mainly the simulated data and experimental data have been compared. Various types of hull have been used there of different L/D ratio ranging from 4 to 10. For the computation method finite volume method based on Reynolds-average Navier-Stoke (RANS) equations have been used for computing the viscous drag. For making the problem more realistic turbulent flow past the axisymmetric

Analysis of Available Yawing Moment of an Autonomous Underwater Vehicle Model in Simulation Frame

Pritam Ghosh*, Anwesha Das and Pranibesh Mandal

Department of Mechanical Engineering, Jadavpur University, 132, Raja Subodh Chandra Mallick Rd, Jadavpur, Kolkata, West Bengal 700032, India
E-mail: pghosh_me@yahoo.com; anweshadas1808@gmail.com; pranibesh.mandal@jadavpuruniversity.in
*Corresponding Author

Abstract

Research endeavors on the design and control techniques of Autonomous Underwater Vehicles (AUVs) have been going on for a long time. In the present study, the yaw motion of a small submerged underwater vehicle is investigated and visualized as a direct result of changes in the rudder tilt angle and forward velocity. The numerical analysis is performed in ANSYS-Fluent software. The turbulent flow field has been modeled using Shear Stress Transport (SST) k-ω model. A grid independence test has been conducted to ensure the validity of the findings. The forces on the rudder and the available yaw moment have been obtained for different combinations of the AUV's rudder tilt angle and forward velocity. The trend has intuitively been consistent and agreed with the basic concept of hydrodynamics.

Keywords: Underwater vehicle, yawing moment, rudder tilt angle, shear stress transport (SST) k-ω model, pressure distribution around on AUV rudder, CFD.

Numerical Analysis of Open-Water Propeller Performance and Submarine Hull Drag

Pritam Ghosh[1], Pranibesh Mandal[2]

[1]Department of Mechanical Engineering, Heritage Institute of Technology, Kolkata-700107, India
[2]Department of Mechanical Engineering, Jadavpur University, Kolkata-700032, India

ABSTRACT

The selection of appropriate propeller size meets the need of a submarine to move forward with the desired velocity against hull drag. In the present study, the Open-water behavior of a B-series four-bladed propeller and hull drag of a submarine with a realistic geometry have been studied through numerical simulation by using the ANSYS-Fluent software platform. The rotation of the propeller has been given by frame motion and the Shear Stress Transport (SST) k-ω model has been used for turbulence flow modeling. The grid independence test has also been performed at the onset. The propeller performance coefficients and submarine hull drag have been obtained by varying flow velocity. This result has helped in predicting the maximum thrust of the propeller and maximum velocity of the submarine. For validation purposes, the results of propeller coefficients obtained from numerical simulation have been compared with experimental data of existing literature and found good acceptance.

Keywords: B-series Propeller, Grid Independency, Open-water Performance, Propeller thrust, Submarine hull drag, Turbulence model.

1. INTRODUCTION

In marine propulsion, the widely used propeller and its design play a very crucial role. Moreover, from the point of view of the power estimation, the submarine's hull-propeller interaction has great importance. The main objective of designing a propeller is to provide maximum thrust and minimum torque for the optimum rotational speed. Besides, achieving the maximum efficiency, low noise and lighter weight also fall under the shade of propeller design. Until and unless these designed propellers are not tested through experiments, the actual performance of these propellers cannot be found out. However, such experiments are not only too expensive and time taking, but also assessment of such propeller behind hull where the highly disturbed wake zone exists is really a challenging job [1]. Thanks to the rapid development and advancement of computational fluid dynamics (CFD) technology it is possible to conduct such studies numerically in a simulation frame and to achieve very close prediction of actual propeller performance in real-time. Basically in an open-water test, the propeller is tested in towing tank without the hull. Here, the performance characteristic attributes viz. thrust and torque coefficients as well as the efficiency with advance ratio, are measured as the efficiency of the propulsion system is greatly dependent on these performance attributes.

2. LITERATURE REVIEW AND OBJECTIVE

In 2017, Delen et al. [2] evaluated the power and resistance of a submarine (DARPA SUBOFF) using both numerical analysis and empirical method. In their research, the open-water analysis of propeller was done numerically and finally validated with experimental data. Besides, the self-propulsion of the vehicle was studied using different velocities. They also applied the Actuator Disc Theory in self-propulsion tests with CFD for making the analysis robust. Investigation on resistance characteristic of a DARPA-SUBOFF submarine was done by Budak and Beji [3]. In this study taking the DARPA-SUBOFF submarine as a base model, nine geometric variant models were developed by combining three slightly different bow and three different stern forms with each other. Analysis of these newly developed submarine model had been done using commercial software ANSYS-FLUENT where SST k-ω model was used for computation. Since power is limited to any underwater submarine, minimization of hull drag could provide a longer dive span to the submarine. While designing any submarine hull, one should focus on various hydrodynamic parameters which play very significant role in submarine motion during submerged condition. Drag of submarine is one of them. In 2018 Ghosh and Mandal [4] have worked on pressure and shear stress distribution on an autonomous underwater vehicle's hull. A 3D submarine hull in the simulation frame has been used to conduct the study using ANSYS-FLUENT software and analyze the distribution of pressure and shear stress distribution over the external hull of the submarine. Taskar et al. [5] have worked on propulsion system of a ship to investigate the propulsion at different wave conditions. To do so they used an inertial shaft model and applied a methodology for estimation of wake in waves. From their study it has been observed that there is a drop in propulsion performance when they considered the engine propulsion dynamics, wake variations and other losses. For power performance of any submarine, hull-propeller interaction plays an important role. In 2014, Nan and Sheng-li [6] studied on five bladed propeller having a high-skew of a submarine

YAW MOTION CONTROL STRATEGY FOR AUTONOMOUS UNDERWATER VEHICLES (AUVs)

P. Ghosh, P. Mandal

Department of Mechanical Engineering, Jadavpur University, Kolkata, India

ABSTRACT

Autonomous Underwater Vehicles (AUVs) are advanced marine robots designed to navigate the ocean's complex environments. A crucial aspect of their navigation capability is the yaw control, which determines the vehicle's horizontal orientation and direction of motion. Efficient yaw control ensures precise maneuvering, enabling AUVs to carry out intricate tasks and navigate through challenging underwater terrains with accuracy. To control its yaw motion, an AUV needs a system that ensures it moves correctly. This study developed and compared yaw control using both Proportional (P) and Proportional Integral (PI) methods. Simulations revealed that the PI-Controller performs better, with fewer oscillations and errors than the P-Controller.

Keywords: Autonomous Underwater Vehicle (AUV), Yaw motion, Control system, Yawing moment.

NOMENCLATURE

- F Force (N)
- I Mass moment of inertia (kg-m^2)
- K Controller gain (dimensionless)
- M Moment (N-m)
- r Distance (m)
- Y Hydrodynamic coefficient (Dimensionless)

Greek Symbols
- α Rudder tilt angle (radian)
- ψ Yaw angle (radian)

Subscripts
- d Drag
- dim Demand
- i Integral
- p Proportional
- r Rate of change of yaw angle
- v Sway velocity
- y Yaw
- z z-axis

1.   INTRODUCTION

In recent decades, there has been a marked progression in research on unmanned systems. While initial developments were concentrated on aerial operations, these systems have progressively demonstrated their potential on terrestrial terrains and even beneath the water's surface. Originating with the pioneering prototype in the 1980s, the Unmanned Underwater Vehicle (UUV) has carved a niche for itself in diverse areas of our everyday lives. AUVs are employed in military operations [1], marine resource utilization, underwater mapping [2,3], chemical plume tracking [4], and other diverse roles.

The evolution of yaw motion control in AUVs has been a subject of extensive research over the years, given its fundamental role in maintaining the desired underwater orientation. Key research, such as

Fossen's [5] foundational text on ocean vehicle dynamics, introduced the community to rudimentary control methods like PID controllers. As AUVs encountered various underwater uncertainties, the demand for adaptive controllers increased, a trend captured in the 2019 study by Yu et al. [6]. Neural networks' potential to predict yaw motion and enhance feedback control was recognized early in 1993 by Healey and Lienard [7]. Alongside, there were significant strides in sliding mode control, emphasizing disturbance robustness, as illustrated by Swaroop et al. [8] and Valeriano et al. [9]. An innovative approach surfaced with Model Predictive Control (MPC), with studies like Lapierre & Soetanto's [10] showcasing its prowess. The 1990s also saw the integration of fuzzy logic into yaw control strategies, offering enhanced performance under specific conditions, as evidenced by Li et al. [11] work. Bai et al. [12] developed a self-adjusting and adaptive control method for the yaw dynamics of an autonomous underwater vehicle, combining fuzzy logic with a classical gain compensator, which, when calibrated, offers consistent control across different conditions, outperforming standalone fuzzy logic and classical state feedback controllers. While hybrid control methods emerged, blending methodologies like neural networks, and sliding mode control, as showcased by Roy et al. [13], a holistic approach integrating yaw control with other motion dimensions was also pursued and exemplified by Lefeber et al. in [14]. The challenge of disturbances, particularly from underwater currents, was addressed through sliding mode techniques, as presented by Rodriguez et al. [15]. The turn of the recent decade has ushered in a fresh perspective on deep reinforcement learning, with researchers like Carlucho et al. [16] emphasizing its significance in AUV control.